1-1-2013

Multifunctional Nanomaterials of DNA Block Copolymers: Synthesis, Self- Assembly, Thermodynamic Studies and Biomedical Applications

Xi-Jun Chen
University of Pennsylvania, mschemmaniac@gmail.com

Multifunctional Nanomaterials of DNA Block Copolymers: Synthesis, Self- Assembly, Thermodynamic Studies and Biomedical Applications

Abstract
Oligonucleotide-conjugated bio-hybrid nanomaterials with a dense DNA layer on the surface have been shown to possess extraordinary selectivity and sensitivity for DNA detection as well as promising results as delivery agents, as demonstrated with the exceptional example of polyvalent oligonucleotide-conjugated gold nanoparticles. However, progress in this field has been slowed, since achieving high DNA density functionalization on the nanoparticle surface for materials other than gold is a major challenge. In this body of work, we have developed a general system to conjugate a dense layer of DNA on the surface of nanoparticles by the self-assembly of DNA block copolymer. These hybrid nanostructures demonstrated enhanced DNA binding, where the DNA strands on the surface of the nanoparticles can recognize and bind to complementary DNA strands without the addition of salt, a condition where free DNA strands do not form duplex. These assemblies are also selective in DNA recognition; they can distinguish different number base mismatches of the complementary DNA. It was determined that these assemblies possess a surface DNA density that is four times higher than that of DNA-conjugated gold nanoparticles of the same size, the highest DNA functionalization reported in the literature in this size range. These assemblies were also effectively taken up by cells without the use of a co-transfecting agent. The high DNA density also protects the degradation of the DNA, making them ideal candidates for DNA delivery and antisensing applications. Lastly, these assemblies have been tested for their antisensing capability, and found that they can effectively down regulate a targeted protein.

Degree Type
Dissertation

Degree Name
Doctor of Philosophy (PhD)

Graduate Group
Chemistry

First Advisor
So-Jung Park

Second Advisor
Ivan J. Dmochowski

Keywords
biomedical, DNA block copolymer, enhanced binding, nanoparticle, polymer, self-assembly

Subject Categories
Chemistry | Mechanics of Materials | Polymer Chemistry

MULTIFUNCTIONAL NANOMATERIALS OF DNA BLOCK COPOLYMERS: SYNTHESIS, SELF-ASSEMBLY, THERMODYNAMIC STUDIES AND BIOMEDICAL APPLICATIONS

Xi-Jun Chen

A DISSERTATION

in

Chemistry

Presented to the Faculties of the University of Pennsylvania

in

Partial Fulfillment of the Requirements for the

Degree of Doctor of Philosophy

2013

Supervisor of Dissertation

_____

So-Jung Park
Associate Professor of Chemistry

Graduate Group Chairperson

_____

Gary A. Molander
Professor of Chemistry

Dissertation Committee
Ivan J. Dmochowski, *Associate Professor of Chemistry*
Christopher B. Murray, *Professor of Chemistry and Materials Science and Engineering*
Daniel A. Hammer, *Professor of Chemical Engineering and Biological Engineering*

MULTIFUNCTIONAL NANOMATERIALS OF DNA BLOCK COPOLYMERS: SYNTHESIS, SELF-ASSEMBLY, THERMODYNAMIC STUDIES AND BIOMEDICAL APPLICATIONS

To my grandmothers, my father and my mother for valuing and for ingraining in me the importance of education and hard work.

To all the dissatisfied and persistent graduate students spending nights and weekends in the lab searching and researching:
"It is better to be a human being dissatisfied than a pig satisfied; better to be Socrates dissatisfied than a fool satisfied." – John Stuart Mill (1906)[1]

[1] Mill, John Stuart (1906). *Utilitarianism*. Chicago, IL: University of Chicago Press

ACKNOWLEDGMENT

Many thanks to:

My graduate advisor, Dr. So-Jung Park, for all her support and guidance during my graduate studies.

My undergraduate advisor, Dr. Donald Hirsh for nurturing my interest in research during my undergraduate studies and for encouraging me to pursue a graduate degree.

Dr. Michael Fryd, for his invaluable advice on polymer synthesis and for his wisdom in life matters.

My committee members, Dr. Ivan Dmchowski, Dr. Christopher Murray, Dr. Daniel Hammer and Dr. Yoko Yamakoshi for insightful comments and suggestions.

Xin Jing Tang for teaching and helping me with solid-state DNA synthesis.

Chih-Jung Hsu for teaching me cell culturing techniques and for going above and beyond in helping me push my antisensing project forward.

Former and current Park lab members: Dr. Timothy Duncan, Dr. Yongri Jung, Dr. Sang-Jae Park, Dr. Brenda Sanchez, Dr. Amanda Kamps, Dr. Robert Hickey, Helen Cativo, Zhaoxia Qian, Qingjie Luo, Benjamin Young, Ngoc Tran and Tianna Whiting for providing a fun and stimulating working environment.

My family for always being there for me. My parents for having the courage to give up everything they have and moved to a new country for our education. My father for teaching me to always question and be inquisitive. My mother for her unconditional love and patience. My older sister for being my confidant and someone I can look up to. My younger siblings for looking up to me.

ABSTRACT

MULTIFUNCTIONAL NANOMATERIALS OF DNA BLOCK COPOLYMERS: SYNTHESIS, SELF-ASSEMBLY, THERMODYNAMIC STUDIES AND BIOMEDICAL APPLICATIONS

Xi-Jun Chen

So-Jung Park

Oligonucleotide-conjugated bio-hybrid nanomaterials with a dense DNA layer on the surface have been shown to possess extraordinary selectivity and sensitivity for DNA detection as well as promising results as delivery agents, as demonstrated with the exceptional example of polyvalent oligonucleotide-conjugated gold nanoparticles. However, progress in this field has been slowed, since achieving high DNA density functionalization on the nanoparticle surface for materials other than gold is a major challenge. In this body of work, we have developed a general system to conjugate a dense layer of DNA on the surface of nanoparticles by the self-assembly of DNA block copolymer. These hybrid nanostructures demonstrated enhanced DNA binding, where the DNA strands on the surface of the nanoparticles can recognize and bind to complementary DNA strands without the addition of salt, a condition where free DNA strands do not form duplex. These assemblies are also selective in DNA recognition; they can distinguish different number base mismatches of the complementary DNA. It was determined that these assemblies possess a surface DNA density that is four times higher than that of DNA-conjugated gold nanoparticles of the same size, the highest DNA functionalization reported in the literature in this size range. These assemblies were also

effectively taken up by cells without the use of a co-transfecting agent. The high DNA density also protects the degradation of the DNA, making them ideal candidates for DNA delivery and antisensing applications. Lastly, these assemblies have been tested for their antisensing capability, and found that they can effectively down regulate a targeted protein.

CONTENTS

LIST OF TABLES

LIST OF FIGURES

Chapter 5

LIST OF SCHEMES

LIST OF EQUATIONS

LIST OF ABBREVIATIONS
(*Alphabetical Order*)

AuNP: gold nanoparticles

cDNA: complementary DNA

CPG: controlled pore glass

CuAAC: copper-catalyzed azide-alkyne cycloaddition

DLS: dynamic light scattering

DMEM: Dulbecco's modified Eagle medium

DMF: dimethylformamide

DNA: deoxyribonucleic acid

dsDNA: double stranded DNA

EDC: carbodiimide

EDTA: ethylenediaminetetraacetic acid

E_{FRET}: FRET efficiency

EGFP: enhanced green fluorescent protein

EMT: epithelial–mesenchymal transition

FAM: fluorescein

FBS: fetal bovine serum

FRET: Förster/fluorescent resonance energy transfer

GFP: green fluorescent protein

GPC: gel permeation chromatography

HeLa: Henrietta Lacks cells

HUVEC: human umbilical vein endothelial cells

ICP-MS: inductively-coupled plasma mass spectrometry

IMR32: human Caucasian neuroblastoma cells

LNA: locked nucleic acid

MNP: magnetic nanoparticles

mRNA: messenger RNA

NHS: N-Hydroxysuccinimide

NIR: near infrared (wavelength = ~ 700 – 1400 nm)

NMR: nuclear magnetic resonance

Opti-MEM®: medium use during cationic lipid transfections

PBO: polybutylene oxide
PBS: phosphate buffer saline
PC: photocleavable
PCL: polycaprolactone
PCR: polymerase chain reaction
PEO/PEG: polyethylene oxide (polyethylene glycol)
PL: photoluminescent
PLGA: poly(lactic-co-glycolic acid)
PMA: polymethylacrylate
PNA: peptide nucleic acid
PPO: polypropylene oxide
PS: polystyrene
PTA: phosphotungstic acid
RISC: RNA-induced silencing complex
RNA: ribonucleic acid
RNAi: RNA interference
RT-PCR: real time PCR
SERS: surface enhanced Raman spectroscopy
siRNA: small interfering RNA
SPR: surface plasmon resonance
SPRS: surface plasmon resonance spectroscopy
ssDNA: single-stranded DNA
TAT: trans-activating transcriptional activator
TBTA: tris-(benzyltriazolylmethyl)amine
TEM: transmission electron microscopy
THF: tetrahydrofuran
THPTA: tris(3-hydroxypropyltriazolylmethyl)amine
Tm: melting temperature
tRNA: transfer RNA

Chapter 1. Introduction

1.1 Dissertation Overview

Bio-inorganic hybrid nanomaterials have long been an actively pursued topic in the field of nano-biotechnology and nano-medicine, mainly owing to their interesting properties and versatile applications in the fields of biology and medicine. The interest of this Ph.D. dissertation lies in the synthesis and medical applications of bio-conjugated inorganic hybrid nanostructures. More specifically, the goals of this body of work involve: i) the fabrication and analysis of novel DNA-inorganic nanoparticulates composed of DNA diblock copolymer assemblies and functional nanoparticles (see **Chapters 2 and 3**), and ii) the application of these hybrid nanostructures in the delivery of conventional and genetic drugs (such as polynucleotides, in this case DNA) (see **Chapters 4 and 5**).

A comprehensive overview on the basic principles and background on the subject is provided here in **Chapter 1**, and an outlook on the future directions of this research project is discussed in **Chapter 6**.

1.2 Deoxyribonucleic Acid (DNA)

1.2.1 Structure

The blueprint of all living organisms, from bacteria to plants and animals, is encrypted in the biopolymer deoxyribonucleic acid (DNA). In eukaryotes (cells with a nucleus), this biopolymer resides in the nucleus and the mitochondria. The backbone of this biopolymer is composed of alternating negatively charged phosphate groups attached to the 3' and 5' carbon of 2-deoxyribose sugar rings (**Figure 1-1**). The encryption for all life forms encoded in DNA is made up of random mixing of four nitrogenous bases attached to the 1' carbon on the five-carbon pentose ring. The four nitrogenous bases belong to two groups, adenine (A) and guanine (G) belonging to the purine group and cytosine (C) and thymine (T) belonging to the pyrimidine group.

James D. Watson and Francis Crick correctly postulated in 1953 that the structure of naturally occurring DNA is composed of two helical chains.[1] The DNA double helix structure is held together by hydrogen bonding and base stacking from the nitrogenous bases, with A paired with T and C paired with G. Double helix DNA can exist in mainly three different conformations, A, B and Z-conformation. Under physiological conditions, DNA exists as the B-form. The diameter of duplex DNA is about 2.0 nm, with each helical turn containing about 10.4 base pairs measuring 3.4 nm per turns, thus each base pair is roughly 3.4 Å.[2]

1.2.2 The Central Dogma of Molecular Biology

DNA contains the genetic codes for amino acids that made up proteins that are necessary to sustain normal functions of cells and thus life. In the human genome, there are roughly three billion nucleotides. In the extended form the entire genome measures to about 2 -3 meters in length, which is super condensed in the nucleus which is roughly $1x10^{-16}$ m^3 in volume. Segments of the DNA that code for a specific protein are called genes. In the human genome as much as 98% of the DNA are non coding.[3] There are only roughly 24,5000 genes in a human genome that are translated into proteins, with 3000 possible "pseudo genes" that do not code for any protein.[4]

DNA does not directly get translated into proteins. Protein production is first initiated by the transcription of DNA to messenger ribonucleic acid (mRNA), follow by the translation of the mRNA to protein through a process known as the central dogma of molecular biology. RNA is another type of nucleic acid, and there are two main differences between RNA and DNA (**Figure 1-1**). One is the pentose sugar rings, where RNA has a hydroxyl substituent at the 2'-carbon instead of hydrogen. The consequence of this makes DNA more stable than RNA since it is less reactive. The other difference between RNA and DNA is RNA uses a nitrogenous base called uracil (U) instead of thymine in DNA.

The protein production process (**Figure 1-2**) begins with the unzipping of the double helix DNA strands from its super-condensed form, and the enzyme RNA polymerase docks on to the coding strand and begin the transcript process and produces mRNA. After a plethora of post-transcription modifications of the transcripted mRNA, the matured mRNA leaves the nucleus to the cytoplasm to be translated into proteins. The

mRNA in the cytoplasm is being read by transfer RNA (tRNA) via a trinucleotide genetic code, where three nucleotides codes for a specific amino acid. The chain of amino acid resulting from the translation process called polypeptides will become part of a protein.

1.2.3 Mutations and Genetic Diseases

A mutation is defined as an inherited change in genetic information; the descendants may be cells produced by cell division or individual organisms produced by reproduction.[2] Mutations in genes can be beneficial as it provides genetic variations and thus is a fundamental aspect of evolution. Without mutations and the variation they generate, organisms could not adapt to a changing environment and risk extinction. However, in some cases the results can be detrimental to the health of the organism. Many of the diseases (skin, heart, cancer) found in human are the unfortunate result of mutations in the genome and in the case of single nucleotide polymorphism (the change of one base).[5, 6]

There are naturally occurring mutations and induced mutations. The former happens due to mistakes that happen duirng DNA replication. DNA is a highly stable molecule that replicates with an amazing accuracy, nevertheless, changes in DNA structure and errors of replication do occur. The process of DNA replication is fairly a complex mechanism that involves a lot of check points in order to prevent DNA material damage as well as unwanted alterations on its structures and base pairs, ultimately leading to mutations. Other ways that can lead to naturally occurring mutation can be due to the loss of a purine base or amine groups in the bases.[2] In the case of induced mutations, viruses, chemical means or radiation modifies the bases on the DNA.

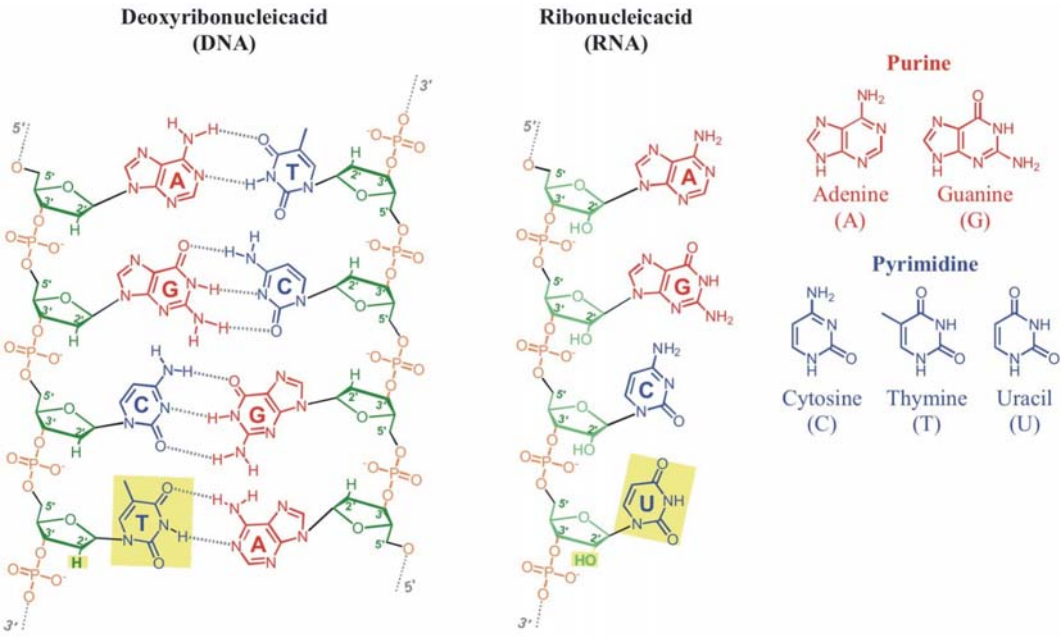

Figure 1-1. Chemical structures of DNA and RNA and different purine and pyrimidine nitrogenous bases.

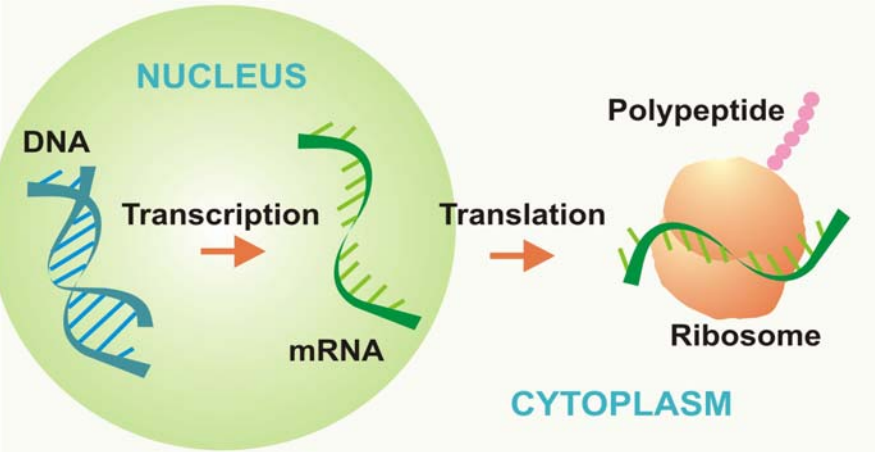

Figure 1-2. Transcription and translation

1.3 Conventional DNA Detection Methods

The important function of DNA causes detrimental consequence when this blueprint for life is mutated or damaged. It is critical to be able to identify and pinpoint the segment of the DNA where this mutation occurred, thus highly sensitive and selective DNA detection is essential. Ideal DNA/RNA biosensors should possess high selectivity (i.e. the ability to distinguish single nucleotide polymorphism) and sensitivity (i.e. low detection limit), as well as simplicity in terms of sample preparation and method of operation. The follow sections will discuss the various methods conventionally used for DNA detection that do not involve nanoparticles and their advantages and limitations.

1.3.1 Radioactive Decay Method

Early DNA detection methods were heavily radioactive based using the decay of ^{32}P (half life: 14.3 days) isotope of phosphorus to expose x-ray film. The limitations of this method are exposure time can take up to 24 hours or more, and it has to be performed at -70°C. A modified method called Southern Blotting invented by Edwin Southern in 1975 which combines agarose gel electrophoresis for size separation of DNA with methods to transfer the size-separated DNA to a filter membrane for radioactive probe hybridization.[7] In this method, target DNA is bound to radioactive probes, and then this band will be exposed on x-ray film. The limitation of this method is that it requires a large amount of DNA. The major disadvantage of radioactive methods in general is the need to work with radioactive materials.

1.3.2 Polymerase Chain Reaction (PCR)

Invented by Kary Mullis in 1983 and was subsequently awarded the Nobel Prize for Chemistry in 1993 for the invention of this method. It revolutionized DNA/RNA detection, specifically targets and amplifies a single sequence.[8] This method mimics DNA replication in cells, need a DNA template, primers, polymerase and nucleotides. This method involves several steps: 1. denaturation (95°C) of DNA duplex, 2. anneal (55°C), 3. synthesis (72°C), 4. repeat cycle 20-40x. It has the ability to detect RNA via reverse-transcription PCR by forming complementary DNA (cDNA) via reverse transcription step prior to PCR of cDNA. It can amplify target DNA strand exponentially, and the products of PCR can be analyzed/purified by gel electrophoresis. The main disadvantage of this method includes the lack of 3′→5′proof-reading activity of Taq DNA polymerase used in PCR that is commonly present in other polymerases. Where Taq mis-incorporates 1 base in 104, therefore, in a 400 base pair (bp) target will contain an error in 33% of molecules after 20 cycles. In addition, the error distribution will be random.

1.3.3 Real-Time Polymerase Chain Reaction (RT-PCR)

A modified and more modern version of the PCR method is real-time PCR (RT-PCR), which utilizes the incorporation of fluorescent dyes in the replication process.[9] RT-PCR allows for detection of PCR amplification during the early phases of the reaction by monitoring the fluorescence emitted during each PCR cycle in real time as opposed to endpoint detection. There are basically two general methods used in RT-PCR, dye

incorporation and probes which include techniques such as Molecular Beacon®, Taqman® and Scopion®.

1.3.3.1 Dye Incorporation Method: SYBR® Green I

In the denaturation step, unbound SYBR® Green I dye exhibits little fluorescence, as shown in the annealing step, the SYBR® dye binds to minor groove of double stranded (dsDNA), and fluorescent intensity increases upon binding. Then in the polymerization step, more and more dye molecules bind to the newly synthesized DNA, and the increase in fluorescence can be monitored in real-time. In the next cycle, the denaturation step where the dye molecules are released and the fluorescence signal returns to background. This method has the advantage of being relatively cheap and does not require probe design; however, this method suffers from non-specificity in the dye incorporation that can lead to false positives.

1.3.3.2 Molecular Beacons

The core principle of this method is that the probe is designed to be complementary to a sequence in the middle of the expected amplicon. In the denaturation step, the molecular beacons assume a random coil configuration and fluoresce. In the annealing step, the stem hybrids form rapidly thus preventing fluorescence. However, in the presence of target, the molecular beacons also bind to the amplicons and generate fluorescence. In the polymerization step, molecular beacons dissociate from their targets, and fluorescence is again quenched. A new hybridization takes place in annealing step of every cycle, and intensity of the resulting fluorescence indicates the amount of

accumulated amplicon at the end of the previous cycle. The advantages of this method include great specificity, reversible fluorescence that ultimately translates to lower background noises. The main limitation is some non-specific interactions between hairpins can lead to false positives.

1.3.3.3 TaqMan®

In the denaturation step, sequence-specific probe connects fluorophore and quencher. The proximity of the two dyes quenches the signal from the fluorescent dye at the 5'- end of probe. In the annealing step, the probe binds to amplicon. Then in the polymerization step, the probe displaced and hydrolyzed by Taq polymerase. The fluorescent dye is released from its proximity to the quencher, and fluorescence is detected. The signal for this method is directly proportional to the number of molecules present. This method has the advantage of specificity, and different colors can be used in multiplex assays. However, this method has the limitation of possessing some background noise due to irreversibility of the reaction.

1.3.3.4 Scorpion®

This method combines fluorescent probe and primer, where the probe is quenched by quencher. PCR blocker prevents unwanted polymerization. The advantages of this method include high specificity and faster cycling. The disadvantage of this method is the design of the probe/primer is complex and expensive.

1.3.3.5 General Disadvantages of RT-PCR

RT-PCR also suffers from the limitation of PCR which includes lacks the 3′→5′proof-reading activity Taq DNA polymerase as mentioned for PCR In addition, the disadvantages mentioned for each RT-PCR method discussed in the above sections can be generalized as followed: the disadvantage for dye incorporation is non-specificity and for probe RT-PCR is that the probes are difficult to design and can be expensive., there are a couple general limitations that RT-PCR suffers from.

1.3.4 DNA Microarray

DNA microarray, also known as DNA chip, biochips, gene chips, gene array, genome chips or genome arrays, it is an array of DNA sequences on solid support (chip), where each chip contains thousands of genes (probes). In standard microarrays, the probes are synthesized and then attached to a solid surface by a covalent bond to a chemical matrix (e.g. epoxy-silane, amino-silane, lysine, polyacrylamide or others). The solid surface can be glass or a silicon chip. DNA arrays are different from other types of microarray only in that they either measure DNA or use DNA as part of its detection system. The advantages of the DNA microarray detection method include its cost effectiveness and high throughput. Disadvantages include incomplete coverage which can lead to false positives and also the lack of sensitivity compared to PCR

1.3.5 Portable DNA/RNA Detection Technologies

There are several commercially available DNA/RNA detection technologies that provides quick and on the spot analysis without the need of analysis in a laboratory

setting. One of the more outstanding performing ones include the LightCycler® 2.0 by Roche that uses dye incorporation and hybridization probe methods.[10] The other is Idaho Tech Ruggedized Advanced Pathogen Identification Device (R.A.P.I.D.), a portable real-time PCR system designed to identify biological agents, used in military field hospitals, first responders and other rough environments.[11]

1.4 Gene Therapy

One of the long-term goals of this dissertation research project is to develop a non-viral delivery system using DNA block copolymer self-assembled nanostructures, for the efficient and effective transportation and release of therapeutic nucleic acids such as DNA and siRNA. Effective gene delivery techniques can provide a new route to combat genetic diseases when conventional medical treatments fall short. Ideal gene delivery carriers should possess great stability in terms of the structural integrity and the integrity of the payload, high processability, low toxicity and biocompatibility, efficient uptake by cells, capability to bypass or escape endocytosis pathways and efficient release of the DNA payload for intended purposes.

In this section, a basic principle of gene therapy is presented. An overview in delivery methods and the types of therapeutic nucleic acids is discussed to provide better understanding on how the process can be better regulated with therapeutic nucleic acids when the organism's internal regulation mechanism fails.

1.4.1 Brief Background

The definition of gene therapy is to transfer (or transfection) of genetic information to specific cells to direct the synthesis of a specific protein, with the agenda to cure diseases caused by the mutation or to prevent diseases caused by pathogens (producing antigens).[12] The goal of gene therapy is to fix diseases that are caused by genetic mutations at the root of the problem, thus, either delivering the correct gene or stopping the incorrect gene from being translated into proteins. In gene therapy, the genetic materials being delivered into the targeted cells can be long DNA sequences that contain genes up to thousands of base pairs, or short oligonucleotides around 25 base pairs. The delivery of short oligo-DNA has the benefit of stopping the expression of proteins post transcription, at the mRNA stage. The mechanism of mRNA degradation, unlike the RISC complex in the case of siRNA, is through the enzymatic degradation by RNAseH.

1.4.2 Therapeutic Nucleic Acid Agents

Depending on the goal of the therapy, different types of nucleic acid has been considered for therapeutic purposes in gene therapy. These different types of therapeutic nucleic acids can range from polynueclic acids thousands of base pairs in length to as few as 25 basepairs. The structure of the nucleic acid can also be modified, that is the phosphate backbone and ribose ring can be replaced into to avoid issues such as charger repulusion and ezymne degradation in the original DNA and RNA structure. These artifical nucleic acids are often used to prolong the circulation of the therapeutic nucleic

acids since naturally occuring nucleic acid degrading ezynmes can not degrade the modified backbones.

1.4.2.1 Long Nucleic Acid: Plasmids, Genes

Long nucleic acids such as plasmids and genes have been used to replace mutated genes. Generally viral carriers and cationic lipids are used to carry these long nucleic acids into the cell. These carriers usually have nuclear targeting moieties since the nucleus is the final destination of the therapeutic nucleic acids, where they integrate into the host genome. Some successful examples have been reported [ref].

1.4.2.2 Short Nucleic Acid: siRNA, Antisensing Oligonucleotides

The discovery of short interference RNA (siRNA) in post transcriptional gene silencing by David Baulcombe's group at the Sainsbury Laboratory in Norwich, England in plants[13] and in mammals by Thomas Tuschl and colleagues[14], where both showed short double strands of antisense RNA can be used to down regulation the expression of a targeted protein created an immensely booming field of siRNA delivery for biomedical applications. Since then, it has been discovered that short strands of antisense DNA can also be used which regulations the translation of mRNA via RNaseH mechanism. (**Chapter 5**).

1.4.2.3 Short Modified Nucleic Acid: Peptide Nucleic Acid (PNA), Phosphotioate DNA, Morpholinio DNA, Lock DNA

Different DNA derivatives have been developed for delivery applications that would overcome the degradation challenges of regular DNA. The structure of these derivative nucleic acids can deviate from the original structure by replacing one substituent on either the pentose or phosphate groups, to the case of peptide nucleic acid (PNA) and morpholino DNA replacing the entire phosphate-pentose backbone that regular DNA possesses.

1.4.3 Endocytotic Mechanism

There are generally four steps involved in the delivery of short oligo-DNA and they are 1) adsorption on the cell membrane, 2) uptake by endocytosis, 3) escape from endosomes and 4) intracellular release. For the delivery of longer DNA such as the case of a gene, there are two additional steps such as 5) nuclear targeting and 6) nuclear entry and gene expression.[15] In both cases, the efficiency of the tranfection dependent on both the efficiency of DNA delivery, that is the fraction of DNA molecules getting into nucleus) and efficiency of DNA expression, that is the fraction of nuclear DNA molecules that undergo transcription.

1.4.4 Major Challenges

There are several major challenges in gene therapy for the delivery of DNA: 1) by-passing the lipid bilayer plasma membrane, 2) degradation of DNA payload by DNA

degrading enzymes (DNAse) inside and outside of the cell, 3) release of DNA payload from endosmes once inside the cell, and 4) functional DNA payload after release. For delivery of a gene, there are additional challenges where 5) nuclear targeting and 6) integrate DNA into genome and express normally.

1.4.5 Gene Delivery Methods

The following subsections present the various methods used for the delivery of genetic materials into cells. Some of these methods utilize mechanical or electrical energy to by-pass the plasma membrane without the need for cellular uptake through endocytosis, such as in the case of microinjection, electroporation and gene gun. While other methods involve cellular uptake in order to cross the plasma membrane such as the use of viruses, recombinant proteins and liposomes.

1.4.5.1 Microinjection

The basic principle of this technique involves the direct injection of naked plasmid DNA into a cell. This method has the advantage of being highly efficient; however, this method can only inject one cell at a time, thus not applicable for research with a large number of cells or in vivo DNA delivery.

1.4.5.2 Electroporation

This method does not require endocytosis by the use of low voltage electric pulses to transiently cause proration in cell membrane, through which DNA can pass and directly enter into the cytoplasm. When the pores close again, DNA is trapped inside the

cell. The advantages of this method is that it is easy to perform and efficient. However, the eclectic pulses can cause high cell mortality due to electrocution. The condition used needs to be optimization for every cell line, and a high concentration of DNA is required. In addition, the efficiency varies greatly with cell type.

1.4.5.3 Gene Gun

The use of gene guns to delivery DNA has been commonly used to genetically modified plants. This "biolistic" particle delivery method relies on the shooting of DNA-functionalized gold (or tungsten) nanoparticles that are accelerated at high velocity into target tissues or cells. The advantages of the gene gun method allows DNA to penetrate directly through cell membranes into cytoplasm or even nucleus, thus bypassing endosomes and avoiding enzymatic degradation of the payload DNA. However, this method is limited by the shallow penetration into the tissue. The depth of penetration using gene gun into skeletal muscle of mouse did not exceed 0.5 mm, and the transfection efficiency is only 10-20% in skin epidermal cells and 1-5% in muscle cells. Furthermore, in vivo gene-gun application only result in short-term and low level gene expression.

1.4.5.4 Viruses

The basic principle of this method utilizes genetically engineered, tissue-specific virus carrying a payload of DNA to deliver to host cells. This method was first demonstrated on Salmonella in 1952. The use of viral carriers is the oldest method and most efficient for gene transfer due to the evolutionary, and the ability to integrate its own genetic information into the host cell's genome. The main advantage of viral carriers

is their innate abilities in crossing the plasma membrane and integrating the genetic material they carry into the genome of the host cells. However, host cells have also evolved to defend against these advantages of viruses, such as serious risk of immunogenicity, inflammation, and carcinogenicity.

1.4.5.5 Recombinant Proteins

Recombinant proteins are proteins produced from recombinant DNA, which are synthetic DNA composed of DNA segments from different sources recombinded together by recombinant technology. Trans-activating transcriptional activator (TAT) proteins are a special type of DNA carrier which contain a nuclear localization sequence; they are capable of penetrating a cell membrane and especially overcome nuclear-membrane barrier to deliver genetic material. Such proteins may include polylysine segments, protamine, or histones to bind DNA and to form stable complexes which help protect DNA and to form stable complexes, to help protect DNA from intracellular degradation. The advantage of this method is that the material used is highly biocompatible, however, the downside is the material can be expensive.

1.4.5.6 Cationic Lipids and Polymers

The use of cationic species for the delivery of DNA is one of the most common non-viral methods used in cell biology. This method involves the use of electrostatic attraction between negatively charged nucleic acid and cationic carriers, such as cationic polyelectrolytes (e.g. polylysine), block-copolymer with cationic block or liposomes/micelles from cationic surfactants. The complexes of the cationic carriers and

DNA are then uptake by the cell. The advantage of this method is the easy preparation, and wide availability of commercial cationic lipids. However, this method has limited efficiency. In addition, the major downside with this method is the cytotoxicity of the cationic polymers and lipids, due to the electrostatic interaction between the cationic species and the negatively charged plasma membrane. The cationic species can integrate and disturb the packing of the phospholipids of the plasma membrane and can even disrupt the bi-layer plasma membrane.

1.4.6 Bio-hybrid Nanoparticle Carriers

To overcome the limitations of conventional gene delivery methods, tremendous interest has been aimed at the development of non-viral bio-hybrid inorganic nanoparticle carriers. The premises for the interest are based on the fact that cells take up nanoparticles, and that the chemistry of inorganic nanoparticles is highly advanced. Inorganic nanoparticles such as nobel metal nanoparticles such as gold, silver and platinum, and non-metallic nanoparticles such as iron oxides (FexOy), carbon nanotube, double hydroxides/clays, silica, calcium phosphate and quantum dots. The advantages of these classes of materials involve the ease of preparation and functionalization and ability for size control. Furthermore, nanoparticles have intrinsic properties, such as optical, magnetic and fluorescent.

1.4.7 Viral Carriers versus Non-viral Carriers

Conventionally, gene therapy is mainly done with viral carriers by hijacking the genetic material inside viruses and replaces them with the therapeutic genetic material.

Since viruses have evolved with the capability of bypassing the plasma membrane of its host. However, there are several disadvantages that are inherent in viral carriers, such as the possibility of inducing immunogenicity and carcinogenicity from the host organism's innate immune response to viruses developed through evolution. For those reasons, efforts have been invested to develop safer non-viral carriers. With thoughtful design and engineering, non-viral carriers not only can overcome the safety issues that viral carriers have, moreover, they can also have the advantages of being easy to process and manufacture, better and easier quality control and thus commercially more appealing.

1.5 DNA-conjugated Nanomaterials for DNA Detection and Delivery[2]

Liposomes are the most widely used non-viral gene delivery agents. These liposomes are commonly made up of positively charged phospholipids that are commercially available such as Lipofectamine. One drawback with these cationic carriers is cytotoxicity at high concentrations, speculated to be due to the integration of the cationic lipids into the cell membrane bilayer, thus disrupting the integrity of the cell membrane. For that reason, other classes of material are being actively explored as alternative to the cationic species. One class of nanomaterial that showed tremendous promise is gold metal nanoparticles conjugated with synthetic alkyl-thiol oligonucleotide developed by Chad Mirkin's group from Northwestern University.

---

[2] Reprinted with permission from Chen, X.-J.; Sanchez-Gaytan, B. L.; Qian, Z.; Park, S.-J.: *Noble metal nanoparticles in DNA detection and delivery*. Wiley Interdisciplinary Reviews: Nanomedicine and Nanobiotechnology. **2012**;4(3):273-290..Copyright 2012 Wiley-VCH Verlag GmbH & Co. KGaA

DNA-conjugated metal nanoparticles have attracted enormous attention for biological and medical applications, owing to their unusual DNA melting characteristics as well as unique optical and catalytic properties. The combination of these unique properties has not only led to the development of DNA detection technologies with remarkably high selectivity and sensitivity, but also to the development of gene therapeutic agents with high efficacy and efficiency. In this section, a brief history that led up to the development of DNA-conjugated nanoparticles is presented, followed by a more in-depth discussion from the synthesis to the applications of these DNA-conjugated nanoparticles.

1.5.1 Brief History

The field of nanomaterials and nanotechnology has been gaining tremendous momentum since the early 1990's. Nanometer-sized noble metal particles exhibit fascinating optical, catalytic, and magnetic properties that are distinct from their bulk counterparts.[16-20] The unique size- and shape-dependent properties of metal nanoparticles have impacted many different areas of modern science and technology, especially in the biological and medical fields.[21-24] Gold and silver nanoparticles decorated with proteins have long been used in immunocytochemistry for the past few decades as electron microscopy markers.[25, 26] However, it was not until the mid 1990s that researchers began actively exploring the unique nanometer scale phenomena of metal particles for various biological and medical applications. Research in this area was greatly facilitated in the last decade by the remarkable advances made in the synthesis and characterization of

nanomaterials. These research efforts resulted in a number of highly sensitive and selective biological detection technologies, particularly for nucleic acid targets.

The size range of nanomaterials falls in the range of proteins and DNA. Bio-conjugated nanoparticles have received tremendous interest in the past decade due to their potential in a wide range of biomedical applications. Of the different types of bio/inorganic hybrid nanomaterials, DNA-conjugated nanoparticles and their biological and medical applications has been one of the more extensively studied examples. Which gave rise to outstanding performance in numerous applications such as biosensing[27], medical imaging[28], drug delivery[29] and gene regulation[30].

1.5.2 Metal Nanoparticles: Synthesis and Properties

Many of the interesting properties of metal nanoparticles, which gave rise to their vast applications in biology and medicine, are highly dependent on the size and shape of the nanoparticles as well as their compositions. For example, gold and silver nanoparticles are brilliantly colored due to their strong surface plasmon resonance (SPR) absorption.[17, 31] As presented in **Figure 1-3**, the position and intensity of the SPR bands can drastically change by varying the shape of the nanoparticles (**Figure 1-3**). In general, solid isotropic metal nanoparticles show SPR bands in the visible region, whereas the SPR band of anisotropic and hollow particles can be tuned to the near infrared (NIR) region.[17, 31] Note that anisotropic particles with SPR bands in the NIR region are of great interest for in vivo applications because NIR light has greater penetration depths in tissues. Thus, synthetic methods for size- and shape-controlled nanoparticles have been actively sought after in the past two decades.[32-36] **Table 1-1** summarizes standard

synthetic methods, common sizes, and unique physical properties of several representative metal nanoparticles of different shapes. For more information about the synthesis and properties of metal nanoparticles, readers are encouraged to read review articles focused on these topics.[33, 37-40]

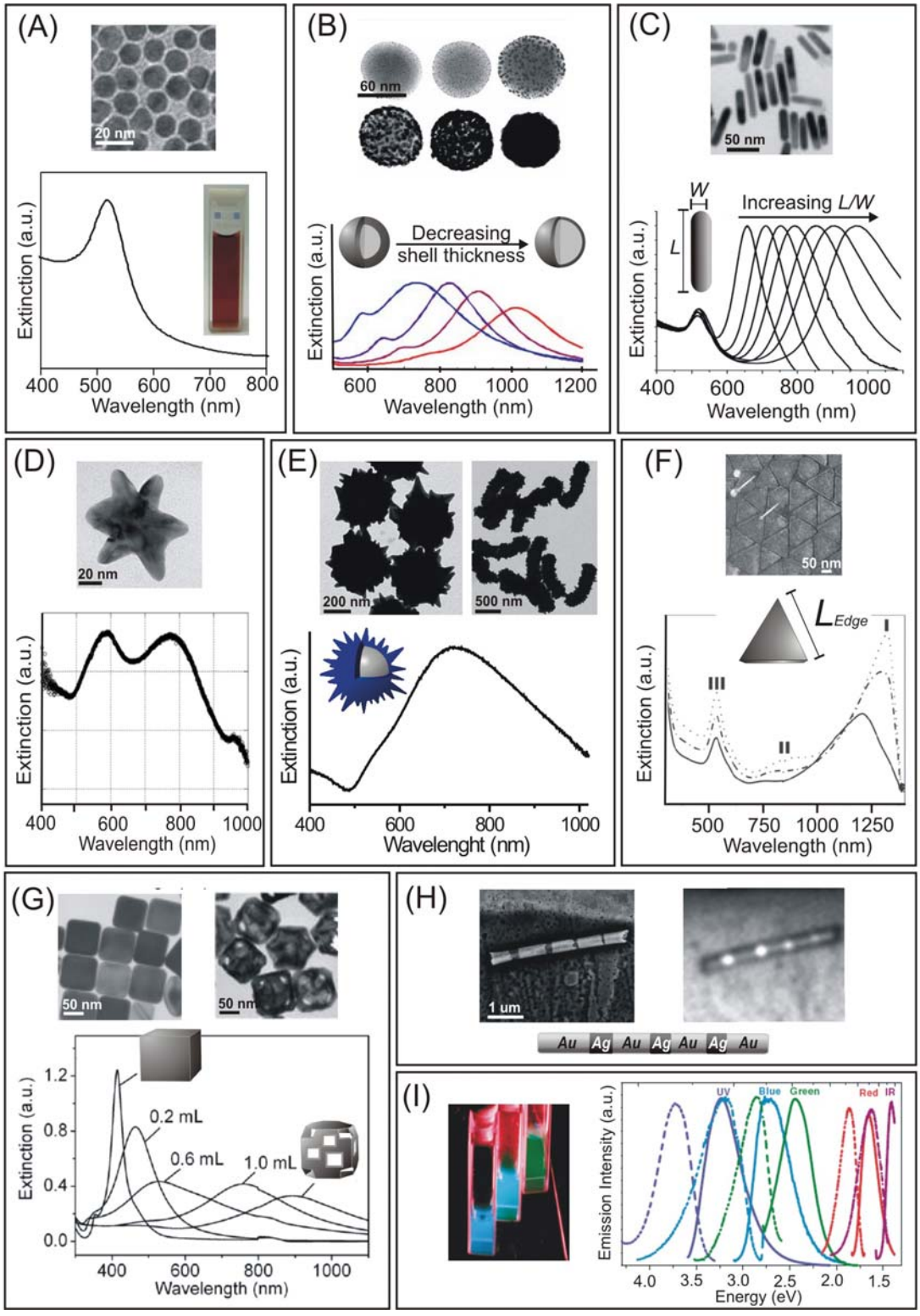
(A)
20 nm
Extinction (a.u.)
400 500 600 700 800
Wavelength (nm)
(B)
60 nm
Decreasing
shell thickness
Extinction (a.u.)
600 800 1000 1200
Wavelength (nm)
(C)
50 nm
W
L
Increasing L/W
Extinction (a.u.)
400 600 800 1000
Wavelength (nm)
(D)
20 nm
Extinction (a.u.)
400 600 800 1000
Wavelength (nm)
(E)
200 nm
500 nm
Extinction (a.u.)
400 600 800 1000
Wavelenght (nm)
(F)
50 nm
L Edge
I
II
III
Extinction (a.u.)
500 750 1000 1250
Wavelength (nm)
(G)
50 nm
50 nm
0.2 mL
0.6 mL
1.0 mL
Extinction (a.u.)
1.2
0.8
0.4
0.0
400 600 800 1000
Wavelength (nm)
(H)
1 um
Au Ag Au Ag Au Ag Au
(I)
UV
Blue
Green
Red
IR
Emission Intensity (a.u.)
4.0 3.5 3.0 2.5 2.0 1.5
Energy (eV)

Figure 1-3. (A) A transmission electron microscope (TEM) image, an extinction spectrum, and a picture of 13 nm gold nanosphere solution. (B) TEM images of silica particles coated with different amounts of gold for the formation of a gold nanoshell. Extinction spectra of nanoshells with different core to shell ratios show that the SPR band of nanoshells red-shifts with decreasing shell thicknesses. (C) A TEM image and extinction spectra of gold nanorods. Extinction spectra of nanorods with different aspect ratios show that the longitudinal SPR band of nanorods red-shifts with increasing aspect ratios. (D) A TEM image and an extinction spectrum of gold nanostars. (E) TEM images of spiky gold nanoshells with spherical and rod cores and an extinction spectrum of spiky gold nanoshells made with spherical cores. (F) A TEM image of gold nanoprisms and extinction spectra of nanoprisms with different edge lengths. (G) TEM images and extinction spectra of silver nanocubes and gold nanocages. (H) Scanning electron microscope (left) and optical microscope (right) images of a multicomponent nanowire. (I) Three different sized small gold clusters with UV (Au5), blue (Au8) and green (Au13) emission under UV irradiation and their corresponding excitation (dotted) and emission (solid) spectra. (B: reprinted with permission from ref [41] with kind permission from from Springer Science + Business Media; C: reprinted with permission from ref [42] Copyright Wiley-VCH Verlag GmbH & Co. KGaA; D: reprinted with permission from ref [43]. Copyright 2006 American Chemical Society; F: reprinted with permission from ref [44]. Copyright Wiley-VCH Verlag GmbH & Co. KGaA.; G: reprinted with permission from ref [45]. Copyright Wiley-VCH Verlag GmbH & Co. KGaA.; H: reprinted with permission from ref [46]. Copyright 2004 by the American Physical Society; I: adapted from ref [47], reprinted with permission from AAAS.) Figure reprint with permission from ref [48].Copyright 2012 Wiley-VCH Verlag GmbH & Co. KGaA

Table 1-1. Syntheses and Characteristics of Representative Metal Nanoparticles

Metal	Shape	Size	Synthesis Method	Stabilizing Agent	Distinctive Property	Reference
Au, Ag	Sphere	10 – 150 nm	Turkevich/ Frens	Citrate	Surface Plasmon Band: ~520 – 580 nm (Au) ~ 390 – 430 nm (Ag)	[49-51]
Au	Sphere	1.5 – 15 nm	Brust*/ Modified Brust	Alkanethiols	Surface Plasmon Band: ~520 nm	[52-55]
Au, Ag	Shells	Core: 50 – 500 nm Shell Thickness: 5 – 30 nm	Templated	–	Tunable Surface Plasmon Band: 700 nm – 2.2 μm	[56, 57]
Au	Spiky Shells	Diameter: 60 nm – 1 μm	Templated	CTAB	Surface Plasmon Band: ~800 nm	[58]
Au, Ag	Rod/Wire	Aspect ratio: Au: 1.5 –350 Ag: 3 – 20	Seed growth method	CTAB	Tunable longitudinal SPR band from visible to IR region: 650 nm – > 1μm	[42, 59-61]
Au, Ag, Pt, Pd, Ni, Co, Cu	Wire (barcode)	Length: ~ 4.5 μ m Width: ~400 nm	Electrochemical deposition	–	Different metallic segments provide multiplexing capability	[46]
Au	Triangle Plate	Edge length: ~90 nm to ~220 nm	Modified seed growth method	CTAB	Tunable surface plasmon to near-IR region: ~700 nm – 1 μM	[44, 62]
Ag	Triangle Plate	Edge length: 50 to 200 nm Thickness: ~30nm	Solvent reduction/polyol method	PVP	Surface Plasmon Band: ~600 – ~700 nm	[63, 64]
Ag	Triangle Plate	Edge length: ~100 nm Thickness: ~15.5 nm	Photoinduced	BSPP and citrate	Surface Plasmon Band: ~700 nm	[64]
Au	Star, branched	100 nm	Seed growth method	CTAB	Surface Plasmon Band ~800 nm	[43]
Au	Star, branched	40 nm	Seed growth method	PVP	Surface Plasmon Band ~750 nm	[65]
Au, Ag	Cube	Edge length: Au ~3 nm and ~85 nm; Ag ~20 to 115 nm	Solvent reduction/ polyol method	Au: DDT, HDD Ag: PVP	Tunable surface plasmon to near-IR region ~400 – ~700 nm	[66, 67]
Au	Cage	Edge length: >20 nm	Galvanic replacement of Ag in Ag cubes in $HAuCl_4$	PVP	Tunable surface plasmon to near-IR region: ~400 – ~900 nm	[45]

Au, Ag	Cluster	< 2nm	Dendrimer stabilized/ $NaBH_4$ reduction	Dendrimer	Tunable photoluminescence: ~330 – ~860 nm (Au) 533 nm – 648 nm (Ag)	[68, 69]
Ag	Cluster	< 2nm	DNA templated/ $NaBH_4$ reduction	DNA	Tunable photoluminescence: ~475 to ~725 nm	[70]

CTAB: cetyltrimethylammonium bromide; TDAB: tetradecylammonium bromide; BDAC: benzyldimethylhexadecylammonium chloride; BSPP: bis(p-sulfonatophenyl) phenylphosphine dihydrate dipotassium salt ; PVP: poly(vinylpyrrolidone); DDT: 1-dodecanethiol; HDD: 1,2-hexadecanediol.
* Nanoparticles synthesized using the Brust method are organic phased and can be transferred to aqueous solutions by various methods.

1.5.3 DNA Conjugation Methods

Among many reported DNA conjugation methods,[71-74] the procedure developed by Mirkin and coworkers has been widely used for biomedical applications because of the ease of preparation, high stability, and high DNA density on particle surface **(Figure 1-4A)**.[74] In this procedure, thiol-modified oligonucleotides were first incubated with citrate stabilized gold nanoparticles, followed by the slow addition of salts to screen the charge repulsions in the DNA backbone. This method yields gold nanoparticles densely functionalized with oligonucleotides (approximately ~70 strands/15 nm particles).[75] Due to the high DNA density, these DNA-conjugated gold nanoparticles are stable in salt solutions and are resistant to nonspecific agglomerations, which is an important requirement for their applications in DNA detection and delivery. Moreover, nanoparticles heavily functionalized with thiol-modified oligonucleotides exhibit unusual DNA melting characteristics, such as sharp melting transitions **(Figure 1-4B)** and high binding constants.[76, 77] These properties, which are shown to be associated with closely spaced DNA strands on the nanoparticle surface,[18, 77] are responsible for the high selectivity and sensitivity of DNA detection methods based on DNA-conjugated gold nanoparticles (see below). Note that it is the combination of the high DNA density and the useful optical and catalytic properties of metal particles that make DNA-conjugated metal nanoparticles extremely useful for DNA detection and delivery applications.

1.5.4 Polyvalence Effect

As mentioned above, the unique properties of DNA-conjugated gold nanoparticles lies in their polyvalency, or in other words a dense layer of DNA decorated on the surface of the nanoparticles. This polyvalence effect is ubiquitous in Nature where many biological systems use this for their associations such as in the case of viruses. Cooperative interactions between interacting systems are highly selective (i.e. high recognition ability). Forces behind cooperative interactions are mainly weak non-covalent interactions, hence reversible. The structures of interacting biological systems optimize the amount of weak non-covalent interactions

1.5.5 In Vitro DNA Detection

This section covers representative in vitro DNA detection techniques using metal nanoparticles including some recent new developments and improvements. DNA-conjugated metal nanoparticles have also been utilized in detection of small molecules[78, 79] , ions[80], proteins[78] and cancer cells.[81] However, in order to provide a tighter focus on the topic at hand, we will only review recent advances in DNA detection. These methods are also summarized in **Table 1-2**.

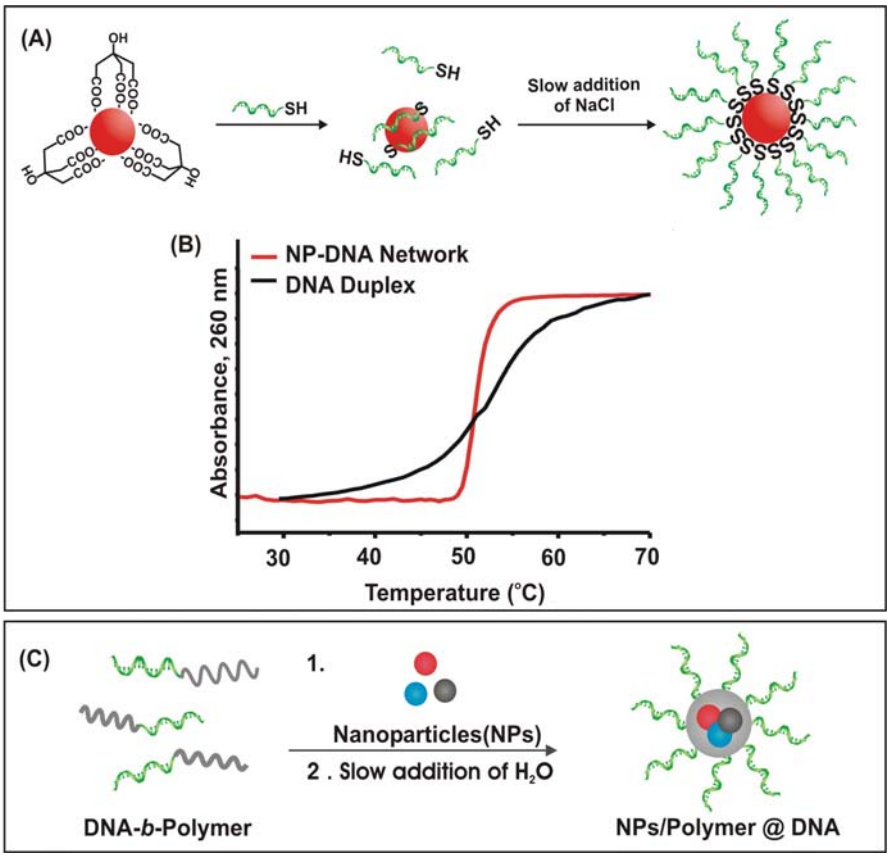

Figure 1-4. Preparation of nanoparticles densely functionalized with DNA. (A) A widely used conjugation method using citrate-stabilized gold nanoparticles and thiol-modified DNA. (B) DNA dissociation curves of DNA-modified nanoparticles and unlabeled DNA, showing that the nanoparticle probes exhibit unusually sharp melting transitions. (C) A DNA functionalization method based on the self-assembly of DNA block-copolymers and nanoparticles. This method can be used to coat different types of nanoparticles with a dense layer of DNA. Figure reprint with permission from ref [48].Copyright 2012 Wiley-VCH Verlag GmbH & Co. KGaA

Table 1-2. DNA Detection Methods Using Gold Nanoparticles

Detection Format	Particle Type	Property	Attribute	Detection Limit	Selectivity	Target Length (base pair)	Reference
Colorimetric	13 nm Au spheres	Distance-dependent SPR	Simple, high selectivity	~ 1 nM	Single base mismatch	24 bp	[74]
Colorimetric	13 nm Au spheres	Salt-induced aggregation	Label-free, fast	4.3 nM*	single base mismatch	24 bp	[82]
Scanometric	13 nm Au spheres	Catalytic	Simple, high selectivity/ sensitivity	200 fM	single base mismatch	119 bp	[83]
Electrical	13 nm Au spheres	Catalytic and conductivity	Portable	500 fM	single base mismatch	27 bp	[18]
Bio-Barcode	13 nm Au spheres	Barcodes	Ultrahigh sensitivity	500 zM	Single base mismatch	27 bp	[84]
SPRS	Gold film/13 nm Au spheres	Surface Plasmon	Suitable for kinetic studies	1.38 fM	single base mismatch	39 bp	[85]
SERS	13 nm Au spheres	Raman	Multiplex Detection	20fM	single base mismatch	30 bp	[86]

* Concentration calculated based on the detection limit given in moles and volume indicated in reference.

1.5.5.1 Colorimetric Method

In 1996, Mirkin and coworkers reported that macroscopic networks of gold nanoparticles can be formed by the hybridization of complementary DNA strands attached on gold particles **(Figure 1-5A)**.[87] This work was a landmark in the development of a new generation of metal nanoparticle-based DNA detection methods, which have been extensively studied since then. The so-called colorimetric method is based on the distance-dependent optical properties of metallic nanoparticles. In the detection method,[88] two sets of gold nanoparticles are functionalized with two different sequences of thiol-modified DNA that are complementary to the target DNA. Thus, in the presence of complementary target DNA, DNA-modified nanoparticles are connected into macroscopic aggregates by duplex formation **(Figure 1-5A)**, which results in the shift of the characteristic surface plasmon band of gold nanoparticles from ~520 nm to ~570 nm, turning the red color of colloidal gold to purple.[88] This color change provides a simple and inexpensive route for DNA detection since it does not require sophisticated equipment. In addition, owing to the unusually sharp melting transitions of DNA-modified gold nanoparticles **(Figure 1-4B)**,[76, 77] the colorimetric method can accurately detect single-base mismatches. In fact, the unique melting characteristics of DNA-conjugated metal nanoparticles have led to the development of a number of detection methods with exceptionally high selectivity (**Table 1-2**).[27] The colorimetric method, however, has a relatively low sensitivity with a detection limit of ~ 1 nM.[50] Recently Liu and coworkers showed that the sensitivity of the colorimetric method can be increased to about 10 pM by employing a nicking endonuclease-assisted amplification scheme,[89] shedding light on the development of sensitive colorimetric methods.

Rothberg and Li recently reported a label-free colorimetric detection method that does not require the pre-functionalization of nanoparticles **(Figure 1-5B)**.[82] In their method, single stranded DNA (ssDNA) or duplex DNA containing the target DNA (dsDNA) was added to citrate-stabilized gold nanoparticles followed by the addition of a salt solution. The ssDNA readily binds to the surface of citrate-stabilized nanoparticles because DNA bases have high affinities to the gold surface, thereby stabilizing the nanoparticles in salt solutions **(Figure 1-5B, top)**.[82] On the other hand, dsDNA does not bind to the gold surface as efficiently because DNA bases are buried in the helical structure. Thus, the addition of salts to the duplex/nanoparticle mixture results in the aggregation of nanoparticles **(Figure 1-5B, bottom)**. Therefore a red to purple color change upon salt addition indicates the presence of target DNA. The detection limit of this label-free method was similar to that of the colorimetric method using DNA-modified nanoparticles described in **Figure 1-5A**.

Plaxco and coworkers improved the sensitivity of the label-free colorimetric approach by using polyelectrolytes in place of salts.[78] In this work, ssDNA or dsDNA was added to citrate stabilized gold nanoparticles followed by the addition of a cationic conjugated polyelectrolyte. The addition of polyelectrolytes to the ssDNA/nanoparticle mixture caused aggregation of ssDNA-decorated nanoparticles due to the interaction between ssDNA and polyelectrolytes. On the other hand, the addition of polyelectrolytes to the duplex/nanoparticle mixture did not induce nanoparticle aggregation because the interaction of dsDNA with polyelectrolytes is weaker than that of ssDNA. This method,

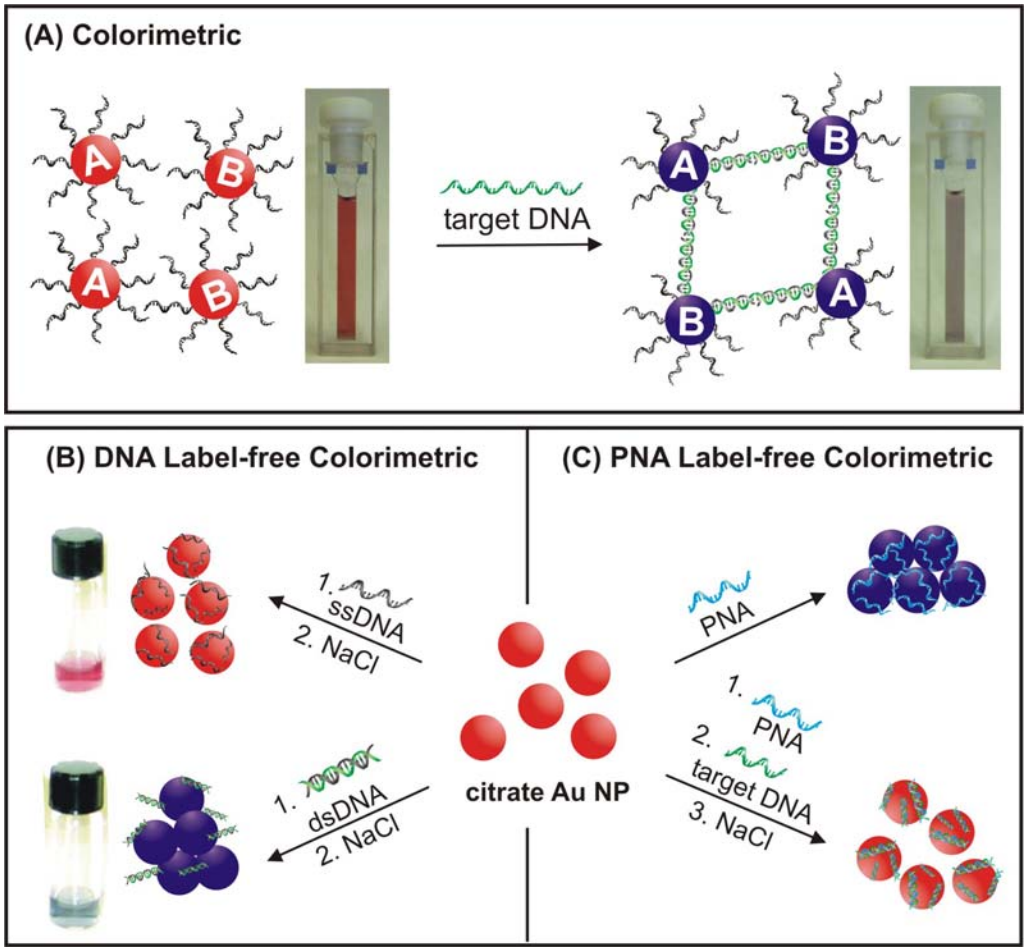

Figure 1-5. Colorimetric DNA detection methods using DNA-modified gold nanoparticles (A) and unmodified gold nanoparticles (B, C). These methods depend on the change in color (e.g. shift in the SPR band) upon nanoparticle aggregation or de-aggregation. (A) The presence of target DNA strands that are complementary to the DNA strands immobilized on gold nanoparticles results in the formation of nanoparticle aggregates and red to purple color change. (B) A label-free colorimetric detection method using citrate-stabilized gold nanoparticles. In the absence of target DNA, the binding of ssDNA on citrate-stabilized gold nanoparticles stabilizes the particles in salt solutions. When dsDNA containing target DNA was added, on the other hand, nanoparticles aggregate in salt solutions, causing red to purple color change. (C) A label-free colorimetric detection using PNA. Citrate-stabilized gold nanoparticles aggregate upon the addition of PNA. Subsequent addition of complementary DNA targets redisperses nanoparticles, causing a purple to red color change. (B: Pictures of the nanoparticle solutions with ssDNA and dsDNA after the addition of salt are adapted from ref [90]. Copyright 2004 National Academy of Sciences, U.S.A.) Figure reprint with permission from ref [48].Copyright 2012 Wiley-VCH Verlag GmbH & Co. KGaA

however, has a rather low selectivity and can only differentiate completely complementary DNA from DNA strands with 3 or more base mismatches.

Gold nanoparticles conjugated with peptide nucleic acid (PNA) were also used in colorimetric detection, taking advantage of the more stable duplex formation between PNA and DNA compared to DNA-DNA duplex formation.[91] Unlike DNA-modified nanoparticles, PNA-modified gold nanoparticles agglomerate in aqueous solutions because of the charge neutrality of PNA. The addition of complementary target DNA to the aggregates of PNA-modified nanoparticles results in the redispersion of nanoparticles, due to the binding of negatively charged DNA strands to neutral PNA-modified nanoparticles. Thus, in this detection scheme, the presence of target DNA is detected by the purple to red color change. Label-free colorimetric technique was also demonstrated using PNA **(Figure 1-5C)**.[92, 93] In this approach, the addition of PNA to citrate-stabilized gold nanoparticles induced the aggregation of nanoparticles as PNA binds to the gold surface. The subsequent addition of complementary target DNA to the solution induced the redispersion of nanoparticles and the characteristic purple to red color change upon binding of negatively charged DNA to PNA-coated nanoparticles. Detection by the purple to red color change (aggregation to dispersion) is advantageous because nanoparticles have a general tendency to aggregate in complex detection media, which can give false positive results for dispersion to aggregation detection methods.

In addition to spherical particles, anisotropic nanoparticles such as gold nanorods have also been utilized for both labeled[94,95] and label-free detection methods,[96] taking advantage of the larger extinction coefficient of nanorods. However, the sensitivity was not significantly improved by employing nanorods in these studies. The development of

more robust functionalization protocols for anisotropic particles might improve their performance in DNA detection.

1.5.5.2 Scanometric Method

The scanometric method is a simple chip-based detection method that overcomes the low sensitivity of colorimetric detection methods described above.[97] It involves two main steps: 1) the binding of DNA-modified gold nanoparticle to the capture DNA strands immobilized on a glass surface through the hybridization of target DNA and 2) subsequent signal amplification by the catalytic silver deposition on gold nanoparticles **(Figure 1-6A)**.[98] The silver enhancement permits visualization of the hybridization event with the naked eye or by a flatbed scanner. This detection system is now commercially available (Nanospheres Inc.).[83]

The scanometric technique has high selectivity and can reliably detect single base mismatches by using a procedure called stringency wash. The stringency wash is a typical procedure used to improve the selectivity in DNA detection. It utilizes the difference in melting temperatures of noncomplementary strands and completely complementary strands. The temperature of the wash solution is adjusted so that a large fraction of noncomplementary DNA strands are dehybridized off of the surface while a large fraction of complementary DNA strands remain on the surface. Owing to the sharp melting transition (**Figure 1-4B**) of nanoparticles densely functionalized with DNA, detection methods utilizing the nanoparticle probes offers a significantly higher selectivity ratio than molecular probes. However, the temperature of the wash solution must be carefully controlled in order to obtain the ideal selectivity ratio. Recently, Liu

and coworkers showed that the washing step can be simplified by covalently coupling the DNA strands on DNA–conjugated nanoparticles to the captured DNA strands on the glass surface using sequence selective enzymatic DNA ligation.[99]

The sensitivity of the scanometric method is also very high; the latest paper on scanometric method reported a sensitivity of 200 fM.[83] The high sensitivity of the scanometric method was even further improved by combining the scanometric detection platform with an amplification technique called the biobarcode assay.[100] Using the biobarcode assay, a detection limit of 500 zeptomolar has been achieved, which essentially removes the need for polymerase chain reaction (PCR) in DNA detection.[84] The biobarcode assay has been reviewed in other review papers along with the scanometric method, and readers are encouraged to read those review articles for more in-depth coverage on the topic.[27, 101]

A similar detection scheme has been applied to develop a DNA detection system with simple electrical read-out (**Figure 1-6B**).[18] In this method, a small gap between two electrodes is functionalized with capture DNA strands. The detection procedure is almost identical to the scanometric method except for the readout and chip fabrication steps. In this method, target DNA strands bring gold nanoparticles to the electrode gap. Subsequent catalytic deposition of silver closes the gap and allows electrical current to flow between the electrodes. Therefore, an increase in the conductivity measured between the two electrodes is indicative of the presence of target DNA, which provides a simple readout system that can be readily implemented in portable devices.[18]

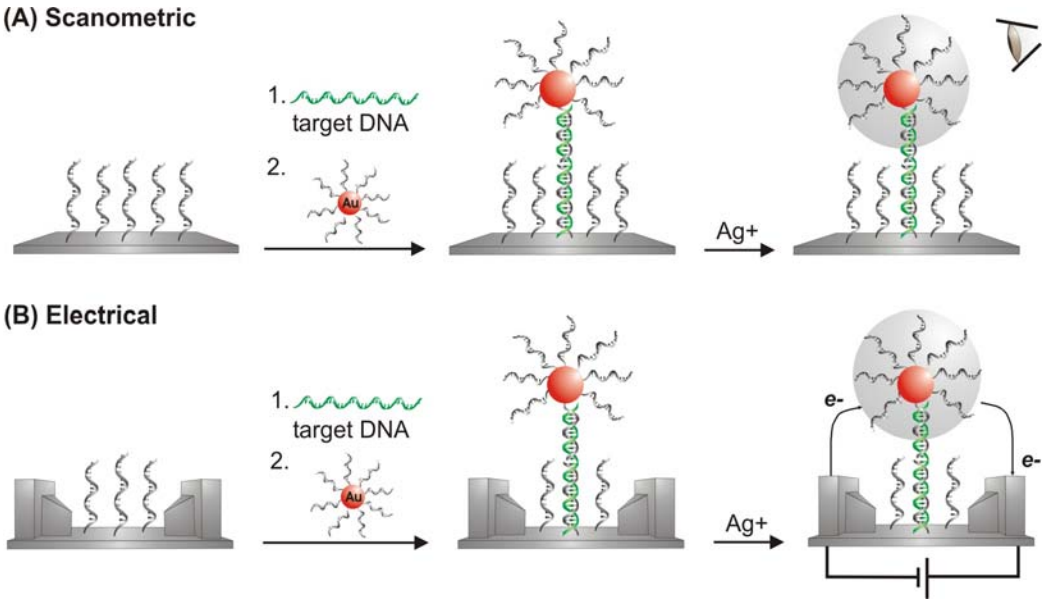

Figure 1-6. Schematic representations for the detection of DNA using the scanometric (A) and electrical (B) methods. The two methods are similar in design with the major difference in the read-out step, where the results of the scanometric method can be detected by a scanner or the naked eye and the electrical method provides an electrical signal. Figure reprint with permission from ref [48].Copyright 2012 Wiley-VCH Verlag GmbH & Co. KGaA

1.5.5.3 Surface Enhanced Raman Spectroscopy (SERS)

Metal nanoparticles have been shown to be extremely useful for several spectroscopic techniques due to the strong electric fields generated on metal nanoparticles upon illumination.[17] The most impressive example is surface enhanced Raman spectroscopy (SERS).[102] Raman spectroscopy is a useful analytical technique that provides molecular fingerprints. However, its low sensitivity prevents it from becoming an efficient sensing tool on its own. In SERS, the Raman signal is enhanced by many orders of magnitude when analytes are attached to metallic nanostructures.[103] Since the discovery of the phenomenon, it has been used to detect and study various chemical and biological molecules including DNA.[104] Cao et al. have demonstrated that SERS can be used for multiplexed DNA detection **(Figure 1-7A)**. This method is based on the scanometric detection system **(Figure 1-6A)**. The only difference in the procedure is that the gold nanoparticles used in the SERS-based detection are functionalized with oligonucleotides containing Raman-active dyes as identification tags.[86] Silver deposition on the nanoparticles enhances the Raman signal of the dyes, providing the identification of the DNA sequence for multiplexed detection.

Note that silver nanostructures offer much higher enhancement factors than gold nanostructures.[105, 106] The enhancement factor also depends highly on the shape of nanoparticles; because of the high electric field generated at the sharp tips of anisotropic nanoparticles, nonspherical particles such as nanorods **(Figure 1-3C)**, nanostars (**Figure 1-3D**), spiky nanoshells (**Figure 1-3E**) and nanotriangles **(Figure 1-3F)** are of great interest for SERS applications. The enhancement factor further increases when analytes

are located at the junction between two particles. The enhancement factor for nanoparticle aggregates can be high enough to even detect single molecules.[107]

The signal increase upon particle aggregation has been used in homogeneous DNA detection **(Figure 1-7B)**.[108] The detection procedure is similar to that of colorimetric detection (**Figure 1-5A**). In the homogeneous SERS based detection, silver nanoparticles are functionalized with dye-labeled DNA. The addition of target DNA strands causes the aggregation of nanoparticles, which is detected by an increase in the SERS signal. An advantage of this SERS-based method over the colorimetric method described above (**Figure 1-5A**) is that it can potentially offer a higher sensitivity, because an increase in the SERS signal can be detected even from small clusters of nanoparticles that do not induce the signature red-to-purple color change. The authors reported that they achieved a detection limit of 20 fM. Again, this method takes advantage of the high enhancement factor of analytes located at nanoparticle junctions. However, in the detection scheme, the nanoparticle-nanoparticle distance is longer than ideal, thus only small numbers of hot spots might be responsible for the increased SERS intensity. Nam and coworkers have recently showed that the distance between DNA-linked metal particles can be reduced by depositing silver shells around gold nanoparticles (**Figure 1-7C)**.[105, 109] The gap between the two particles was controlled by varying the amount of silver deposition. Using this strategy, they were able to detect single Raman dyes located at the small gap between two particles.

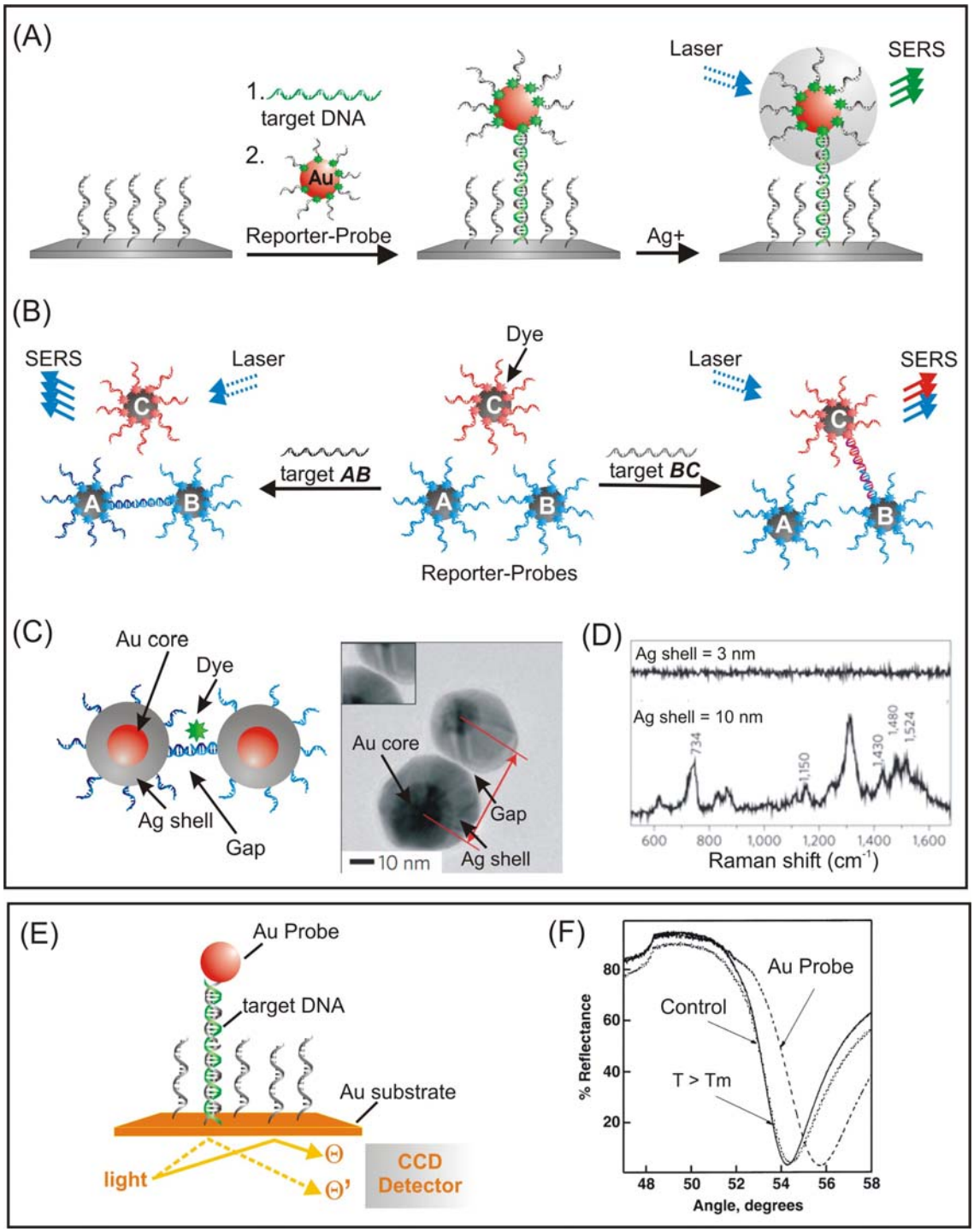

Figure 1-7. (A) Schematic description of chip-based DNA detection using SERS. The SERS signal from reporter dyes is increased by the catalytic silver deposition on nanoparticles. Different reporter dye molecules show different SERS spectra, providing

this method the capability for multiplexing. (B) A homogeneous DNA detection method based on SERS. SERS signal is increased in the presence of target DNA because Raman enhancement factor is higher in nanoparticle aggregates than in isolated nanoparticles. (C) Scheme and TEM image of a Au-Ag core-shell nanoparticle dimer prepared from DNA-functionalized gold nanoparticles. (D) SERS spectra of Au-Ag core-shell dimers with 3 nm (top) and 10 nm (bottom) thick Ag shell, showing that the dimer with a narrower gap yields higher SERS signal. (E) A diagram for a DNA detection scheme based on SPRS. (F) SPRS spectra showing that the binding of gold nanoparticles through DNA hybridization results in a large shift in SPR positions. (C and D: adapted from ref [109], reprinted with permission from AAAS; F: adapted with permission from ref [110]. Copyright 2000 American Chemical Society.) Figure reprint with permission from ref [48].Copyright 2012 Wiley-VCH Verlag GmbH & Co. KGaA

1.5.5.4 Surface Plasmon Resonance Spectroscopy (SPRS)

Surface plasmon resonance spectroscopy (SPRS) is a well-established analytical tool in life sciences, which measures the molecular adsorption and desorption on metal films. The detection principle is based on the observation that the conditions for the SPR excitation of metal films change sensitively to the refractive index of medium.[111] SPRS is a particularly useful technique for kinetic studies as it can monitor binding events in real time.[112, 113]

SPRS has been used to analyze many different types of biological molecules including DNA.[114-117] However, the sensitivity of SPRS is not high enough to be used as an ultra-sensitive DNA detection tool on its own. It has been shown that the detection limit of SPRS can be drastically enhanced by using DNA-conjugated gold nanoparticles as a signal enhancer (**Figure 1-7E**).[110, 118] This signal enhancement strategy takes advantage of the high dielectric constant of gold nanoparticles and the electromagnetic coupling between the metal surface and nanoparticles. In this approach, the gold film and the nanoparticles are functionalized with DNA strands that are complementary to different parts of the target DNA. Upon the addition of the target DNA and nanoparticle probes to the DNA modified metal film, the target DNA brings the gold particles to the metal surface, forming a sandwich-type structure **(Figure 1-7E)**. A detection limit of 10 pM of target DNA was achieved using the sandwich geometry **(Figure 1-7E, F).**[68] Yao et al. reported a quantification limit of 1.38 fM of DNA when the metal surface was coated with a layer of dextran to reduce non-specific binding of nanoparticles.[85]

1.5.6 DNA Delivery Applications

Nanoparticles are attractive alternatives to conventional viral vectors in gene delivery applications because of potentially lower adverse immune responses, ease of production, more flexible manipulation in terms of size and shape as well as methodologies for releasing DNA payloads.[119] In this section, we present recent studies on DNA-conjugated metal nanoparticles as a new generation of DNA carriers.

1.5.6.1 DNA-Conjugated Metal Nanoparticles as Gene Carriers

The use of metal nanoparticles to deliver oligonucleotides into cells was first demonstrated through the use in gene guns. This method has been used in plants to insert genetic materials into the genome of host cells.[120] The main disadvantage of gene guns, however, is the shallow penetration depth (~ 100 to 200 micrometers), therefore making the delivery of genetic materials into deeper tissues impossible.

Recently, Mirkin and coworkers demonstrated that DNA-functionalized gold nanoparticles are effective vectors for DNA delivery with a cellular uptake efficiency higher than 99%.[30] In the study, they used gold nanoparticles conjugated with antisense DNA strands to inhibit the expression of enhanced green fluorescent protein (EGFP) in C166-EGFP cells **(Figure 1-8A)**.[30] They found that C166-EGFP cells treated with the antisensing gold nanoparticles showed a noticeable decrease in EGFP expression **(Figure 1-8B, C),** with a higher knock-down efficiency than commercial cationic transfecting agents (Lipofectamine™). In addition, the immobilized oligonucleotides were shown to be highly resistant to degradation by nucleases.[30] Small interference RNA (RNAi) has also been delivered using RNAi-functionalized gold nanoparticles.[121]

Another report by the same group used a similar design to create an intracellular RNA detection system called "nano-flare". The "nano-flare" probe shown in **Figure 1-16D** is prepared by hybridizing shorter fluorescently labeled DNA strands to the longer DNA strands attached to gold nanoparticles.[122] The technique uses the fluorescence quenching capability of gold nanoparticles for the quantification of intracellular RNA **(Figure 1-8E)**. The binding of target RNA to the DNA-modified nanoparticles releases the short fluorescently labeled DNA from nanoparticles, which results in the increased in fluorescence intensity. The cellular uptake efficiency of the nano-flares was shown to be extremely high (99%), and their signal-to-noise ratio is superior when compared with conventional molecular beacons.[122]

Leong and coworkers demonstrated that plasmid DNA can be delivered into cells by using metal nanorods with cell-targeting proteins.[123] In this work, Au-Ni multi-segment nanorods were used to immobilize both GFP-encoding plasmid and targeting proteins on the rods; DNA plasmids were immobilized on Ni segments and the cell-targeting proteins were bound to Au segments. The bifunctional nanorods exhibited increased gene expression by 22% compared to nanorods that are functionalized with DNA plasmids alone, due to the targeting capability of the bifunctional nanorods.[123]

It is interesting to note that the DNA-modified gold nanoparticles described above **(Figure 1-4A)** show extremely high cellular uptake efficiencies without any targeting agents. Although the exact origin is not fully understood, it is believed to be associated with a high DNA density on the nanoparticle surface.[124] The low nuclease activity on these nanoparticles was also shown to be associated with the high DNA density and the high local salt concentration.[124] These observations demonstrate that the performance of

nanoparticles in DNA delivery applications can depend highly on the exact make-up of nanoparticles (e.g. DNA density, size and shape of nanoparticles), thus it is important to fully characterize them for their successful implementation in gene delivery.

1.5.6.2 Release of DNA Payload

The strong light absorption and the high heat capacity of metal nanoparticles have been used to control the local temperature surrounding nanoparticles and to release DNA loads in DNA delivery applications.[125,126] Hollow metal particles (e.g., gold nanoshells[127] and nanocages[45], **Figure 1-3B, G**) and non-spherical particles such as gold nanorods (**Figure 1-3C**),[128] whose SPR band is located in the NIR region, are particularly useful for this application because the NIR light has deeper penetration depths in tissues. Halas and coworkers demonstrated that DNA strands that are hybridized to the DNA immobilized on nanoshells can be dehybridized and released from nanoshells by increasing the local temperature through NIR irradiation **(Figure 1-9A)**.[128,127] Yamashita et al. have recently reported the release of hybridized DNA strands from DNA-conjugated Au nanorods in mice using NIR irradiation, demonstrating that an irradiation-based release method is feasible in animal models.[129] It has also been shown that DNA directly adsorbed on nanorod surfaces can be released by NIR irradiation with a pulsed laser.[130,131, 132] For example, Wu et al. attached EGFP-encoding plasmid DNA to gold nanorods, and delivered them to cultured HeLa cells.[133] When irradiated with 800 nm light, EGFP plasmid DNA was released from the nanorods, which was accompanied by the shape transformation of gold nanorods to nanospheres **(Figure 1-9B)**. No GFP

expression was observed when cells were not irradiated. Recently, Hamad-Schifferli et al. were able to selectively release two different oligonucleotides using two sets of gold nanorods with different aspect ratios (i.e. short nanorods and longer nano-dogbones). It was achieved by the selective excitation of gold nanorods through irradiation at their longitudinal SPR peaks (800 nm for the short nanorods or 1100 nm for the nano-dogbones).[134] They found that the released DNA strands were not damaged by this process and can still hybridize to the complementary DNA.

Radio-frequency (RF) has also been used to control the hybridization of DNA attached to gold nanoparticles **(Figure 1-9C)**.[135] The application of a RF field resulted in an increased local temperature due to the high heat capacity of gold, which was enough to induce the dehybridization of DNA duplexes.[135] This was also demonstrated using magnetic nanoparticles.[136]

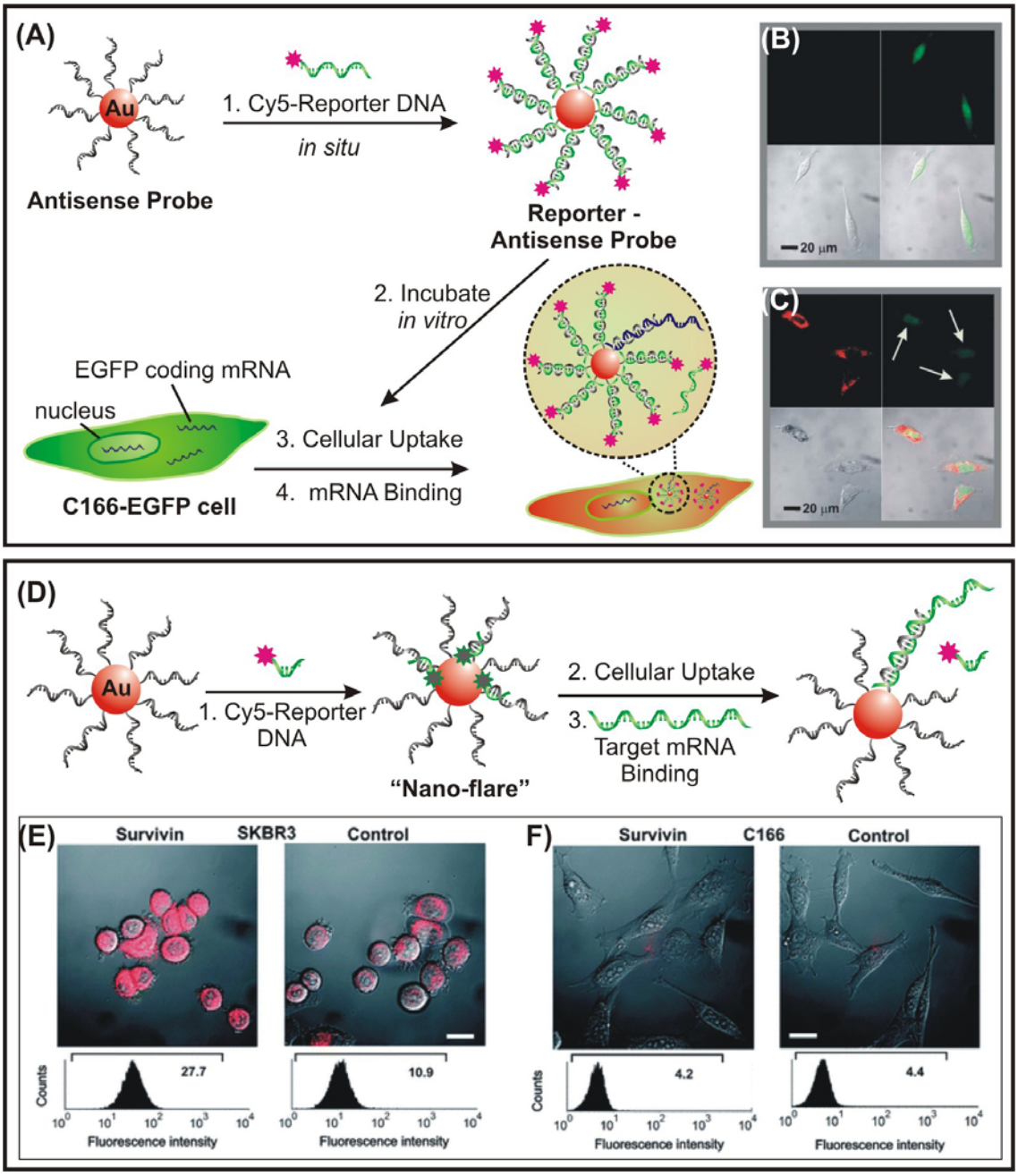

Figure 1-8. (A-C) Gene delivery and regulation using DNA functionalized gold nanospheres. In this method, antisense DNA strands that inhibit the expression of EGFP were first immobilized on gold probes. Cy5-modified reporter DNA strands, which were used to monitor the cellular uptake, were hybridized to the antisense DNA and then the nanoparticle probes were incubated with C166-EGFP cells. Confocal fluorescence microscopy images of C166-EGFP cells before and after the treatment with the

nanoparticle probes are shown in (B) and (C), respectively. (upper left: Cy5 emission, upper right: EGFP emission, lower left: transmission image, lower right: overlay of the three channels). Results indicate that the reporter-antisense probes were effectively taken up by cells (appearance of red fluorescence from Cy5 in C) and reduced the expression of EGFP in the cells (reduced green fluorescence from EGFP in C). (D-E) Intracellular RNA detection method based on DNA-modified nanoparticles called "nano-flares". In this work, Cy5-modified reporter DNA strands were hybridized to the Survivin antisense DNA on nanoparticles in a way that Cy5 dyes were close to the gold surface. In that geometry, fluorescence of Cy5 was completely quenched by gold. In the presence of mRNA, the short Cy5 labeled reporter strands are dehybridized from the nano-flares and therefore become fluorescent (left image in (E)). Shown in (E) are cells treated with nano-flares (left: cells containing survivin, right: cells without survivin). Shown in (F) is another control where cells are treated with non-Survivin antisense nano-flares (left: cells containing survivin, right: cells without survivin); neither show any fluorescence from the reporter. (B and C were adapted from ref [30], reprinted with permission from AAAS; E and F were reprinted with permission from ref [122]. Copyright 2007 American Chemical Society) Figure reprint with permission from ref [48].Copyright 2012 Wiley-VCH Verlag GmbH & Co. KGaA

1.3.5.3 Disadvantages as Carriers

As discussed in the previous sections, DNA-conjugated gold nanoparticles with high DNA density functionalization have been extensively studied for various biological and medical applications such as bio-imaging and sensing[137], medical diagnostics[27], drug delivery[29] and gene regulation.[30] This system has shown great promises in DNA detection owing to their unusual DNA melting characteristics (i.e. sharp melting transitions and high binding constants) that originated from cooperative interactions of closely spaced DNA strands on the nanoparticle surfaces, i.e. high DNA density on the surface of the nanoparticles.[138, 139] Importantly, these unique properties have led to the development of DNA detection technologies with exceptionally high selectivity and sensitivity.[27]

Nevertheless, there are several disadvantages associated with DNA-conjugated metal nanoparticles that are not easily overcome, such as the need to have modified DNA for the delivery of drugs. It is also difficult to incorporated a different type of physical property such as magnetic or fluorescence into the structure. While the benefit of extending these properties onto other types of functional nanoparticles (e.g. magnetic particles and quantum dots) is obvious, however, progress in these studies has been hindered by the ability to obtain high density DNA on the surfaces of those nanoparticles.

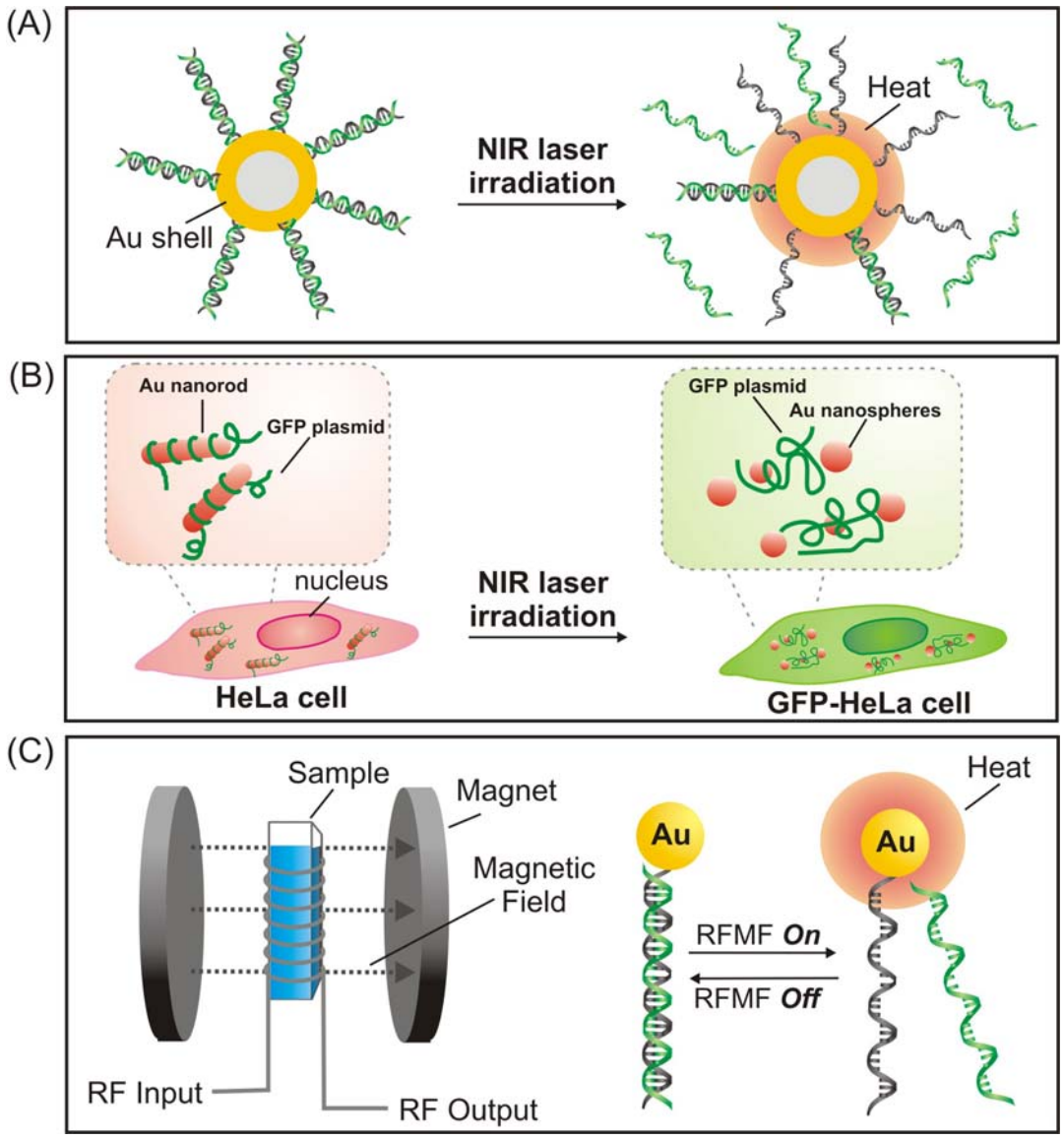

Figure 1-9. (A) Release of DNA strands hybridized to complementary DNA immobilized on gold nanoshells by NIR irradiation. (B) Release of green fluorescent protein (GFP) coding plasmid from Au nanorod through the shape transformation by pulsed laser irradiation. (C) Experimental set-up and schematic description of RF-field induced DNA dehybridization. Figure reprint with permission from ref [48].Copyright 2012 Wiley-VCH Verlag GmbH & Co. KGaA

1.6 Our Novel System: Multifunctional DNA Block Copolymer Assemblies

In many instances, the effectiveness of these DNA-conjugated gold nanoparticles in the intended applications is attributed to the densely packed DNA layer on the nanoparticle surface.[76, 77, 124] While in principle, any type of functional nanoparticle (e.g. other noble metal nanoparticles, magnetic nanoparticles and semiconductor nanoparticles) with a high DNA density on the surface can demonstrate the same effectiveness shown by DNA-conjugated gold nanoparticles, nevertheless, progress in this direction has been slow due to the difficulty in achieving high DNA density functionalization for other types of nanoparticles. To this end, DNA-conjugated gold nanoparticles are still the "gold standard" in terms of high DNA density functionalization on nanoparticles.

To circumvent this challenge, a general method was developed to achieve high DNA density on any type of nanoparticle using the self-assembling capability of DNA diblock copolymers (**Scheme 1-1**). In this strategy, hydrophobic nanoparticles are incorporated into amphiphilic DNA block copolymer micelles, resulting in nanoparticle/polymer hybrid particles with high DNA density on their surfaces. These unique nanostructures not only possess a high DNA density layer on the surface, but they also acquire the functionalities of the encapsulated nanoparticles. In principle, this synthetic strategy can be extended to virtually any type of nanoparticles, and thus can be used to generate a wide range of multifunctional nanostructures with the extraordinary DNA hybridization properties mentioned above. The advantages of these DNA block-copolymer assemblies over DNA-functionalized nanoparticles include their flexibility in

the design, i.e. sequence of DNA can be easily changed and the makeup of the polymer can also be changed depending upon the intended application.

1.6.1 Background on DNA Block Copolymer

There are a handful of literature reports on the synthesis of DNA block copolymer, in which short synthetic oligonucleotides are covalently attached to a polymer strand. There are also reports of hybrids such as DNA/lipid and DNA/peptide, but we will only consider systems that are closer to ours, that is single strands of short synthetic DNA covalently attached to a single strand of synthetic organic polymer. DNA block copolymer and their self-assembled structures have been previously reported, and the structures reported were mainly simple micelles[140-142] We are the first to report the successful incorporation of nanoparticles into the hydrophobic polymer core to create multifunctional DNA block copolymer assemblies.[143]

1.6.2 Advantages Over DNA-conjugated Nanoparticles

Our approach to over come the disadvantages of gold conjugated nanoparticles is to prepare nanostructures decorated with high DNA density using the self-assembly of DNA block copolymer and nanoparticles to create multifunctional nanoparticles. The advantages of this method over DNA-conjugated metallic nanoparticles are the universality, multifunctionalities, easy to change components to materials that are biodegradable. DNA block copolymers (DNA BCP) and their self-assemblies, and their potential applications as gene and drug delivery vehicles.

This method has the additional advantages over direct functionalization methods in that additional functionalities can be easily engineered into the organic polymer block, and small molecules such as pharmaceutical drugs can be incorporated into the core of the assemblies to create multifunctional bio-inorganic hybrid nanostructures, which can be used for a variety of biomedical applications.

Scheme 1-1. Self-assembly of DNA block copolymer with nanoparticles (A) and delivery applications (B).

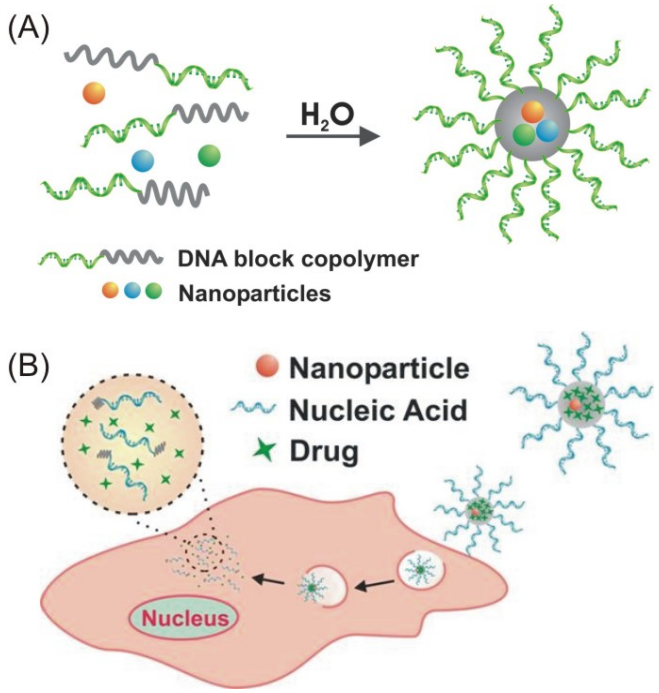

1.7 References

1. Watson, J. D. & Crick, F. H. Molecular structure of nucleic acids:a structure for deoxyribose nucleic acid. Nature 171, 737–738 (1953).
2. Voet, D., Voet, J. G. & Pratt, C. W. Fundamentals of Biochemistry: Life at the Molecular Level (2012).
3. Elgar, G. & Vavouri, T. Tuning in to the signals: noncoding sequence conservation in vertebrate genomes. Trends in Genetics 24, 344-352 (2008).
4. Pennisi, E. A Low Number Wins the GeneSweep Pool. Science 300, 1484 (2003).
5. Venter, J. C. et al. The Sequence of the Human Genome. Science 291, 1304-1351 (2001).
6. Burton, P. R. et al. Genome-wide association study of 14,000 cases of seven common diseases and 3,000 shared controls. Nature 447, 661-678 (2007).
7. Southern, E. M. Detection of specific sequences among DNA fragments separated by gel electrophoresis. Journal of Molecular Biology 98, 503-517 (1975).
8. Mullis, K. B., Faloona, F. A. & Ray, W. in Methods in Enzymology 335-350 (Academic Press, 1987).
9. Bustin, S. A. Absolute quantification of mRNA using real-time reverse transcription polymerase chain reaction assays. Journal of Molecular Endocrinology 25, 169-193 (2000).
10. Roche(TM).
11. BioFire(TM).
12. Putnam, D. Polymers for gene delivery across length scales. Nat Mater 5, 439-451 (2006).
13. Hamilton, A. J. & Baulcombe, D. C. A Species of Small Antisense RNA in Posttranscriptional Gene Silencing in Plants. Science 286, 950-952 (1999).
14. Elbashir, S. M. et al. Duplexes of 21-nucleotide RNAs mediate RNA interference in cultured mammalian cells. Nature 411, 494-498 (2001).

15. Sokolova, V. & Epple, M. Inorganic Nanoparticles as Carriers of Nucleic Acids into Cells. Angewandte Chemie International Edition 47, 1382-1395 (2008).
16. Sharma, V., Park, K. & Srinivasarao, M. Colloidal dispersion of gold nanorods: Historical background, optical properties, seed-mediated synthesis, shape separation and self-assembly. Materials Science and Engineering: R: Reports 65, 1-38 (2009).
17. Xia, Y. & Halas, N. J. Shape-controlled synthesis and surface plasmonic properties of metallic nanostructures. Mrs Bulletin 30, 338-344 (2005).
18. Park, S.-J., Taton, T. A. & Mirkin, C. A. Array-based electrical detection of DNA with nanoparticle probes. Science 295, 1503-1506 (2002).
19. Schmid, G. & Simon, U. Gold nanoparticles: assembly and electrical properties in 1-3 dimensions. Chemical Communications, 697-710 (2005).
20. Yamamoto, Y. & Hori, H. Direct observation of the ferromagnetic spin polarization in gold nanoparticles: A review. Reviews on Advanced Materials Science 12, 23-32 (2006).
21. Wagner, V., Dullaart, A., Bock, A.-K. & Zweck, A. The emerging nanomedicine landscape. Nat Biotech 24, 1211-1217 (2006).
22. Nie, S., Xing, Y., Kim, G. J. & Simons, J. W. Nanotechnology Applications in Cancer. Annual Review of Biomedical Engineering 9, 257-288 (2007).
23. Jain, P. K., Huang, X., El-Sayed, I. H. & El-Sayed, M. A. Noble Metals on the Nanoscale: Optical and Photothermal Properties and Some Applications in Imaging, Sensing, Biology, and Medicine. Accounts of Chemical Research 41, 1578-1586 (2008).
24. Cobley, C. M., Chen, J., Cho, E. C., Wang, L. V. & Xia, Y. Gold nanostructures: a class of multifunctional materials for biomedical applications. Chemical Society Reviews 40, 44-56 (2011).
25. Raikhel, N. V., Mishkind, M. & Palevitz, B. A. Immunocytochemistry in plants with colloidal gold conjugates. Protoplasma 121, 25-33 (1984).

26. Hodges, G. M., Southgate, J. & Toulson, E. C. Colloidal gold--a powerful tool in scanning electron microscope immunocytochemistry: an overview of bioapplications. Scanning Microscopy 1, 301-318 (1987).
27. Rosi, N. L. & Mirkin, C. A. Nanostructures in biodiagnostics. Chemical Reviews 105, 1547-1562 (2005).
28. Song, Y. et al. Multimodal Gadolinium-Enriched DNA-Gold Nanoparticle Conjugates for Cellular Imaging. Angewandte Chemie International Edition 48, 9143-9147 (2009).
29. Dhar, S., Daniel, W. L., Giljohann, D. A., Mirkin, C. A. & Lippard, S. J. Polyvalent Oligonucleotide Gold Nanoparticle Conjugates as Delivery Vehicles for Platinum(IV) Warheads. Journal of the American Chemical Society 131, 14652-14653 (2009).
30. Rosi, N. L. et al. Oligonucleotide-Modified Gold Nanoparticles for Intracellular Gene Regulation. Science 312, 1027-1030 (2006).
31. Kelly, K. L., Coronado, E., Zhao, L. L. & Schatz, G. C. The Optical Properties of Metal Nanoparticles:The Influence of Size, Shape, and Dielectric Environment. The Journal of Physical Chemistry B 107, 668-677 (2002).
32. Tao, A. R., Habas, S. & Yang, P. Shape Control of Colloidal Metal Nanocrystals. Small 4, 310-325 (2008).
33. Grzelczak, M., Perez-Juste, J., Mulvaney, P. & Liz-Marzan, L. M. Shape control in gold nanoparticle synthesis. Chemical Society Reviews 37, 1783-1791 (2008).
34. Xia, Y., Xiong, Y., Lim, B. & Skrabalak, S. E. Shape-Controlled Synthesis of Metal Nanocrystals: Simple Chemistry Meets Complex Physics? Angewandte Chemie International Edition 48, 60-103 (2009).
35. Murphy, C. J. et al. Anisotropic Metal Nanoparticles: Synthesis, Assembly, and Optical Applications. Journal of Physical Chemistry B 109, 13857-13870 (2005).
36. Hu, M. et al. Gold nanostructures: engineering their plasmonic properties for biomedical applications. Chemical Society Reviews 35, 1084-1094 (2006).

37. Murphy, C. J., Sau, T. K., Gole, A. & Orendorff, C. J. Surfactant-Directed Synthesis and Optical Properties of One-Dimensional Plasmonic Metallic Nanostructures. MRS Bulletin 30, 349-355 (2005).
38. Xia, Y., Xiong, Y., Lim, B. & Skrabalak, S. Shape-Controlled Synthesis of Metal Nanocrystals: Simple Chemistry Meets Complex Physics? Angewandte Chemie International Edition 48, 60-103 (2009).
39. Cobley, C., Skrabalak, S., Campbell, D. & Xia, Y. Shape-Controlled Synthesis of Silver Nanoparticles for Plasmonic and Sensing Applications. Plasmonics 4, 171-179 (2009).
40. Lu, X., Rycenga, M., Skrabalak, S. E., Wiley, B. & Xia, Y. Chemical Synthesis of Novel Plasmonic Nanoparticles. Annual Review of Physical Chemistry 60, 167-192 (2009).
41. Hirsch, L. et al. Metal Nanoshells. Annals of Biomedical Engineering 34, 15-22 (2006).
42. Huang, X., Neretina, S. & El-Sayed, M. A. Gold Nanorods: From Synthesis and Properties to Biological and Biomedical Applications. Advanced Materials 21, 4880-4910 (2009).
43. Nehl, C. L., Liao, H. & Hafner, J. H. Optical Properties of Star-Shaped Gold Nanoparticles. Nano Letters 6, 683-688 (2006).
44. Millstone, J. E., Métraux, G. S. & Mirkin, C. A. Controlling the Edge Length of Gold Nanoprisms via a Seed-Mediated Approach. Advanced Functional Materials 16, 1209-1214 (2006).
45. Skrabalak, S. E. et al. Gold Nanocages for Biomedical Applications. Advanced Materials 19, 3177-3184 (2007).
46. Nicewarner-Pena, S. R. et al. Submicrometer Metallic Barcodes. Science 294, 137-141 (2001).
47. Zheng, J., Zhang, C. & Dickson, R. M. Highly Fluorescent, Water-Soluble, Size-Tunable Gold Quantum Dots. Physical Review Letters 93, 077402 (2004).

48. Chen, X.-J., Sanchez-Gaytan, B. L., Qian, Z. & Park, S.-J. Noble metal nanoparticles in DNA detection and delivery. Wiley Interdisciplinary Reviews: Nanomedicine and Nanobiotechnology 4, 273-290 (2012).
49. Turkevich, J., Stevenson, P. C. & Hillier, J. A Study of the Nucleation and Growth Processes in The Synthesis of Colloidal Gold. Discussions of the Faraday Society, 55-75 (1951).
50. Ji, X. et al. Size Control of Gold Nanocrystals in Citrate Reduction: The Third Role of Citrate. Journal of the American Chemical Society 129, 13939-13948 (2007).
51. Frens, G. Controlled Nucleation for the Regulation of the Particle-Size in Monodisperse Gold Suspensions. Nature-Physical Science 241, 20-22 (1973).
52. Brust, M., Walker, M., Bethell, D., Schiffrin, D. J. & Whyman, R. Synthesis of Thiol-Derivatized Gold Nanoparticles in a 2-Phase Liquid-Liquid System. Chemical Communications, 801-802 (1994).
53. Hostetler, M. J., Green, S. J., Stokes, J. J. & Murray, R. W. Monolayers in Three Dimensions: Synthesis and Electrochemistry of ω-Functionalized Alkanethiolate-Stabilized Gold Cluster Compounds. Journal of the American Chemical Society 118, 4212-4213 (1996).
54. Shimizu, T., Teranishi, T., Hasegawa, S. & Miyake, M. Size Evolution of Alkanethiol-Protected Gold Nanoparticles by Heat Treatment in the Solid State. The Journal of Physical Chemistry B 107, 2719-2724 (2003).
55. Jana, N. R. & Peng, X. Single-Phase and Gram-Scale Routes toward Nearly Monodisperse Au and Other Noble Metal Nanocrystals. Journal of the American Chemical Society 125, 14280-14281 (2003).
56. Brinson, B. E. et al. Nanoshells Made Easy: Improving Au Layer Growth on Nanoparticle Surfaces. Langmuir 24, 14166-14171 (2008).
57. Jackson, J. B. & Halas, N. J. Silver Nanoshells: Variations in Morphologies and Optical Properties. The Journal of Physical Chemistry B 105, 2743-2746 (2001).
58. Sanchez-Gaytan, B. L. & Park, S.-J. Spiky Gold Nanoshells. Langmuir 26, 19170-19174 (2010).

59. Gole, A. & Murphy, C. J. Seed-Mediated Synthesis of Gold Nanorods: Role of the Size and Nature of the Seed. Chemistry of Materials 16, 3633-3640 (2004).
60. Jana, N. R., Gearheart, L. & Murphy, C. J. Wet chemical synthesis of silver nanorods and nanowires of controllable aspect ratio. Chemical Communications, 617-618 (2001).
61. Nikoobakht, B. & El-Sayed, M. A. Preparation and Growth Mechanism of Gold Nanorods (NRs) Using Seed-Mediated Growth Method. Chemistry of Materials 15, 1957-1962 (2003).
62. Ha, T. H., Koo, H.-J. & Chung, B. H. Shape-Controlled Syntheses of Gold Nanoprisms and Nanorods Influenced by Specific Adsorption of Halide Ions. The Journal of Physical Chemistry C 111, 1123-1130 (2006).
63. Pastoriza-Santos, I. & Liz-Marzan, L. M. Synthesis of Silver Nanoprisms in DMF. Nano Letters 2, 903-905 (2002).
64. Jin, R. et al. Photoinduced Conversion of Silver Nanospheres to Nanoprisms. Science 294, 1901-1903 (2001).
65. Rodríguez-Lorenzo, L., Álvarez-Puebla, R. n. A., de Abajo, F. J. G. a. & Liz-Marzán, L. M. Surface Enhanced Raman Scattering Using Star-Shaped Gold Colloidal Nanoparticles. The Journal of Physical Chemistry C 114, 7336-7340 (2009).
66. Sun, Y. & Xia, Y. Shape-Controlled Synthesis of Gold and Silver Nanoparticles. Science 298, 2176-2179 (2002).
67. Liu, Y. & Walker, A. R. H. Monodisperse Gold–Copper Bimetallic Nanocubes: Facile One-Step Synthesis with Controllable Size and Composition. Angewandte Chemie International Edition 49, 6781-6785 (2010).
68. Zheng, J., Petty, J. T. & Dickson, R. M. High Quantum Yield Blue Emission from Water-Soluble Au8 Nanodots. Journal of the American Chemical Society 125, 7780-7781 (2003).
69. Zheng, J. & Dickson, R. M. Individual Water-Soluble Dendrimer-Encapsulated Silver Nanodot Fluorescence. Journal of the American Chemical Society 124, 13982-13983 (2002).

70. Richards, C. I. et al. Oligonucleotide-Stabilized Ag Nanocluster Fluorophores. Journal of the American Chemical Society 130, 5038-5039 (2008).
71. Kanaras, A. G., Wang, Z., Bates, A. D., Cosstick, R. & Brust, M. Towards Multistep Nanostructure Synthesis: Programmed Enzymatic Self-Assembly of DNA/Gold Systems. Angewandte Chemie International Edition 42, 191-194 (2003).
72. Claridge, S. A. et al. Directed Assembly of Discrete Gold Nanoparticle Groupings Using Branched DNA Scaffolds. Chemistry of Materials 17, 1628-1635 (2005).
73. Zhao, W., Lin, L. & Hsing, I. M. Rapid Synthesis of DNA-Functionalized Gold Nanoparticles in Salt Solution Using Mononucleotide-Mediated Conjugation. Bioconjugate Chemistry 20, 1218-1222 (2009).
74. Storhoff, J. J., Elghanian, R., Mucic, R. C., Mirkin, C. A. & Letsinger, R. L. One-pot colorimetric differentiation of polynucleotides with single base imperfections using gold nanoparticle probes. Journal of the American Chemical Society 120, 1959-1964 (1998).
75. Hurst, S. J., Lytton-Jean, A. K. R. & Mirkin, C. A. Maximizing DNA Loading on a Range of Gold Nanoparticle Sizes. Analytical Chemistry 78, 8313-8318 (2006).
76. Storhoff, J. J. et al. What controls the optical properties of DNA-linked gold nanoparticle assemblies? Journal of the American Chemical Society 122, 4640-4650 (2000).
77. Jin, R., Wu, G., Li, Z., Mirkin, C. A. & Schatz, G. C. What controls the melting properties of DNA-linked gold nanoparticle assemblies? Journal of the American Chemical Society 125, 1643-1654 (2003).
78. Xia, F. et al. Colorimetric detection of DNA, small molecules, proteins, and ions using unmodified gold nanoparticles and conjugated polyelectrolytes. Proceedings of the National Academy of Sciences 107, 10837-10841 (2010).
79. Lee, J.-S., Ulmann, P. A., Han, M. S. & Mirkin, C. A. A DNA-Gold Nanoparticle-Based Colorimetric Competition Assay for the Detection of Cysteine. Nano Letters 8, 529-533 (2008).

80. Lee, J.-S., Han, M. S. & Mirkin, C. A. Colorimetric Detection of Mercuric Ion (Hg2+) in Aqueous Media using DNA-Functionalized Gold Nanoparticles. Angewandte Chemie International Edition 46, 4093-4096 (2007).

81. Wu, Y., Sefah, K., Liu, H., Wang, R. & Tan, W. DNA aptamer-micelle as an efficient detection/delivery vehicle toward cancer cells. Proceedings of the National Academy of Sciences 107, 5-10 (2010).

82. Li, H. & Rothberg, L. Colorimetric detection of DNA sequences based on electrostatic interactions with unmodified gold nanoparticles. Proceedings of the National Academy of Sciences 101, 14036-14039 (2004).

83. Storhoff, J. J. et al. Gold nanoparticle-based detection of genomic DNA targets on microarrays using a novel optical detection system. Biosensors and Bioelectronics 19, 875-883 (2004).

84. Nam, J.-M., Stoeva, S. I. & Mirkin, C. A. Bio-Bar-Code-Based DNA Detection with PCR-like Sensitivity. Journal of the American Chemical Society 126, 5932-5933 (2004).

85. Yao, X. et al. Sub-attomole oligonucleotide and p53 cDNA determinations via a high-resolution surface plasmon resonance combined with oligonucleotide-capped gold nanoparticle signal amplification. Analytical Biochemistry 354, 220-228 (2006).

86. Cao, Y. C., Jin, R. & Mirkin, C. A. Nanoparticles with Raman spectroscopic fingerprints for DNA and RNA detection. Science 297, 1536-1540 (2002).

87. Mirkin, C. A., Letsinger, R. L., Mucic, R. C. & Storhoff, J. J. A DNA-based method for rationally assembling nanoparticles into macroscopic materials. Nature 382, 607-609 (1996).

88. Elghanian, R., Storhoff, J. J., Mucic, R. C., Letsinger, R. L. & Mirkin, C. A. Selective colorimetric detection of polynucleotides based on the distance-dependent optical properties of gold nanoparticles. Science 277, 1078-1080 (1997).

89. Xu, W., Xue, X., Li, T., Zeng, H. & Liu, X. Ultrasensitive and Selective Colorimetric DNA Detection by Nicking Endonuclease Assisted Nanoparticle Amplification. Angewandte Chemie International Edition 48, 6849-6852 (2009).
90. Li, H. & Rothberg, L. Colorimetric detection of DNA sequences based on electrostatic interactions with unmodified gold nanoparticles. Proceedings of the National Academy of Sciences of the United States of America 101, 14036-14039 (2004).
91. Chakrabarti, R. & Klibanov, A. M. Nanocrystals Modified with Peptide Nucleic Acids (PNAs) for Selective Self-Assembly and DNA Detection. Journal of the American Chemical Society 125, 12531-12540 (2003).
92. Su, X. & Kanjanawarut, R. Control of Metal Nanoparticles Aggregation and Dispersion by PNA and PNA-DNA Complexes, and Its Application for Colorimetric DNA Detection. ACS Nano 3, 2751-2759 (2009).
93. Kanjanawarut, R. & Su, X. Colorimetric Detection of DNA Using Unmodified Metallic Nanoparticles and Peptide Nucleic Acid Probes. Analytical Chemistry 81, 6122-6129 (2009).
94. Pan, B. et al. End-to-end self-assembly and colorimetric characterization of gold nanorods and nanospheres via oligonucleotide hybridization. Nanotechnology 16, 1776 (2005).
95. Parab, H. J., Jung, C., Lee, J.-H. & Park, H. G. A gold nanorod-based optical DNA biosensor for the diagnosis of pathogens. Biosensors and Bioelectronics 26, 667-673 (2010).
96. He, W. et al. One-Step Label-Free Optical Genosensing System for Sequence-Specific DNA Related to the Human Immunodeficiency Virus Based on the Measurements of Light Scattering Signals of Gold Nanorods. Analytical Chemistry 80, 8424-8430 (2008).
97. Lee, J.-S. & Mirkin, C. A. Chip-Based Scanometric Detection of Mercuric Ion Using DNA-Functionalized Gold Nanoparticles. Analytical Chemistry 80, 6805-6808 (2008).

98. Taton, T. A., Mirkin, C. A. & Letsinger, R. L. Scanometric DNA array detection with nanoparticle probes. Science 289, 1757-1760 (2000).
99. Xue, X., Xu, W., Wang, F. & Liu, X. Multiplex Single-Nucleotide Polymorphism Typing by Nanoparticle-Coupled DNA-Templated Reactions. Journal of the American Chemical Society 131, 11668-11669 (2009).
100. Nam, J.-M., Park, S.-J. & Mirkin, C. A. Bio-Barcodes Based on Oligonucleotide-Modified Nanoparticles. Journal of the American Chemical Society 124, 3820-3821 (2002).
101. Shim, S.-Y., Lim, D.-K. & Nam, J.-M. Ultrasensitive optical biodiagnostic methods using metallic nanoparticles. Nanomedicine 3, 215-232 (2008).
102. Kneipp, J., Kneipp, H. & Kneipp, K. SERS-a single-molecule and nanoscale tool for bioanalytics. Chemical Society Reviews 37, 1052-1060 (2008).
103. Kneipp, K., Kneipp, H., Itzkan, I., Dasari, R. R. & Feld, M. S. Ultrasensitive Chemical Analysis by Raman Spectroscopy. Chemical Reviews 99, 2957-2976 (1999).
104. Fabris, L. et al. A Heterogeneous PNA-Based SERS Method for DNA Detection. Journal of the American Chemical Society 129, 6086-6087 (2007).
105. Lim, D.-K. et al. Highly uniform and reproducible surface-enhanced Raman scattering from DNA-tailorable nanoparticles with 1-nm interior gap. Nat Nano 6, 452-460 (2011).
106. Bohren, C. F. & Huffman, D. R. Absorption and Scattering of Light by Small Particles (WILEY-VCH Verlag GmbH & Co. KGaA. Weinheim, 2004).
107. Kneipp, K. et al. Single Molecule Detection Using Surface-Enhanced Raman Scattering (SERS). Physical Review Letters 78, 1667-1670 (1997).
108. Graham, D., Thompson, D. G., Smith, W. E. & Faulds, K. Control of enhanced Raman scattering using a DNA-based assembly process of dye-coded nanoparticles. Nat Nano 3, 548-551 (2008).
109. Lim, D.-K., Jeon, K.-S., Kim, H. M., Nam, J.-M. & Suh, Y. D. Nanogap-engineerable Raman-active nanodumbbells for single-molecule detection. Nat Mater 9, 60-67 (2010).

110. He, L. et al. Colloidal Au-enhanced surface plasmon resonance for ultrasensitive detection of DNA hybridization. Journal of the American Chemical Society 122, 9071-9077 (2000).
111. Kurihara, K. & Suzuki, K. Theoretical Understanding of an Absorption-Based Surface Plasmon Resonance Sensor Based on Kretchmann's Theory. Analytical Chemistry 74, 696-701 (2002).
112. Campbell, C. T. & Kim, G. SPR microscopy and its applications to high-throughput analyses of biomolecular binding events and their kinetics. Biomaterials 28, 2380-2392 (2007).
113. Hutter, E. & Pileni, M. P. Detection of DNA hybridization by gold nanoparticle enhanced transmission surface plasmon resonance spectroscopy. Journal of Physical Chemistry B 107, 6497-6499 (2003).
114. Shankaran, D. R., Gobi, K. V. & Miura, N. Recent advancements in surface plasmon resonance immunosensors for detection of small molecules of biomedical, food and environmental interest. Sensors and Actuators B: Chemical 121, 158-177 (2007).
115. Tsoi, P. Y. & Yang, M. Surface plasmon resonance study of the molecular recognition between polymerase and DNA containing various mismatches and conformational changes of DNAâ€“protein complexes. Biosensors and Bioelectronics 19, 1209-1218 (2004).
116. Kindermann, M., George, N., Johnsson, N. & Johnsson, K. Covalent and Selective Immobilization of Fusion Proteins. Journal of the American Chemical Society 125, 7810-7811 (2003).
117. Baird, C. L., Courtenay, E. S. & Myszka, D. G. Surface plasmon resonance characterization of drug/liposome interactions. Analytical Biochemistry 310, 93-99 (2002).
118. Lyon, L. A., Musick, M. D. & Natan, M. J. Colloidal Au-Enhanced Surface Plasmon Resonance Immunosensing. Analytical Chemistry 70, 5177-5183 (1998).
119. Scanlon, K. J. Cancer Gene Therapy: Challenges and Opportunities. Anticancer Research 24, 501-504 (2004).

120. Viktoriya, S. & Matthias, E. Inorganic Nanoparticles as Carriers of Nucleic Acids into Cells. Angewandte Chemie International Edition 47, 1382-1395 (2008).
121. Giljohann, D. A., Seferos, D. S., Prigodich, A. E., Patel, P. C. & Mirkin, C. A. Gene Regulation with Polyvalent siRNA Nanoparticle Conjugates. Journal of the American Chemical Society 131, 2072-2073 (2009).
122. Seferos, D. S., Giljohann, D. A., Hill, H. D., Prigodich, A. E. & Mirkin, C. A. Nano-Flares: Probes for Transfection and mRNA Detection in Living Cells. Journal of the American Chemical Society 129, 15477-15479 (2007).
123. Salem, A. K., Searson, P. C. & Leong, K. W. Multifunctional nanorods for gene delivery. Nature Materials 2, 668-671 (2003).
124. Prigodich, A. E., Alhasan, A. H. & Mirkin, C. A. Selective Enhancement of Nucleases by Polyvalent DNA-Functionalized Gold Nanoparticles. Journal of the American Chemical Society 133, 2120-2123 (2011).
125. Weissleder, R. A clearer vision for in vivo imaging. Nature Biotechnology 19, 316-317 (2001).
126. Lee, S. E., Liu, G. L., Kim, F. & Lee, L. P. Remote Optical Switch for Localized and Selective Control of Gene Interference. Nano Letters 9, 562-570 (2009).
127. Huschka, R. et al. Light-Induced Release of DNA from Gold Nanoparticles: Nanoshells and Nanorods. Journal of the American Chemical Society 133, 12247-12255 (2011).
128. Barhoumi, A., Huschka, R., Bardhan, R., Knight, M. W. & Halas, N. J. Light-induced release of DNA from plasmon-resonant nanoparticles: Towards light-controlled gene therapy. Chemical Physics Letters 482, 171-179 (2009).
129. Yamashita, S. et al. Controlled-release system of single-stranded DNA triggered by the photothermal effect of gold nanorods and its in vivo application. Bioorganic & Medicinal Chemistry 19, 2130-2135 (2011).
130. Link, S., Burda, C., Nikoobakht, B. & El-Sayed, M. A. Laser-Induced Shape Changes of Colloidal Gold Nanorods Using Femtosecond and Nanosecond Laser Pulses. The Journal of Physical Chemistry B 104, 6152-6163 (2000).

131. Takahashi, H., Niidome, Y. & Yamada, S. Controlled release of plasmid DNA from gold nanorods induced by pulsed near-infrared light. Chemical Communications, 2247-2249 (2005).
132. Horiguchi, Y., Niidome, T., Yamada, S., Nakashima, N. & Niidome, Y. Expression of Plasmid DNA Released from DNA Conjugates of Gold Nanorods. Chemistry Letters 36, 952-953 (2007).
133. Chen, C.-C. et al. DNA Gold Nanorod Conjugates for Remote Control of Localized Gene Expression by near Infrared Irradiation. Journal of the American Chemical Society 128, 3709-3715 (2006).
134. Wijaya, A., Schaffer, S. B., Pallares, I. G. & Hamad-Schifferli, K. Selective Release of Multiple DNA Oligonucleotides from Gold Nanorods. ACS Nano 3, 80-86 (2008).
135. Hamad-Schifferli, K., Schwartz, J. J., Santos, A. T., Zhang, S. & Jacobson, J. M. Remote electronic control of DNA hybridization through inductive coupling to an attached metal nanocrystal antenna. Nature 415, 152-155 (2002).
136. Derfus, A. M. et al. Remotely Triggered Release from Magnetic Nanoparticles. Advanced Materials 19, 3932-3936 (2007).
137. Giljohann, D. et al. Gold Nanoparticles for Biology and Medicine. Angewandte Chemie International Edition 49, 3280-3294 (2010).
138. Jin, R. C., Wu, G. S., Li, Z., Mirkin, C. A. & Schatz, G. C. What controls the melting properties of DNA-linked gold nanoparticle assemblies? Journal of the American Chemical Society 125, 1643-1654 (2003).
139. Park, S. J., Taton, T. A. & Mirkin, C. A. Array-based electrical detection of DNA with nanoparticle probes. Science 295, 1503-1506 (2002).
140. Li, Z., Zhang, Y., Fullhart, P. & Mirkin, C. A. Reversible and chemically programmable micelle assembly with DNA block-copolymer amphiphiles. Nano Letters 4, 1055-1058 (2004).
141. Alemdaroglu, F. E., Ding, K., Berger, R. & Herrmann, A. DNA-templated synthesis in three dimensions: Introducing a micellar scaffold for organic reactions. Angewandte Chemie-International Edition 45, 4206-4210 (2006).

142. Jeong, J. H. & Park, T. G. Novel Polymer-DNA Hybrid Polymeric Micelles Composed of Hydrophobic Poly(d,l-lactic-co-glycolic Acid) and Hydrophilic Oligonucleotides. Bioconjugate Chemistry 12, 917-923 (2001).

143. Chen, X.-J. et al. Self-Assembled Hybrid Structures of DNA Block-Copolymers and Nanoparticles with Enhanced DNA Binding Properties. Small 6, 2256-2260 (2010).

Chapter 2. Multifunctional DNA Block Copolymer Nanostructures: Synthesis and Self-Assembly[3]

2.1 Overview

This chapter presents detailed procedures on (1) the synthesis and characterization of DNA di- and tri-block copolymers and (2) the self-assembly of the synthesize DNA block copolymers and encapsulants (e.g. nanoparticles, homopolymers, small molecules, etc). Two different routes are presented for the synthesis of DNA block copolymer, with the major difference in the coupling step of the DNA with the organic polymer.

2.2 Background on DNA Block Copolymer Synthesis

The synthesis of amphiphilic DNA block copolymer has been previously reported by several groups.[1, 2] The first example of DNA block copolymer synthesized using solid

[3] Reprint in parts with permission from Chen, X.-J.; Sanchez-Gaytan, B. L.; Hayik, S. E. N.; Fryd, M.; Wayland, B. B.; Park, S.-J.: *Self-Assembled Hybrid Structures of DNA Block-Copolymers and Nanoparticles with Enhanced DNA Binding Properties.* Small. **2010**;6(20):2256-2260..Copyright 2010 Wiley-VCH Verlag GmbH & Co. KGaA

state synthesis (**Scheme 2-1**) was reported by the Mirkin group from Northwestern for the synthesis of DNA-*b*-PS,[1] followed by the Herrmann group from University of Groningen (The Netherlands) with DNA-*b*-PPO.[2] Other examples of DNA block copolymer synthesized not using solid-state synthesis, that is the DNA and polymer are coupled post DNA synthesis have been reported by a number of groups. The type of chemistry used to covalently link the two blocks together include "click" chemistry such as CuAAC and Michael's Addition, carboiimide-N-hydroxylsuccinimide (EDC-NHS), and dithiol reaction. (**Scheme 2-2**)

It has been shown that all these examples of amphiphilic DNA block copolymer can self-assemble to form micelles in water.[1, 3] It was reported for the case of DNA-*b*-PS that these micellar self-assemblies of the DNA block copolymer have similar properties as DNA functionalized gold particles in terms of sharp melting[1], thus eluting to a high DNA density on micelle surfaces.

2.3 Solid-state Synthesis of DNA Block Copolymers

The following procedures describe the synthesis of one specific example of DNA block copolymer, DNA-*b*-PS, having a fluorescein (FAM)-modified oligonucleotide with sequence of 5'-FAM A_{10} ATC CTT ATC AAT ATT-3' and polystyrene (PS, MW = 10.4 kg/mol) (DNA-FAM-*b*-PS). The polymer is attached at the 5' end of DNA. The DNA block copolymer is prepared by solid-state synthesis by standard phosphoramidite chemistry. [4,1] Briefly, hydroxyl-terminated PS was converted to phosphoramidite-terminated PS, which was subsequently coupled to the 5' end of the oligonucleotides synthesized on controlled pore glass (CPG) beads (**Figure 2-1B**). Unreacted polymers

Scheme 2-1. Solid-state synthesis of DNA block copolymer.

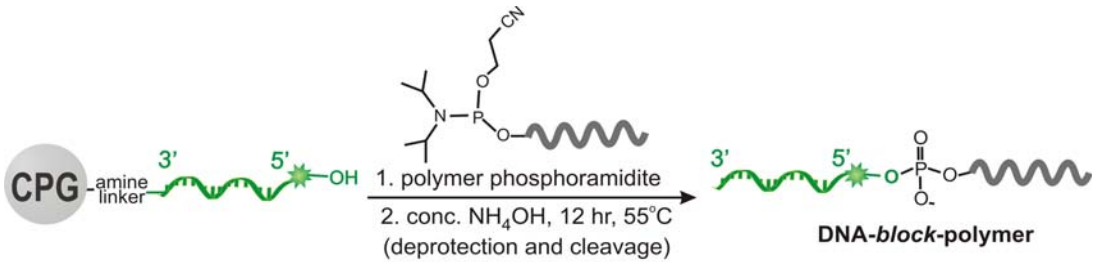

Scheme 2-2. Post-DNA cleaving synthesis of DNA block copolymer.

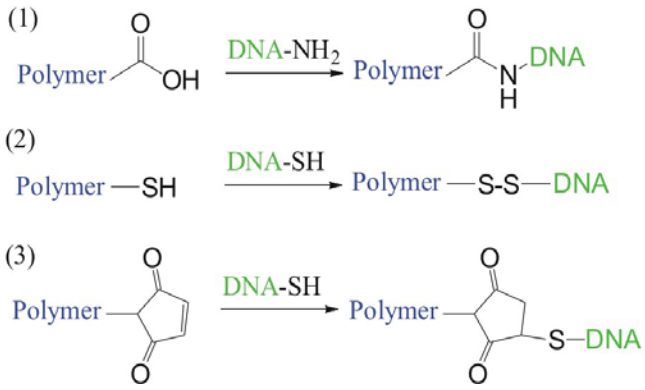

were washed from the CPG beads, and the DNA block copolymers were deprotected and cleaved from the solid support with concentrated ammonium hydroxide. Other types of DNA block copolymers can be synthesized in a similar fashion using different hydroxyl-terminated polymers.

2.3.1 Solid-state DNA Synthesis

A 10 umol scale synthesis of oligonucleotide strand 5'-Fluoracesein-A_{10} ATCCTTATCAATATT-3' was carried out using standard solid state DNA synthesis. Appropriate amounts of anhydrous acetonitrile, 18.77 mL, 10 mL , 8 mL and 1 mL, was added to crimped vials containing dA-CE (1.0 g), dT-CE (0.5 g), dC-CE (0.5g) and 6-fluorescein (100 μmol) phosphoramidites, respectively, and the vials were swirled gently to make sure that the reagents were completely dissolved. A solid state synthesis column for a 10 μmol synthesis was prepared by weighing out 0.33 mg of dT-CE CPG beads (1000Å) and loaded into empty crimped style synthesis columns.

The CPG support column and the CE-phosphoramidite bottles were connected to the appropriate dedicated spots on the DNA synthesizer. Enter the DNA sequence (5'-A_{10} ATC CTT ATC AAT ATT-3'), select 10 μmol synthesis method, choose the option to keep the trityl end group "on", and start the synthesis. When the synthesis is complete, the fluorescein dye (FAM) was added at the 5' end of the oligonucleotide by selecting the 10 μmol synthesis method again, and entering DNA sequence of 5'**X**A3', where X denotes the position of the bottle containing the dye-phosphoramidite on the DNA synthesizer. Select the option to keep the trityl end group "on". The synthesis of a dye-

modified DNA can be performed in one step instead of the two-steps described in the procedure by programming in the sequence (5'-**X**A_{10} ATC CTT ATC AAT ATT-3'), where **X** denotes the position of the FAM phosphoramidite.

2.3.2 Synthesis of Phosphoramidite-Terminated Polymer

For the synthesis of phosphoramidite terminated-PS, 4.16 g (0.4 mmol) of hydroxyl-terminated PS (Mn = 10.4 Kg/mol) was added to a 3-neck round bottom flask equipped with a PTFE-coated magnetic stir bar, a Schlenk line adapter and two rubber stoppers. The reaction flask containing the polymer was vacuumed and then purged with argon three times. Under a gentle flow of argon, 15 mL of anhydrous dichloromethane was added to the reaction flask with stirring to allow the polymer to dissolve completely. 0.378 mL (1.68 mmol) of chlorophosphoramidite and 0.290 mL (1.68 mmol) of anhydrous diisopropylethylamine was added to the reaction flask. The solution was allowed to stir for three hours under a blanket of argon. The crude product is light yellow in color. The product was analyzed by ^{31}P NMR. The signal for phosphoramidite-terminated PS is at δ = 147 ppm. Note that phosphoramidite-terminated polymer is highly prone to oxidation to become phosphate, thus no purification was carried out to avoid the possibility of exposure to oxygen. ^{31}P NMR can be calibrated by adding an internal standard trioctylphosphine (TOP), with a ^{31}P NMR peak at -30 ppm.[17] The hydrolyzed chlorophosphoramidite has a peak at ~0 to 18 ppm. The unreacted chlorophosphoramidite has a peak at 180 ppm.

2.3.3 Synthesis of DNA-block-Polystyrene

The DNA on CPG solid support was manually detriylated by pushing detritylation solution through the supporting column containing the beads using a syringe until no orange color is observed. The beads were dried by blowing a stream of argon gas through the column. The dried CPG beads containing the synthetic oligonucleotides prepared in the previous section was added into the round bottom flask equipped with a stir bar and Schlenk line adapter and two rubber stoppers. 3 mL of anhydrous dichloromethane was added to the CPG beads to avoid static cling while the flask is purged with a gentle stream of argon for ten minutes. The phosphoramidite-terminated PS was transferred to the flask containing the DNA on CPG beads as fast as possible by cannula to reduce the exposure to oxygen. 15 mL of dimethylformamide was then added to make a 1:1 DMF:CH_2Cl_2 solution to resolve the solubility difference between DNA and PS . 2.7 mL of activator solution was added to the flask at 3:1 molar ratio of activator: phosphoramidite-terminated PS. The reaction was stirred for a few hours or overnight under a blanket of argon.

The reaction was stopped and stirring turned off to allow the CPG to settle to the bottom. The supernatant of the reaction was decanted and the beads were washed with 5 aliquots of 10 mL chloroform to remove unreacted polymer. The beads were then dried with a gentle stream of argon, collected, and packed them back into the solid support column. The phosphoramidite was oxidized to phosphate by passing the oxidation solution through the column with a syringe drop wise for 2 min. The beads were rinsed with acetonitrile until no yellow color from the iodine in the oxidation solution is observed on the beads. Dry the beads and transfer them to a scintillation vial. 10 mL of

concentrated ammonium hydroxide was added to the beads and leave undisturbed for 6 to 12 hrs at 55°C. ***Caution****:* During this step, ammonia is produced as a by-product from the degradation of ammonium hydroxide. Therefore, be cautious when opening the vial after the reaction. Cool down the solution to room temperature before opening the vial, and open the vial in a well-ventilated hood.

Separate the supernatant from the CPG beads by gravity filtration This fraction contains mainly uncoupled DNA strands and a small amount of DNA block copolymers. The beads were washed with two 5 mL aliquots of DMF, and collect the DMF solution in a separate vial. This fraction contains mainly DNA block copolymers. The synthesis yield 2 umol of DNA-*b*-PS (2% yield).

The fractions were characterized by UV-visible spectroscopy and photoluminescence (PL) spectroscopy. Emission spectrum of DNA-*b*-PS in water was collected with the excitation wavelength at 490 nm to check the presence of the FAM dye in DNA. The concentration of FAM-modified DNA-*b*-PS in DMF was determined using the extinction coefficient of FAM in DMF at 518 nm (1.3×10^4 $M^{-1}cm^{-1}$) using UV-vis spectroscopy. The extinction coefficient of FAM in DMF was determined by creating a calibration curve by preparing a series of dilutions from a stock solution of FAM in DMF. The extinction coefficient provided is the average of three measurements.

The hydrodynamic diameter of simple micelles of DNA-*b*-PS in water (PS@DNA) was determined by DLS using Malvern Zetasizer. The average of three separate measurements was 15 ± 4 nm (**Figure 2-2C**). The DNA block copolymer product was further characterized by gel electrophoresis using a 3% agarose gel. The gel was prepared by dissolving 1.5g of agarose with 50 mL of 1x TAE buffer with heating in

a microwave oven for 2 min. The gel by pouring the solution into the gel tray and allow it to cool and solidify. 2 μL of loading buffer was added to 10 μL DNA samples (10 pmol). Enough 1x TAE buffer was added to cover the gel, and the sample was loaded into the well and the gel was ran at 60 V for 1 hr. The gel was imaged under UV lamp (**Figure 2-2E**).

2.3.4 Self-Assembly of DNA Block Copolymers

Nano- and meso-scale structures were prepared from the self-assembly of DNA block copolymers by the slow addition of water to the samples containing DNA block copolymers. (**Scheme 2-3**)

2.3.4.1 Simple Micelles

Simple micelles of DNA-FAM-*b*-PS *(PS@DNA)* were prepared by the slow addition of purified water (300 μL) to a solution of DNA block copolymers (3 nmol, 1 mL) in DMF at a rate of 10 μL at every 30 sec time intervals for 15 min. After overnight stirring, 1 mL of purified water was added to the solution, and subsequently dialyzed against water for one day.

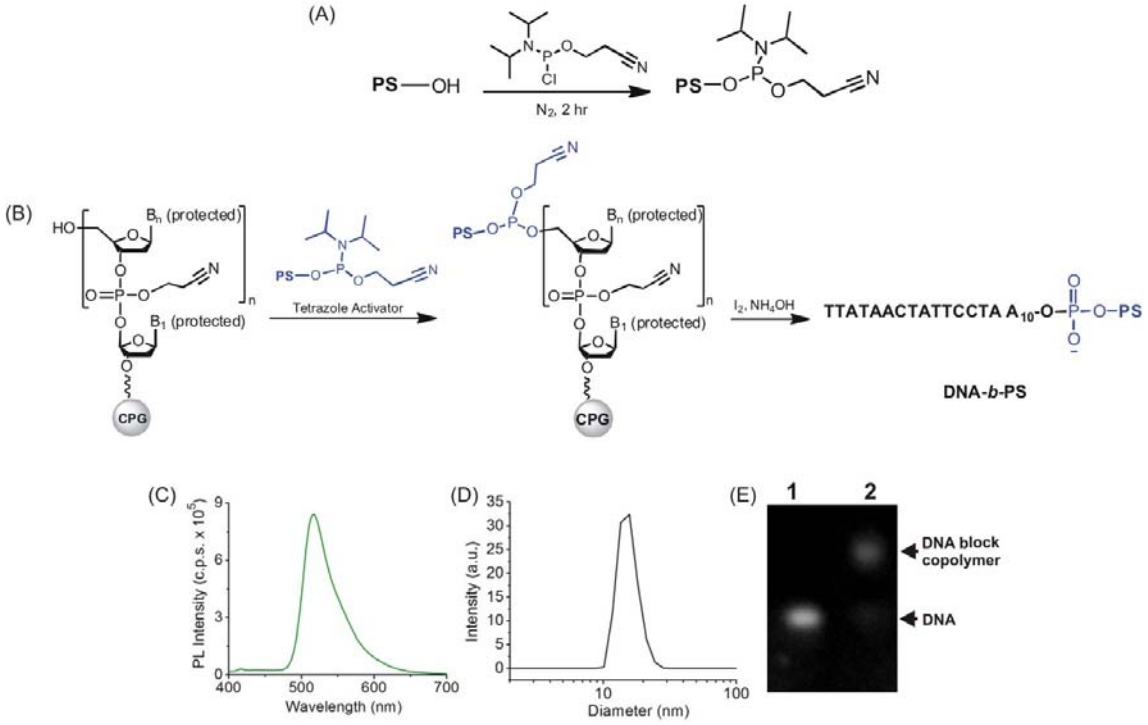

Figure 2-1. (A, B) Solid state DNA synthesis of DNA-*b*-Polystyrene (DNA-*b*-PS), (A) Phosphormaidite-terminated PS and (B) coupling of polymer with DNA on CPG beads. (C) An emission spectrum of FAM- labeled DNA-*b*-PS dispersed in water. (D) DLS data of simple micelles of DNA-*b*-PS (PS@DNA) in water. (E) Gel electrophoresis result for 1) DNA and 2) PS@DNA.

2.3.5 Nanoparticle-Encapsulated Meso-scale Assemblies

2.3.5.1 Synthesis of Oxide and Gold Nanoparticles

Oleic acid-stabilized iron oxide magnetic nanoparticles (MNP) with a diameter of 4.5 nm were synthesized by the thermal decomposition method following a reported procedure.[5] The purified MNP were dispersed in chloroform to make a 5 mg/mL stock solution. Citrate-stabilized gold nanoparticles (AuNP) with a diameter of 36 ± 6 nm were synthesized following a reported procedure.[6] For the preparation of PS-modified AuNP, the AuNP were transferred to dimethylformamide (DMF) by first adding DMF (500 μL) to an aqueous solution of AuNP (500 μL) and redispersing them in DMF by centrifugation (6,000 rpm, 30 min). This procedure was repeated two more times. The final solution of AuNP dispersed in DMF was concentrated to make a 15 nM solution.

2.3.5.2 Synthesis of Polymer-grafted Nanoparticles

Nanoparticles (50 μL of stock solution) were dispersed in a 500 μL solution of carboxyl-terminated polystyrene in DMF (MW= 6K g/mol, approximately 1000-fold excess to calculated number of surfactants on the nanoparticle). The solution was left stand overnight and precipitated with acetone (1 mL). The supernatant containing un-grafted polymer was decanted and the precipiates were resuspended in DMF. The concentration of purified PS-modified MNP and PS-modified AuNP were adjusted to 1 mg/mL and 1 nM, respectively.

Scheme 2-3. (A) Nano- and (B) meso-scale structures of DNA block copolymer self-assembly.

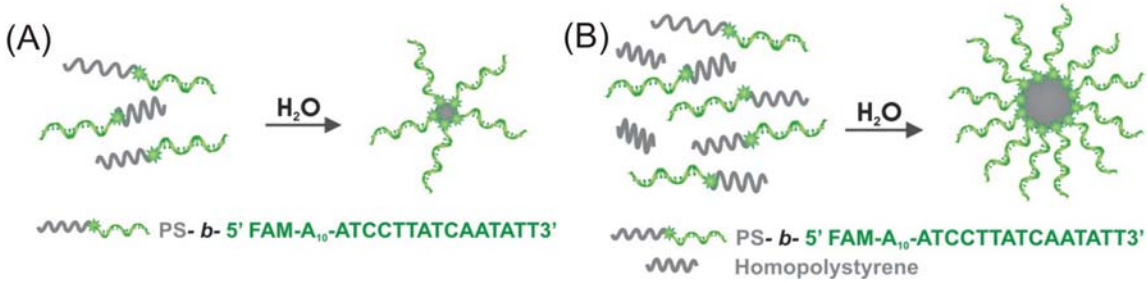

2.3.5.3 Self-assembly of DNA BCP with Nanoparticles

Typically, core-filling polymer-grafted nanoparticles (10 μL, 1 mg/mL) were mixed with a DMF solution of DNA block copolymers (3 nmol, 1 mL). (**Scheme 2-3B**) To induce self-assembly, 300 μL of purified water was slowly added to the nanoparticle/polymer mixture in DMF (10 μL at every 30 sec interval for a period of 15 min). After overnight stirring, 1 mL of purified water was added to the solution and it was subsequently dialyzed against water for one day. PS-filled assemblies were prepared following the similar procedure as polymer-grafted nanoparticles, where 10 μL of a 2 mg/mL PS (MW= 6K g/mol) stock solution was added in place of nanoparticles. The assemblies were then purified by decanting off the supernatant after centrifugation at 14,000 rpm for 45 min. The collected assemblies were subsequently vortexed to suspend them back into water.

2.4 Synthesis of Biodegradable DNA Block Copolymer via Click Chemistry

For the biomedical applications we intended to use the DNA block copolymer assemblies, we have decided to synthesize a new DNA block copolymer that is biocompatible/biodegradable. The first reported biodegrable DNA block copolymer was synthesized by the Park group form KAIST (Korea) consisting of a (PLGA) block.[7] Although, there is a recent report on the solid-state synthesis of DNA-*b*-PCL, and the authors reported micelle structures were obtained. However, the authors failed to characterize the final integrity of the PCL polymer after the harsh cleaving step using

ammonia hydroxide. In a control study, we have observed that PCL degrades rapidly in the presence of concentrated ammonia hydroxide (**Figure 2-2**).

A biocompatible DNA triblock copolymer, DNA-*b*-polyethylene oxide-b-polycaprolactone (DNA-*b*-PEO-*b*-PCL), was synthesized to further the study of the antisensing experiments. Both PCL and PEO constructing the DNA BCP are FDA-approved biocompatible polymers. In addition, PCL is degradable, thus can be used to control the release of the drug payloads when needed, and this can be controlled by the addition of a short polybutylene oxide (PBO) segment to slow down the enzymatic degradation process of the PCL.

2.4.1 Synthesis of DNA-*b*-PEG-*b*-PCL

The triblock copolymer was synthesized in a three-step process (**Scheme 2-4**). Azide-terminated polyethylene oxide-block-polycaprolactone was prepared first by synthesizing a hetero-functionalized polyethylene oxide polymer,[8] with an azide moiety on one end and the hydroxyl group on the other via anionic polymerization (step 1). The hetero-terminated PEO was subsequently used as a macro-initiator for the ring opening polymerization of polycaprolactone to yield a diblock copolymer of azide-terminated PEO-*b*-PCL (step 2). This block copolymer self-assembles with the addition of water into the common organic solvent, in which they are dissolved, into fiber-like structure with the azide moieties on the PEO exposed. The exposed azide grounds were then subsequently coupled with alkyne-terminated DNA via Copper-Catalyzed Azide-Alkyne Cycloaddition (CuAAC), “click” chemistry (step 3).

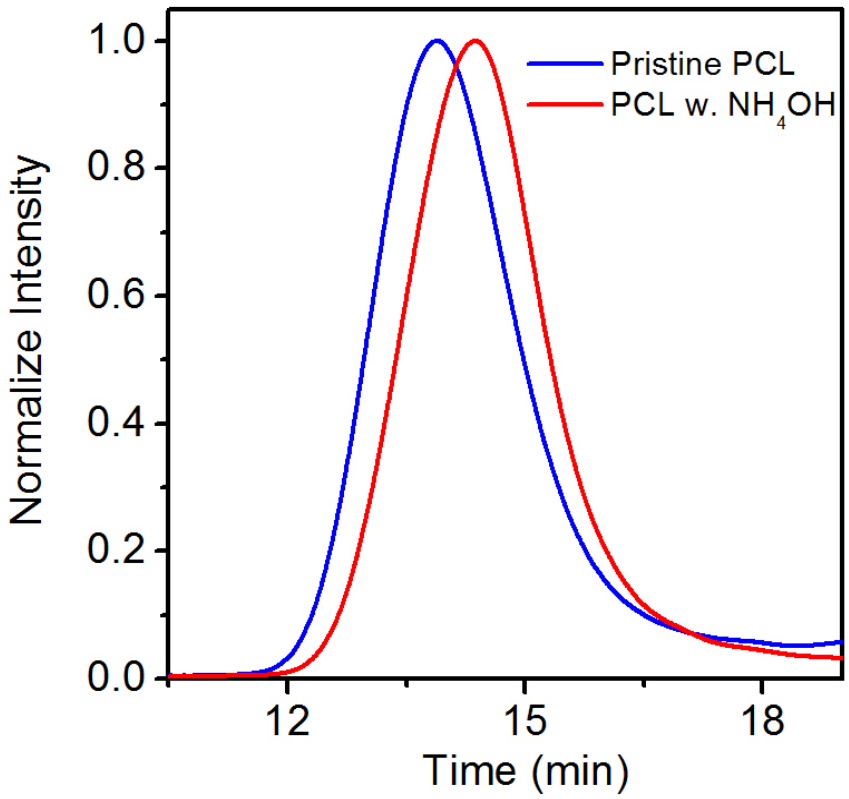

Figure 2-2. GPC chromatograph of pristine PCL and PCL after exposure to concentrated ammonium hydroxide in DMF.

Heterbifunctional polyethylene glycol was synthesize following a previously reported method.[8]

The block copolymer was successfully synthesized. The final and intermediate products were characterized by GPC and/or NMR, **Figure 2-3**.

2.4.1.1 Self-Assembly of PEG-*b*-PCL

Self-assembled structures of azide-terminated PEG-*b*-PCL were prepared by the slow water addition method. In a typical experiment, 400 uL of the block copolymer solution in THF (2mg/mL) was diluted to 1 mL in total volume with THF. Shown in **Figure 2-4** is a plot of the different assembled structures from the different length of PEG-*b*-PCL.

2.4.1.2 Stability of PEG-*b*-PCL

Stability studies on PEG-*b*-PCL were performed on the self-assemblies. It was determined that the structure in water is very stable. As shown in **Figure 2-5**, PEG-*b*-PCL assemblies in water after a period of one month did not show signs of degredation based on GPC.

Scheme 2-4. Synthesis of Biodegradable DNA Triblock Copolymer DNA-*b*-PEO-*b*-PCL

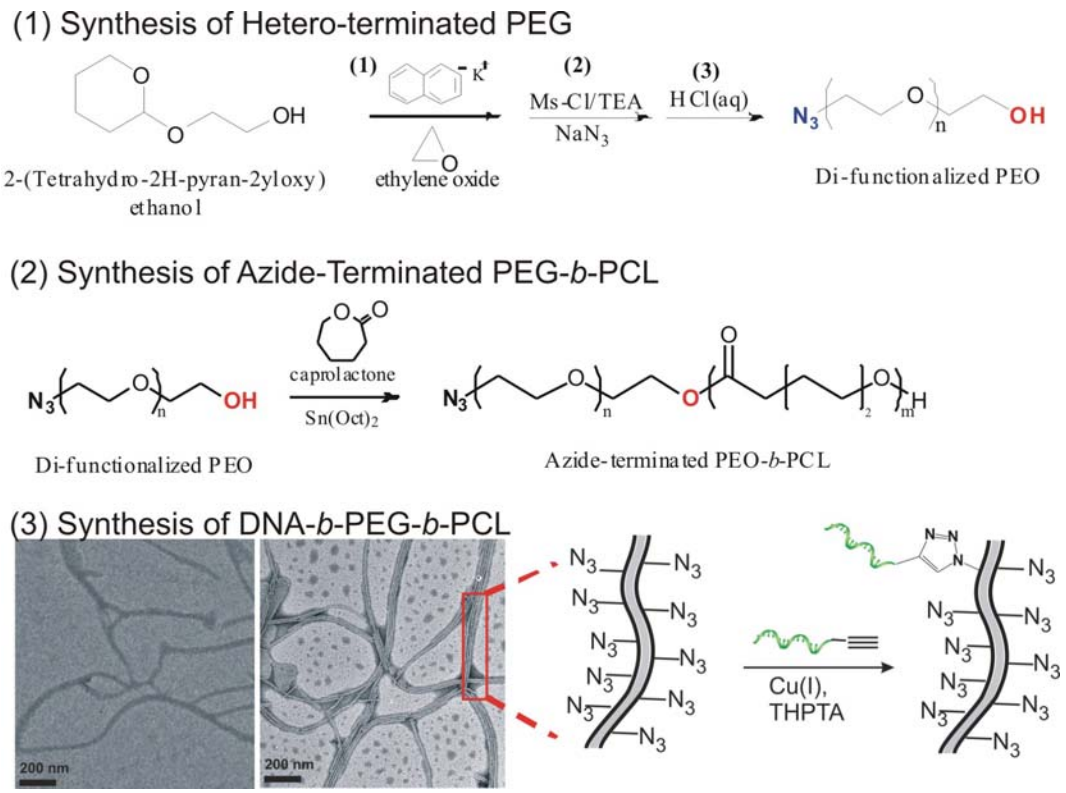

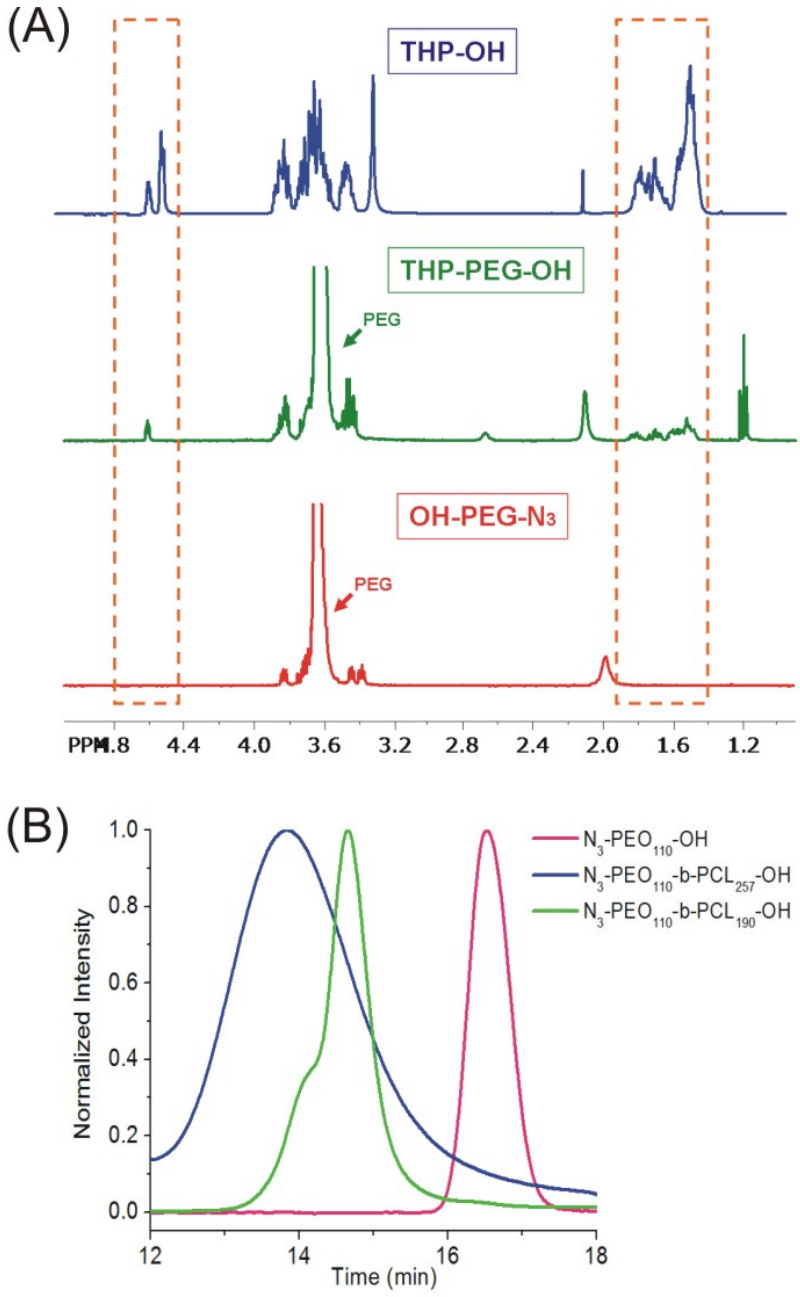

Figure 2-3. Synthesis and characterization of PEG-*b*-PCL (A) THP-PEG, (B) N3-PEG-OH, (C) N3-PEG-*b*-PCL-OH

2.4.1.3 Alternative Synthetic Routes and Their Problems

It has been determined that some of the azide functional groups on the azide-terminated PEG degrade due to high temperature at which the ring-opening polymerization of polycaprolactone is performed. To circumvent this problem, alternative synthetic routes (**Scheme 2-5**) were developed where the azide functionalization step was performed after the ring opening polymerization method. In the first alternative scheme (**Scheme 2-5A**), the order of the PEG and PCL synthesis was reversed, where PCL was synthesized first followed by the anionic synthesis of PEG using hydroxyl terminated PCL as a macroinitiator. The assemblies obtained from the resulting polymer are mainly vesicles and bilayer structures (**Figure 2-6**) that are greater than 500 nm in size, which is not ideal as delivery agents into cells. Moreover, these methods however, were found to degrade PCL during the azide-functionalization steps due to the presence of triethylamine base used in the reaction (**Figure 2-7**). Therefore, we reverted back to the original synthetic scheme for the synthesis of axide-functionalized PEG-*b*-PCL for the CuAAC reaction.

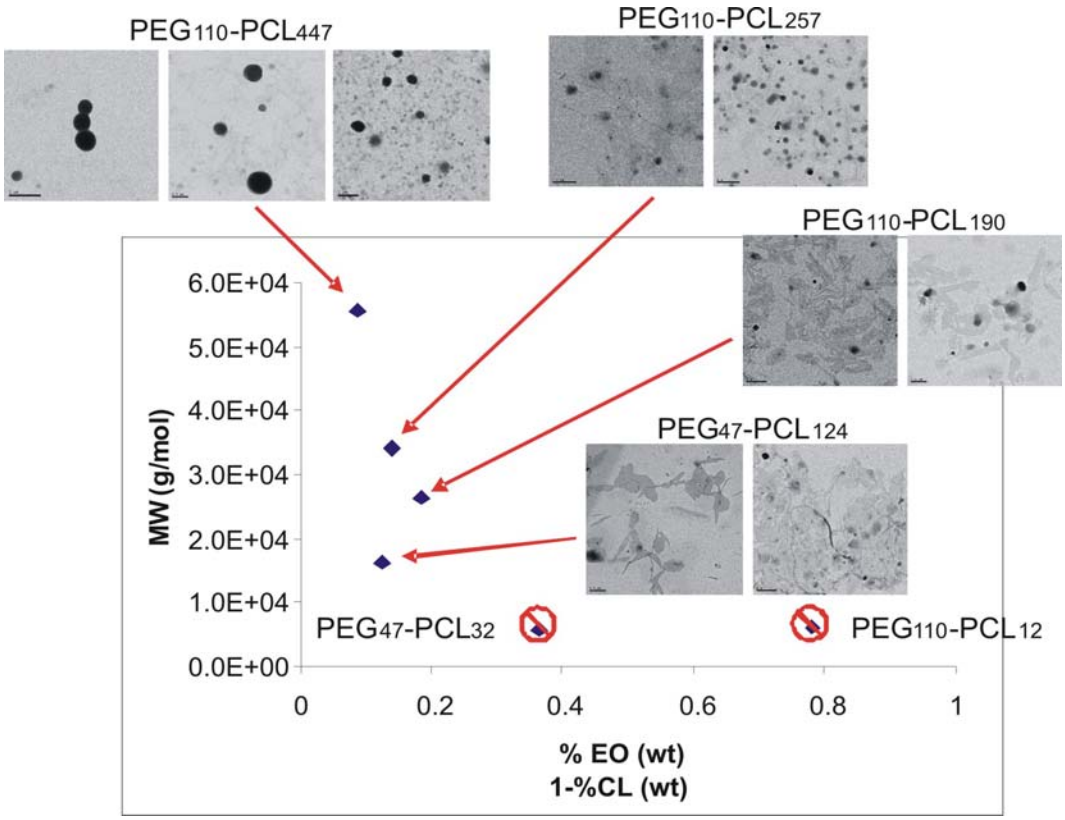

Figure 2-4. Various molecule weights of azide-PEG-*b*-PCL-OH

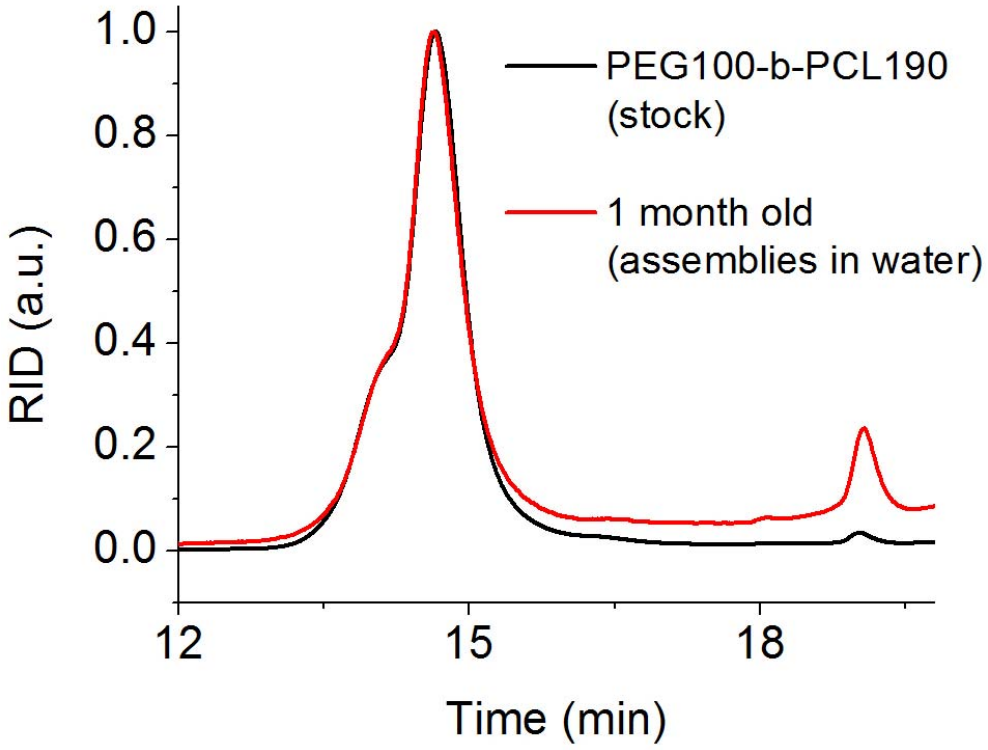

Figure 2-5. GPC chromatograph of pristine PEG-*b*-PCL and PEG-*b*-PCL after being suspended in water in the self-assembled form after a period of one month.

Scheme 2-5. Alternative Synthetic Methods (A) Pyrene-PCL (B) THP-PEG, bi-azide

(A) Alternative Synthesis #1

(1) Synthesis of Pyrene-terminated PCL

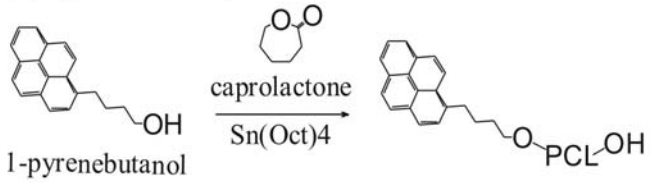

(2) Synthesis of Pyrene-terminated PCL-*b*-PEO

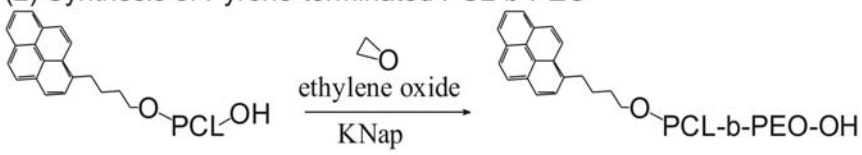

(3) Azide Functionalization Pyrene-terminated PCL-*b*-PEO

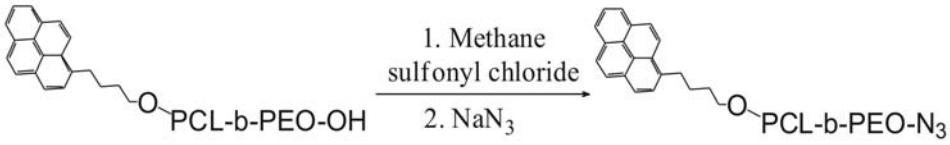

(B) Alternative Synthesis #2

(1) Synthesis of THP-terminated PEO

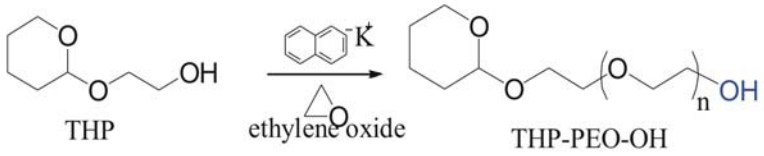

(2) Synthesis of THP-terminated PEO-*b*-PCL

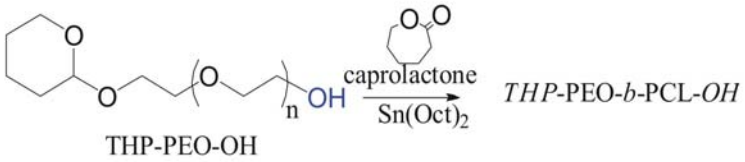

(3) Bis-azide Functionalization of PEO-*b*-PCL

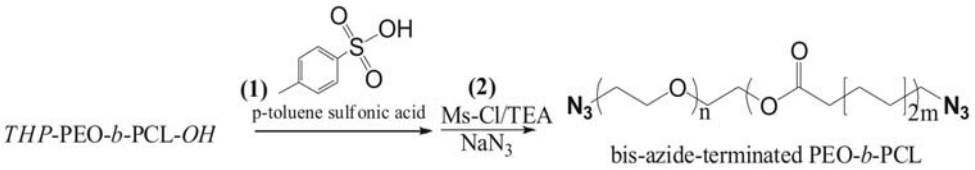

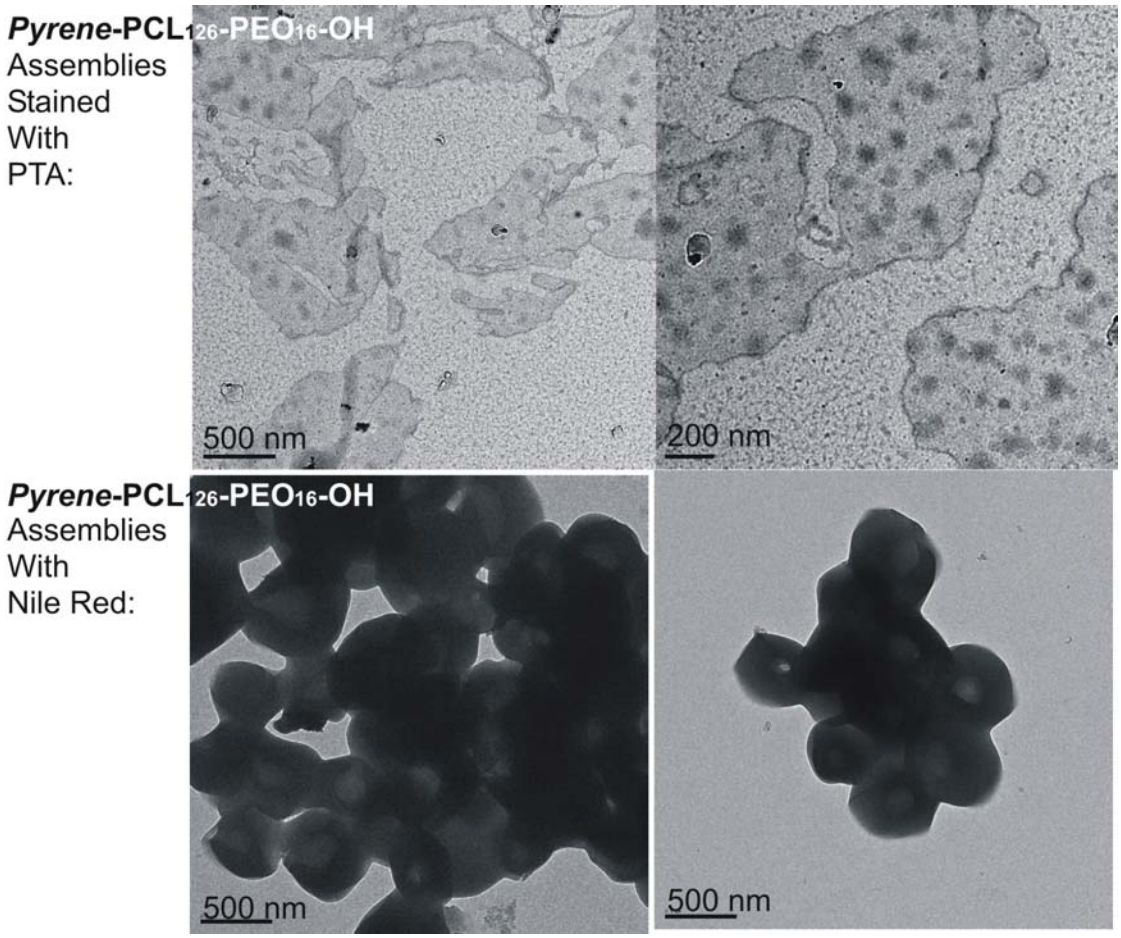

Figure 2-6. Assemblies of Pyrene-PCL-*b*-PEO-OH

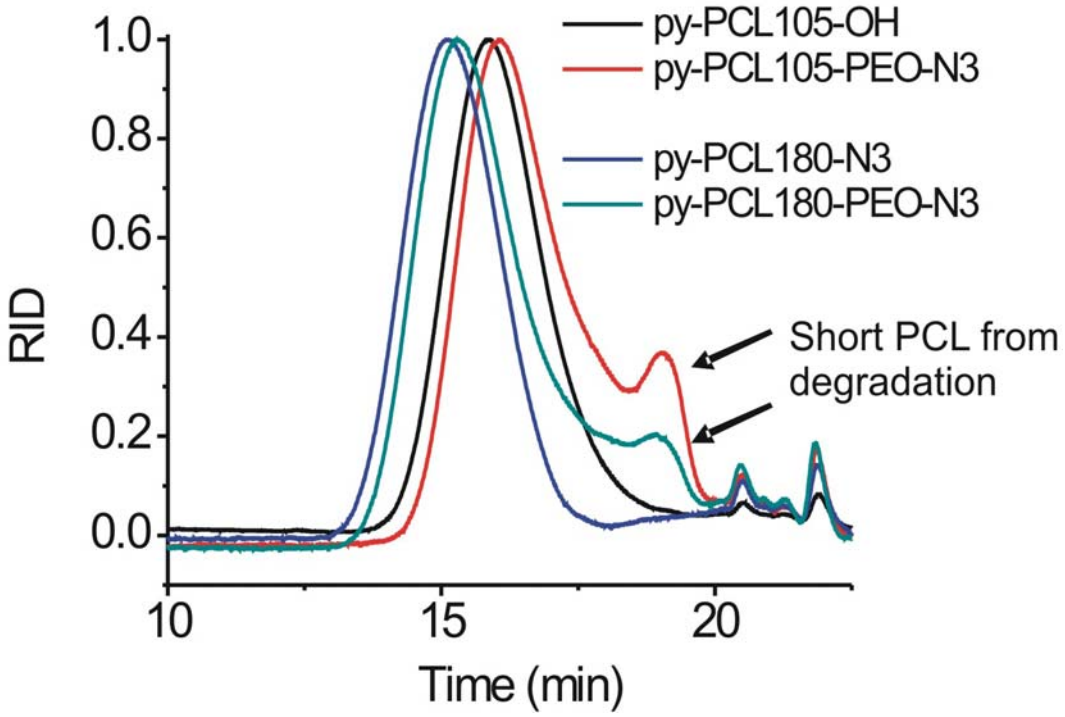

Figure 2-7: Degradation of PCL in alternative synthesis method of PEG-*b*-PCL block copolymer.

2.4.1.4 Synthesis of THPTA

In copper assisted coupling chemistry, the major concern of using CuAAC for the coupling with DNA is the free Cu(I) ions which degrades DNA by cleaving the phosphate backbone. In order to circumvent this problem, it has been reported that the ligand tris[(1-benzyl-1H-1,2,3-triazol-4-yl)methyl]amine (TBTA) are able to stabilize Cu(I) ions during the clicking process. However, as a result of the solubility issue in our synthesis scheme, TBTA cannot be used due to its poor solubility in water. A water-soluble derivative of TBTA, tris(3-hydroxypropyltriazolymethyl)amine (THPTA) was synthesized following the procedures of a previous report.[9]

The synthesis is composed of two steps (**Scheme 2-6**), first is the synthesis of 3-azido-1-propanol which is subsequently used in the synthesis of THPTA. For the synthesis of 3-azido-1-propanol, 3-bromo-1-propanol was converted to the azido form by mixing with sodium azide in a 1:2 mole ratio in water at 45°C overnight, follow by extraction with dimethylchloride and dry with magnesium sulfate. In the second step, the purified 3-azido-1-propanol was mixed with tripropargylamine under inert atmosphere in 4:1 mole ratio in THF. Copper acetate was then added to the solution. The solution was then refluxed overnight. The solution was then concentrated and dissolve in water and then stir in resin to remove copper ions. The filtered product is a yellowish oil/solid, which then was dispersed in acetonitrile and sonicated to break the solid. The product was then analyzed by NMR.

Scheme 2-6. Synthesis of THPTA

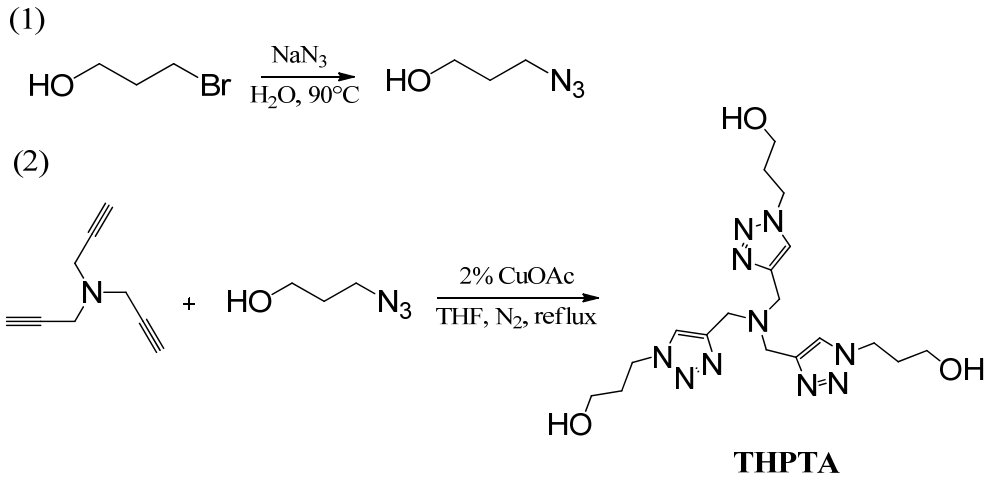

THPTA

2.4.1.5 CuAAC "Click" Chemistry

Self-assembly of azide-terminated PEG-*b*-PCL in water can yield either spherical or more interestingly fibril structure. By TEM, the diameter of the spherical nanostructures is about 100 nm, and the dimension of the fibril structure is roughly 20 nm in diameter and can go up to microns in length. The structure is expected to have a structure with a hydrophobic PCL core and a hydrophilic PEG corona. This is confirmed by selectively staining PEG with phosphotungstic acid (PTA).

In a typical CuAAC "click" reaction, solutions of copper (II) sulfate ($CuSO_4$, 4 mM), THPTA (10 mM) and sodium ascorbate (20 mM) were prepared. PEG-*b*-PCL self-assembled structures suspended in water (100 uL, 20 nmol azide moiety). A stock solution of 5' Alkyne- and FAM-modified DNA (Integrated DNA Technology) was prepared in water. The reaction was carried out with the mole ratio of azide:alkyne:Cu:THPTA:sodium ascrobate of 1:1:30:1:50. The reaction was allowed to stand at room temperature for 6 to 8hr.

The assemblies after DNA conjugation was separated from the uncoupled DNA by centrifugation at 14K for 1hr. To the collected precipitate, a solution of ethylenediaminetetraacetic acid (EDTA) was added to the reaction mixture to quench the reaction by chelation of EDTA to copper ions. The EDTA/Cu complex was then removed by dialysis against water for 3 days with frequent change of the water. The solution with the assemblies were then concentrated to a desired concentration.

2.4.1.6 Integratity of DNA after CuAAC "Click" Reaction

Thermal denaturation on the DNA of the DNA-*b*-PEG-*b*-PCL assemblies were performed to determine the integrity of the DNA after CuAAC "click", as mentioned in **section 2.4.1.4**, the presence of free copper (I) ion can damage the backbone of the DNA. As shown in **Figure 2-8,** DNA strands on the DNA-*b*-PEG-*b*-PCL are nearly identical in terms of melting temperature (T_m) compared to pristine DNA strands what were not exposed to the copper ions.

2.4.2 Synthesis of DNA-*b*-PEG-*b*-PBO-*b*-PCL

As shown in **section 2.4.1.2**, the PEG-*b*-PCL assemblies are stable in water for a long period of time without showing signs of degradation. However, in our preliminary studies with using these constructs as carriers, we have found that these assemblies tend aggregate over time. This observation was confirmed by static scattering experiments with polymer constructs incubated in cell medium under the same conditions used for cell uptake experiments (**Chapter 4**). As shown in **Figure 2-10A**, by measuring the scattering at 800 nm, the scattering of the sample increases over time. This is likely due to the enzyme degradation of the PCL, where PCL chains with PEG cleaved will aggregate to minimize the exposure to water.

To increase the stability of PCL by slowing enzyme degradation by enzymes in cell medium for cell uptake studies, a small block of polybutyleneoxide (PBO) was added in between the PEG and PCL blocks to increase the hydrophobicity of the polymer core and provide a protective layer for the PCL[10], **Scheme 2-7.** For the synthesis of PEG-b-

PBO-*b*-PCL, allyl alcohol was used as the initiator for the anionic polymerization of PEG, followed by the anionic polymerization of PBO. The allyl-PEG-*b*-PBO-OH polymer was then quenched by stirring in methanol. The polymer was dried completely and precipitated in diethyl ether. The purified polymer was then subsequently used as a macroinitiator for the ring opening polymerization of PCL. The triblock copolymer was precipitated into hexanes and dried in vacuum oven. The product was characterized by GPC and NMR, **Figure 2-9**.

2.4.2.1 Self-Assembly of PEG-*b*-PBO-*b*-PCL

Self-assembled structures of azide-terminated PEG-*b*-PBO-*b*-PCL were prepared by the slow water addition method. In a typical experiment, 400 uL of the block copolymer solution in THF (2mg/mL) was diluted to 1 mL in total volume with THF. Then 10 uL of water was added every 30 seconds for a period of 15 min to the polymer solution in THF, and then allowed to stir overnight. 1 mL of water was then added to the solution and dialyzed against water overnight. The resulting assemblies were then precipitated with centrifugation at 14K for 1hr.

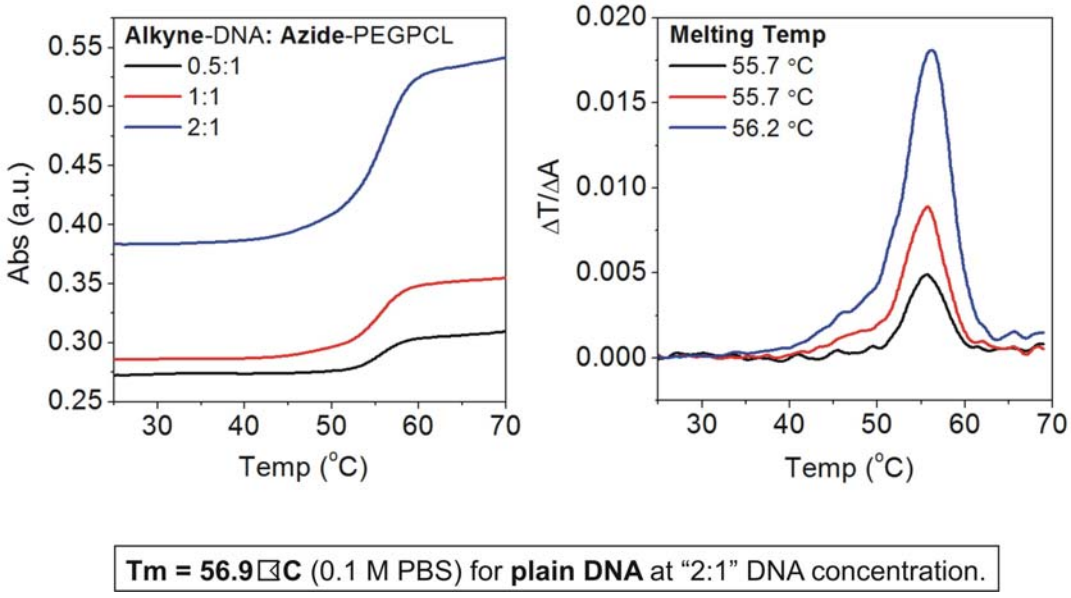

Figure 2-8. Hybridization of DNA TCP with HeLa cells with different DNA density.

Scheme 2-7. Synthesis of DNA-*b*-PEG-*b*-PBO-*b*-PCL

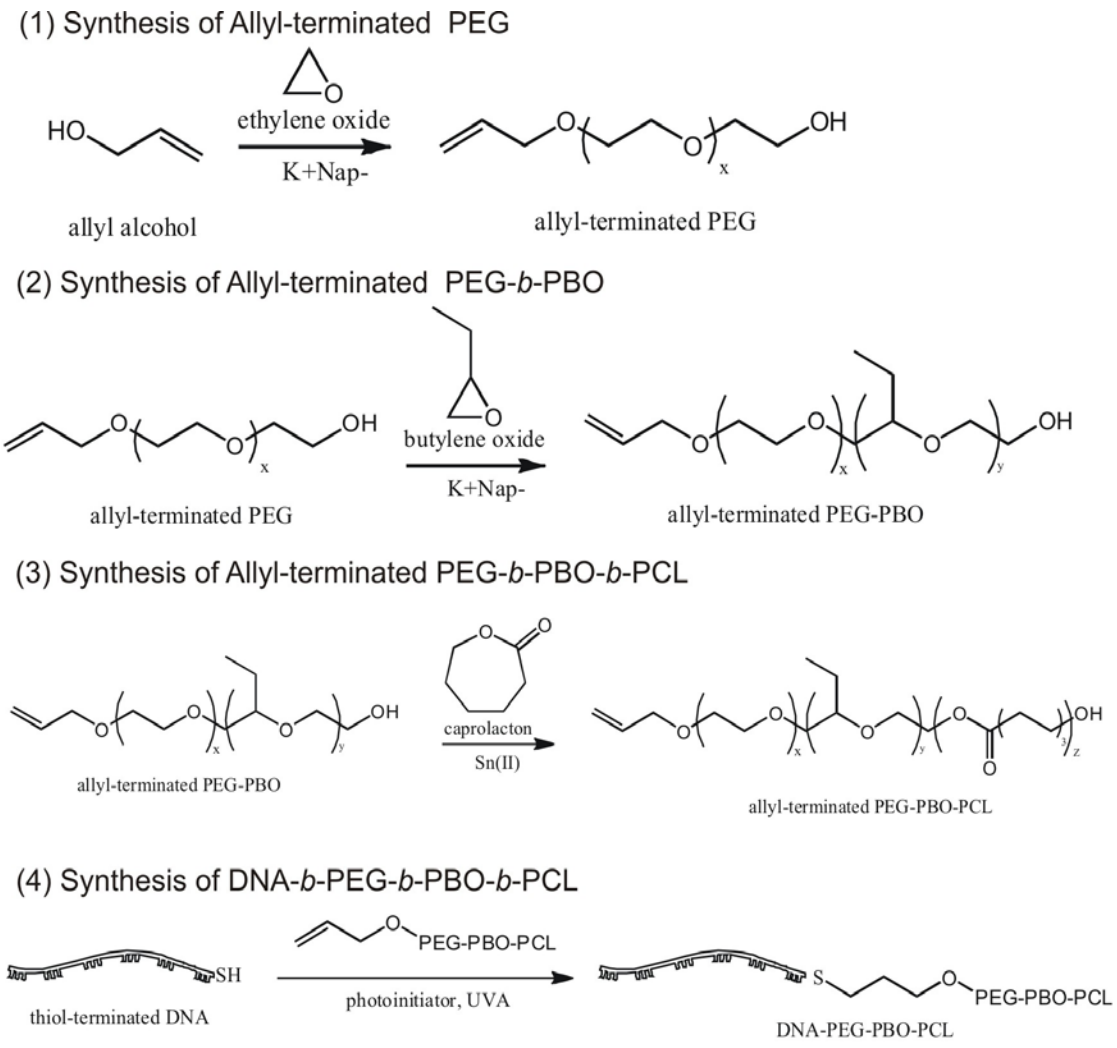

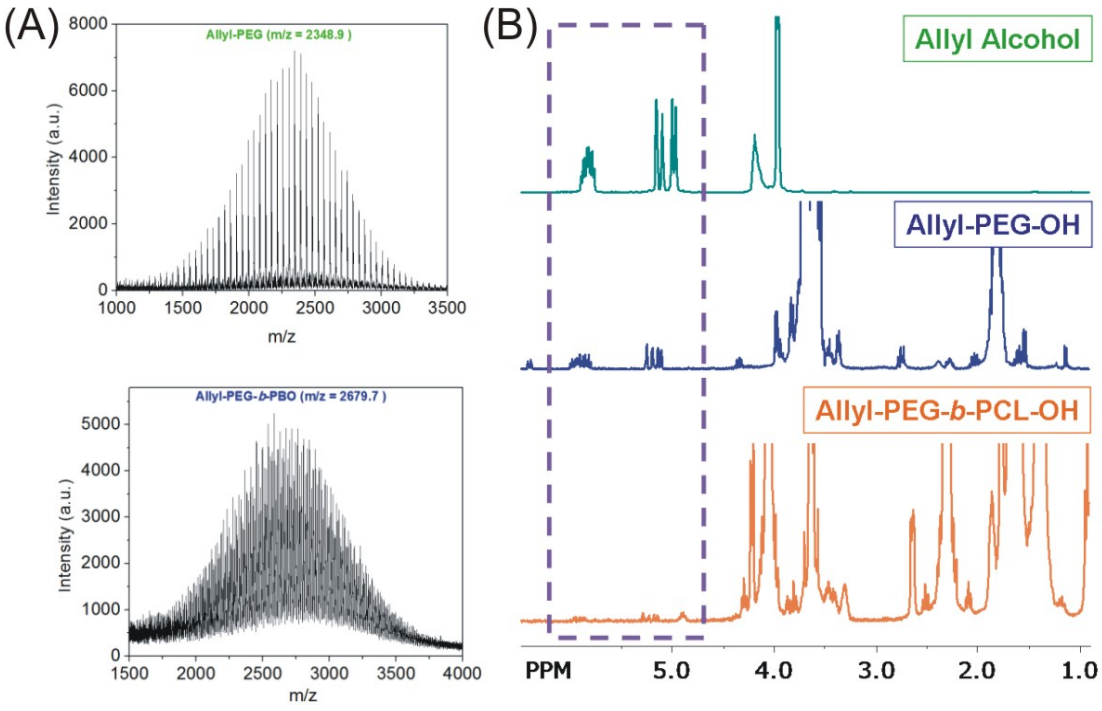

Figure 2-9. Characterization of PEG-*b*-PBO-*b*-PCL and NMR

2.4.2.2 Stability of PEG-*b*-PBO-*b*-PCL

Stability studies on PEG-*b*-PBO-*b*-PCL were performed on the self-assemblies. It was determined that the structure is very stable in cell medium. As monitored by the scattering, where even after 10 days in cell medium under incubation conditions used for cell uptake there is no increase in the scattering indicating no aggergation of the assemblies is taking place inside the medium. (**Figure 2-10B**)

2.4.2.3 Synthesis of DNA-*b*- PEO-*b* PBO-*b*-PCL via Thiolene "Click" Chemistry

For the conjugation of DNA onto the self-assembled structures of allyl-PEO-*b*-PBO-*b*-PCL, the thiol Michael Addtion reaction was used with thiol-modified DNA (Intergrated DNA Technology). Water soluble photoinitatior 4-(2-hydroxyethoxy)phenyl-(2-hydroxy-2-propyl)ketone (Irgacure 2959) was used in 2 mol% to thiol-DNA. The mixture of allyl--PEO-*b*-PBO-*b*-PCL, thiol-DNA and photoinitiaor were irradiated under UV lamp (365nm) for 2 hr. The resulting DNA-*b*- PEO-*b* PBO-*b*-PCL product was then precipitated with centrifugation at 14K for 1hr. The precipitate was then washed 2x with water and clean by precipitation with centrifugation to completely remove any uncoupled DNA and photoinitator.

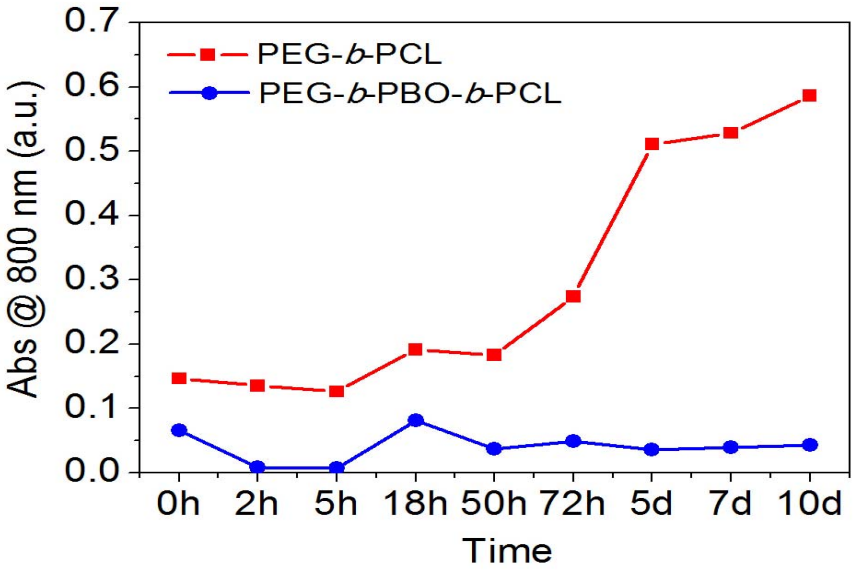

Figure 2-10. Scattering of PEG-PCL and PEG-*b*-PBO-*b*-PCL assemblies in cell medium after different time periods of incubation.

2.5 Summary and Conclusions

We have recently developed a new DNA-functionalization method based on the self-assembly of DNA block copolymers and nanoparticles.[9] In this approach, nanoparticles are encapsulated in DNA block copolymer assemblies by the slow addition of water to the mixture of DNA block copolymers and nanoparticles in a polar organic solvent. The resulting assemblies are composed of nanoparticles embedded in the hydrophobic polymer core and the hydrophilic DNA shell at the exterior. Since this approach is based on self-assembly, it can be applied to virtually any types of nanoparticles. It is also important to note that this methodology leads to a densely packed DNA layer on the surface because every polymer strand is conjugated to DNA. Due to the high density, the DNAs on the assemblies show dramatically enhanced binding properties. For example, they can recognize complementary DNA at low salt concentrations where regular DNA strands do not form duplex structures. While DNA block copolymers have been previously synthesized for other purposes,[1, 3, 7, 11] this work was the first to demonstrate that the self-assembly of nanoparticles and DNA block copolymers can be used to prepare DNA-functionalized nanoparticles with enhancing properties. This enhanced binding property in combination with the capability to load nanoparticles and other small molecules makes the DNA assemblies an excellent material for DNA detection and delivery applications.

2.6 References

1. Li, Z., Zhang, Y., Fullhart, P. & Mirkin, C. A. Reversible and chemically programmable micelle assembly with DNA block-copolymer amphiphiles. Nano Letters 4, 1055-1058 (2004).
2. Alemdaroglu, F. E. & Herrmann, A. DNA meets synthetic polymers - highly versatile hybrid materials. Organic & Biomolecular Chemistry 5, 1311-1320 (2007).
3. Alemdaroglu, F. E., Ding, K., Berger, R. & Herrmann, A. DNA-templated synthesis in three dimensions: Introducing a micellar scaffold for organic reactions. Angewandte Chemie-International Edition 45, 4206-4210 (2006).
4. Chen, X.-J. et al. Self-Assembled Hybrid Structures of DNA Block-Copolymers and Nanoparticles with Enhanced DNA Binding Properties. Small 6, 2256-2260 (2010).
5. Sun, S. & Zeng, H. Size-Controlled Synthesis of Magnetite Nanoparticles. Journal of the American Chemical Society 124, 8204-8205 (2002).
6. Ji, X. et al. Size Control of Gold Nanocrystals in Citrate Reduction: The Third Role of Citrate. Journal of the American Chemical Society 129, 13939-13948 (2007).
7. Jeong, J. H. & Park, T. G. Novel Polymer-DNA Hybrid Polymeric Micelles Composed of Hydrophobic Poly(d,l-lactic-co-glycolic Acid) and Hydrophilic Oligonucleotides. Bioconjugate Chemistry 12, 917-923 (2001).
8. Hiki, S. & Kataoka, K. A Facile Synthesis of Azido-Terminated Heterobifunctional Poly(ethylene glycol)s for "Click" Conjugation. Bioconjugate Chemistry 18, 2191-2196 (2007).
9. Chan, T. R., Hilgraf, R., Sharpless, K. B. & Fokin, V. V. Polytriazoles as Copper(I)-Stabilizing Ligands in Catalysis. Organic Letters 6, 2853-2855 (2004).
10. Zhu, X., Fryd, M., Tran, B. D., Ilies, M. A. & Wayland, B. B. Modifying the Hydrophilic-Hydrophobic Interface of PEG-b-PCL To Increase Micelle Stability: Preparation of PEG-b-PBO-b-PCL Triblock Copolymers, Micelle Formation, and Hydrolysis Kinetics. Macromolecules 45, 660-665 (2012).

11. Chien, M.-P., Rush, A. M., Thompson, M. P. & Gianneschi, N. C. Programmable Shape-Shifting Micelles. Angewandte Chemie International Edition 49, 5076-5080 (2010).

Chapter 3. Enhanced DNA Binding Properties[4] and Thermodynamic Studies

3.1 Overview

This chapter shows efforts toward determining the origin of the enhanced binding mentioned in **Chapter 2**. In general, we hypothesize that the enhanced binding is likely due to the DNA density on the surface of the assemblies, which is supported by the size dependency of the enhanced binding. Thus, we designed experiments to 1) determine the number of DNA strands on the surface of the assemblies, and then 2) we probed the importance of the DNA density by diluting the number of DNA strands on the surface and see what effect that has on the enhanced binding properties. **Table 3-1** summarizes a list of DNA block copolymer assemblies prepared for the studies mentioned in this Chapter.

[4] Reprint in parts with permission from Chen, X.-J.; Sanchez-Gaytan, B. L.; Hayik, S. E. N.; Fryd, M.; Wayland, B. B.; Park, S.-J.: *Self-Assembled Hybrid Structures of DNA Block-Copolymers and Nanoparticles with Enhanced DNA Binding Properties.* Small. **2010**;6(20):2256-2260..Copyright 2010 Wiley-VCH Verlag GmbH & Co. KGaA

3.2 Förster Resonance Energy Transfer (FRET) Monitored DNA Hybridization

3.2.1 FRET

As a result of the strong absorbance of polystyrene at 260 nm, melting denaturation of the DNA duplex to single-stranded DNA transitions were unable to be monitored by conventional UV-vis spectroscopy at 260 nm. Instead, Förster/Fluorescent resonance energy transfer (FRET) was used to monitor the transition, by labeling the DNA strands on the DNA block copolymer with a fluorescein (FAM) and a Cy3 labeling on the complementary strand.

FRET efficiency was determined based on the changes in the fluorescence intensity of FAM (donor) with the addition of Cy3-labeled target oligonucleotide (acceptor) using **Eq.3-1**, where F_D is the donor fluorescence intensity in the absence of acceptor and F_{DA} is donor fluorescence intensity in the presence of acceptor.[1] The donor PL intensity was used for the FRET efficiency calculation because Cy3 PL intensity changes with temperature while there is no significant change in the FAM PL intensity with the temperature range used in the experiments.

$$E = 1 - (F_{DA}/F_D) \qquad \text{(Eq. 3-1)}$$

Table 3-1. List of DNA block copolymer assemblies and their characterization by dynamic light scattering (DLS).

DNA Block Copolymer Assemblies[a]	Description	DNA Sequence(s)[b]	Hydrodynamic Diameter [c] (nm)
PS@DNA	Simple micelles of DNA-*block*-polystyrene (DNA-*b*-PS) in water	5'-FAM A_{10} ATC CTT ATC AAT ATT-3'	15 ± 4
MNP@PS@DNA	Meso-assemblies of DNA-*b*-PS with encapsulated magnetic nanoparticles	5'-FAM A_{10} ATC CTT ATC AAT ATT-3'	161 ± 8
PS@PS@DNA	Meso-assemblies of DNA-*b*-PS with encapsulated homo-polystyrene	5'-FAM A_{10} ATC CTT ATC AAT ATT-3' or 5'- A_{10} ATC CTT ATC AAT ATT-FAM-3' for cellular uptake studies	166 ± 2
PS@PS@dilDNA	Meso-assemblies of DNA-*b*-PS with a mixture of DNA-*b*-PS with different length DNA; with encapsulated homo-polystyrene	5'-FAM –CACAT-3' and 5'-FAM A_{10} ATC CTT ATC AAT ATT-3'	230 ± 2
AuNP@PS@PC-DNA	Meso-assemblies of DNA-*b*-PS with photocleavable-moiety modified DNA; with encapsulated gold nanoparticles	5'- PC-FAM-A_{10} ATC CTT ATC AAT ATT-3'	153 ± 6
PS@PS@dilFAM-DNA	Meso-assemblies of DNA-*b*-PS with a mixture of DNA-*b*-PS with and without FAM-labeled DNA; with encapsulated homo-polystyrene	5'- A_{10} ATC CTT ATC AAT ATT-3' and 5'-FAM A_{10} ATC CTT ATC AAT ATT-3'	174 ± 3

[a]The A@B denotes a core-shell structure composed of A core and B shell.
[b]FAM = fluorescein; A_{10} = AAAAAAAAAA
[c]Standard deviation was taken from three individual measurements.

3.2.2 Enhanced DNA binding of DNA BCP assemblies

Assemblies of DNA-FAM-*b*-PS (DNA concentration: 200 pmol) was mixed with 800 pmol of Cy3-labeled complementary DNA (Cy3-DNA) strands in phosphate buffered saline (PBS) solutions with appropriate salt concentrations or in water (total volume of 800 μL).

The DNA hybridization property of these assemblies was monitored by FRET using FAM/Cy3 donor/acceptor pair (**Figure 3-1A**). It was found that not only did the DNA strands on these MNP@PS@DNA retain their hybridization properties in phosphate buffer saline solution as expected (**Figure 3-1B**), surprisingly they can still hybridize with complementary DNA strands in solutions without added salt (**Figure 3-1C**).

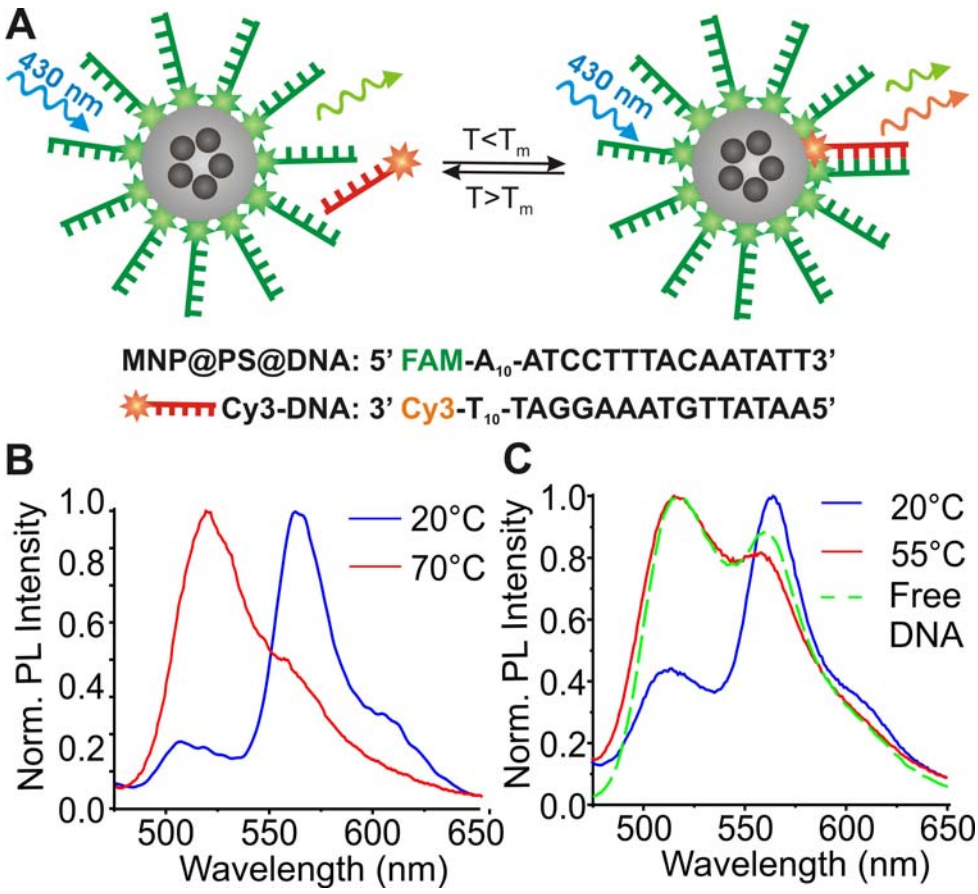

Figure 3-1. **(A)** Schematic description for the binding of Cy3-labeled complementary DNA (Cy3-DNA) to MNP@PS@DNA below DNA melting temperature. **(B)** Fluorescence spectra of MNP@PS@DNA mixed with Cy3-DNA in 0.3 M PBS below and above DNA melting temperature. **(C)** Fluorescence spectra of MNP@PS@DNA mixed with Cy3-DNA in water with no added salt below and above DNA melting temperature. For comparison, a fluorescence spectrum of plain FAM-modified DNA mixed with the complementary Cy3-DNA in the same condition was collected at 20 □C and plotted in green, which reveals negligible FRET. For all spectra, the excitation wavelength was 430 nm, which selectively excites FAM. Figure reprint with permission from ref [2].Copyright 2010 Wiley-VCH Verlag GmbH & Co. KGaA

This enhanced binding by the MNP@PS@DNA was clearly demonstrated in a "competition experiment", where Cy5-labeled DNA strands with the same sequence as that of the DNA strands on the MNP@PS@DNA were added to the solution to compete for the Cy3-labeled target DNA (**Figure 3-2A**). Emission spectra collected reveled that only FRET between the FAM/Cy3 pair is observed (**Figure 3-2B**) and no significant FRET was observed between Cy3/C5 pair (**Figure 3-2C**); ergo the Cy3-labeled target binds mainly to the MNP@PS@DNA.

3.2.3 Selective DNA Binding

These MNP@PS@DNA hybrid assemblies are highly selective in complementary DNA recognition and they can distinguish fully complementary sequence (*i.e.* 0 base mismatch) from strands with small numbers of base pair mismatches. To test the selectivity, DNA hybridization properties were measured for "complementary" DNA strands with 0, 1, 2, 3 base mismatches (**Figure 3-3**). The binding of a fully noncomplementary DNA was also monitored for comparison. All experiments were done in water without added salt. The DNA sequences used for the experiments are given in Figure 4. The FRET efficiency and the melting temperature were determined for the mismatched DNA and presented in Figure 4 along with the data for complementary DNA. Both the FRET efficiency and melting temperature became progressively smaller with a larger number of base mismatches, and there was no detectable DNA binding for fully noncomplementary DNA. Notably, the FRET efficiency is significantly lowered even with one base mismatch, showing that the hybrid assemblies can distinguish a single

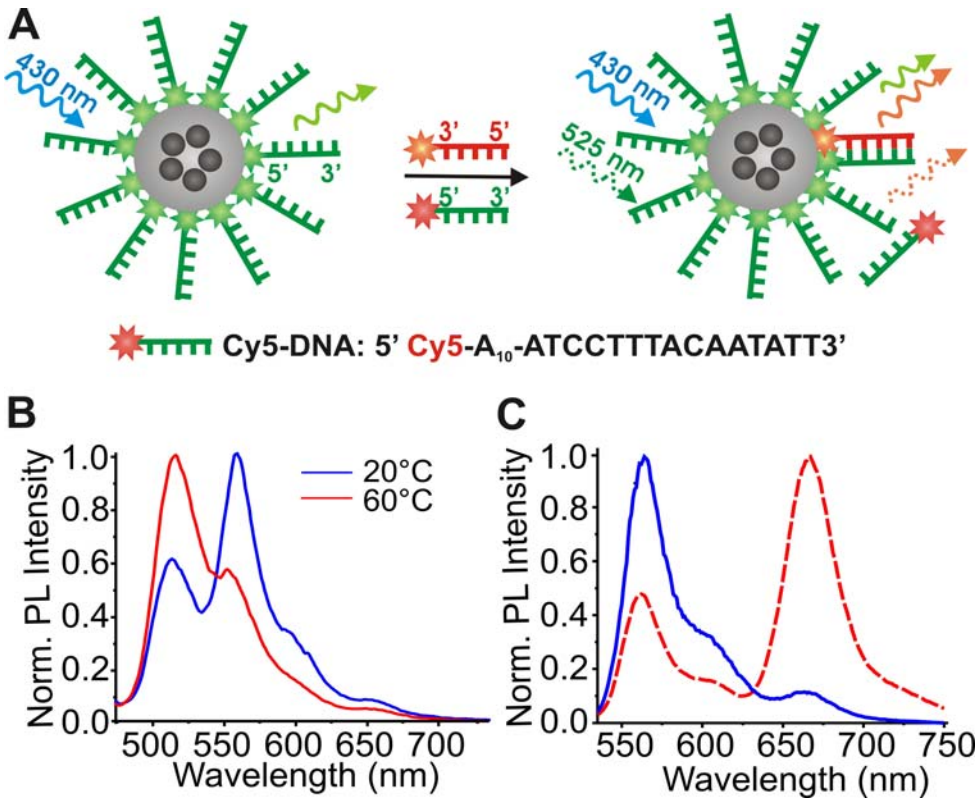

Figure 3-2. **(A)** Schematic description for the preferential binding of Cy3-labeled target DNA to MNP@PS@DNA in the presence of Cy5-labeled competition DNA (*i.e.* plain DNA with same sequence as the DNA of MNP@PS@DNA). All experiments were carried out in water without added salts unless otherwise specified. **(B)** Fluorescence spectra of the competition experiment with MNP@PS@DNA, Cy3-labeled target strands (Cy3-DNA) and Cy5-labled competition strands (Cy5-DNA), showing selective binding of target DNA to MNP@PS@DNA. FRET efficiency of FAM/Cy3 pair, $E_{FRET(FAM\text{-}Cy3)}$ = 36.0 %. Excitation wavelength = 430 nm. **(C)** Room temperature (20 ^{o}C) fluorescence spectrum of the competition experiment with 525 nm excitation (blue), confirming that competition Cy5-DNA strands exist as single stranded DNA ($E_{FRET\ Cy3\text{-}Cy5}$ = <1 %). For comparison, fluorescence spectrum of Cy5-DNA and Cy3-DNA in 0.3 M PBS is also presented (red), which shows intense Cy5 emission via the FRET, $E_{FRET(Cy3\text{-}Cy5)}$ = 74.7 %. Figure reprint with permission from ref [2].Copyright 2010 Wiley-VCH Verlag GmbH & Co. KGaA

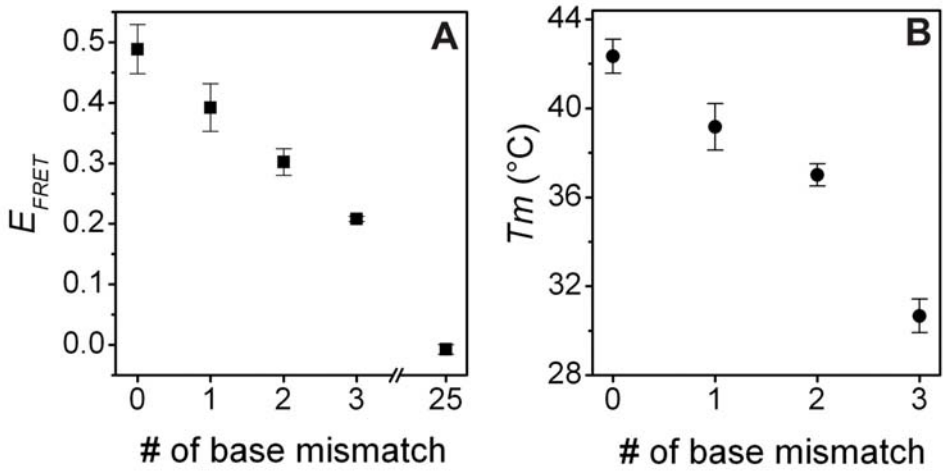

No. Base Mismatch	DNA Sequence
0	3'Cy3-T_{10}TAGGAAATGTTATAA5'
1	3'Cy3-T_{10}TAGGAA**C**TGTTATAA5'
2	3'Cy3-T_{10}TAGGAA**CG**GTTATAA5'
3	3'Cy3-T_{10}TAGGAA**CGC**TTATAA5'
25	3'Cy3-**A_{10}CTGCCGGTTGCAAAG**5'

Figure 3-3. FRET efficiencies (E_{FRET}) (A) and melting temperatures (T_m) (B) for DNA sequences with different numbers of base mismatches (underlined). Figure reprint with permission from ref [2].Copyright 2010 Wiley-VCH Verlag GmbH & Co. KGaA

base mismatch from fully complementary DNA sequence without a thermal treatment. This result also confirms that the DNA binding in the unusual condition (*i.e.*, in purified water with no added salt) is due to sequence specific DNA interaction. Because the MNP@PS@DNA can be used at very low salt concentrations where plain DNA exist as single stranded DNA, the hybrid material should be extremely effective in duplex DNA detection applications.

3.3 Enhanced Binding is Size Dependent

3.3.1 Experimental Method

DNA block copolymers composed of polystyrene (PS) and a fluorescein (FAM)-labeled oligonucleotide strand (DNA-FAM-*b*-PS) were synthesized by coupling phosphoramidite-modified PS to oligonucleotides synthesized on CPG beads following a previously reported procedure.[2,3] The FAM dye was inserted in-between PS and DNA for DNA hybridization studies. The self-assembly of DNA-FAM-*b*-PS was induced by the slow water addition to the DMF solution of DNA-FAM-*b*-PS followed by dialysis in water and centrifugation. The prepared DNA block copolymer assemblies were characterized by dynamic light scattering (DLS) and transmission electron microscopy (TEM).

Assemblies of DNA-FAM-*b*-PS (DNA concentration: 200 pmol) was mixed with 800 pmol of Cy3-labeled complementary DNA (Cy3-DNA) strands in phosphate buffered saline (PBS) solutions with appropriate salt concentrations or in water (total volume of 800 μL)

DNA block copolymer assemblies of two different sizes were prepared to examine the effect of the size and surface curvature of the assemblies on DNA recognition properties.[2] Mesoscale assemblies of DNA block-copolymers were prepared by incorporating PS homopolymers in the core, which resulted in PS-filled DNA block copolymer assemblies (PS@PS@DNA). The diameter of the PS@PS@DNA meso-assemblies was determined to be 166 ± 2 nm by DLS **(Figure 3-4)**. For comparison, simple spherical micelles of DNA block copolymers (PS@DNA) were prepared by the slow addition of water to the DMF solution of DNA block copolymers. The size of the simple micelles was determined to be 15 ± 4 nm by DLS **(Figure 3-4)**, which correspond to the size previously reported.[2,3]

3.3.2 Thermal Denaturation Studies

The DNA binding properties of the PS@DNA and PS@PS@DNA were monitored by Förster resonance energy transfer (FRET) between the FAM (donor dye) on the assemblies and Cy3 (acceptor dye) attached at the 3' end of complementary DNA as depicted in **Figure 3-5A-B**. The photoluminescence (PL) spectra were collected with the excitation wavelength of 430 nm, which selectively excites FAM but not Cy3. Therefore, the high intensity of the Cy3 PL at 564 nm and the drastically quenched fluorescent of FAM in the presence of the Cy3-DNA acceptor are indicative of the binding between Cy3-DNA and FAM-DNA. In typical experiments, DNA assemblies (200 pmol DNA) were mixed with Cy3-labeled complementary DNA (Cy3-DNA, 800 pmol), at a 1:4 ratio, either in a PBS buffer or in water.

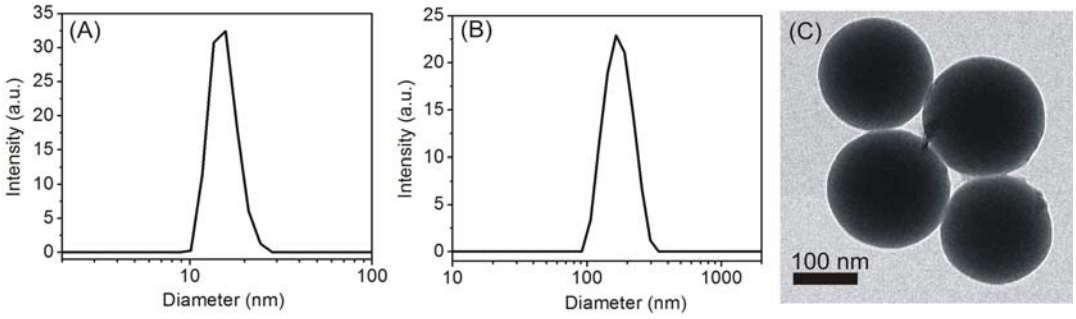

Figure 3-4. DLS measurements of simple micelles (A) and PS-filled meso-assemblies (B). (C) A TEM image of PS-filled meso-assemblies.

Figure 3-5C and D present PL spectra of the donor FAM-labeled PS@DNA simple micelles and PS@PS@DNA meso-assemblies, respectively, in the absence (F_D) and presence (F_{DA}) of the acceptor Cy3-complementary DNA in water and in 0.3 M PBS. In 0.3M PBS solutions, both assemblies showed a strong acceptor emission and reduced FAM emission in the presence of Cy3-DNA (**Figure 3-5C-D, red**), confirming that they both bind to complementary DNA in 0.3 M PBS as expected. The FRET efficiencies in 0.3M PBS were calculated to be 88.9 ± 4.8% and 88.2 ± 3.5% for simple micelles and meso-assemblies, respectively. For comparison, the FRET efficiency for plain DNA at this salt concentration was determined to be 95 ± 2.2%. It is interesting to point out that the E_{FRET} for plain DNA is higher than that of simple micelles and meso-assemblies. This is likely due to steric hindrance of the DNA being closely packed on a surface of DNA block copolymer assemblies. It is expected that there will be considerable interactions from neighboring DNA in assemblies versus in the case of plain DNA where the DNA are freely moving. The steric hindrance effect on the crowded surface of simple micelles and meso-assemblies can also affect the orientation of the dye molecules, and thus the FRET efficiency.

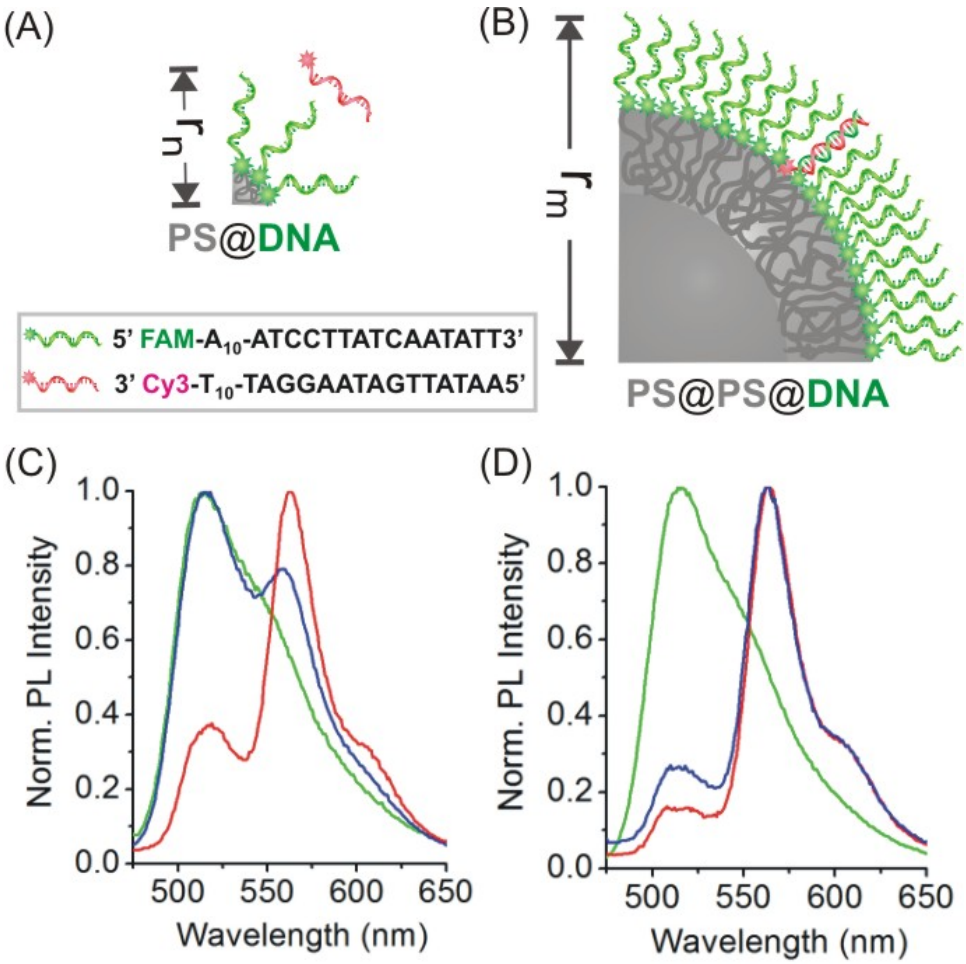

Figure 3-5. (A-B) Pictorial descriptions of PS@DNA (A) and PS@PS@DNA (B), showing how the radius of curvature affects the DNA packing and the duplex formation at a low salt concentration. (C-D) PL spectra of PS@DNA (C) and PS@PS@DNA (D) in the absences of acceptor (green) and in the presences of acceptor (blue) measured in water. The PL spectra of the assemblies in 0.3 M PBS in the presence of acceptor are also presented for comparison (red).

The PL spectrum of the Cy3-DNA and simple micelle mixture in water (**Figure 3-5 C**) shows a strong FAM peak at 520 nm, indicating that the complementary Cy3-DNA does not bind to the small micelles of PS@DNA in water without added salts. On the other hand, the meso-assemblies showed an intense Cy3 peak at 564 nm and a reduction of FAM peak intensity at 520 nm, indicating that Cy3-DNA strands hybridize to the complementary DNA on meso-assemblies at an extremely low salt concentration (**Figure 3-5D**). This behavior is similar to what was found for the assemblies encapsulated with magnetic nanoparticles (MNP@PS@DNA) in our previous report.[2] The FRET efficiency between the meso-assemblies incorporating PS homopolymers and Cy3-DNA in water was calculated to be 74.6 ± 4.1%. This result clearly shows that the enhanced DNA binding property of our meso-assemblies is indeed size-dependent phenomena. It also shows that the enhanced binding is not nanoparticle-specific, such that any core-filled meso-assemblies of DNA block copolymers possess enhanced DNA binding properties regardless of the type of core-filling materials. Thus, one can combine the unusual enhanced binding properties of meso-assemblies with any types of molecular or nanoscale encapsulants.

The FRET efficiency in water (without added salt), however, was much higher for meso-assemblies when the three systems are compared, since simple micelles and regular isolated oligonucleotide strands do not form duplex structure in water without added salt (**Figure 3-6**). Suggesting that meso-assemblies possess significantly enhanced binding constant than simple micelles or plain DNA in low salt conditions.

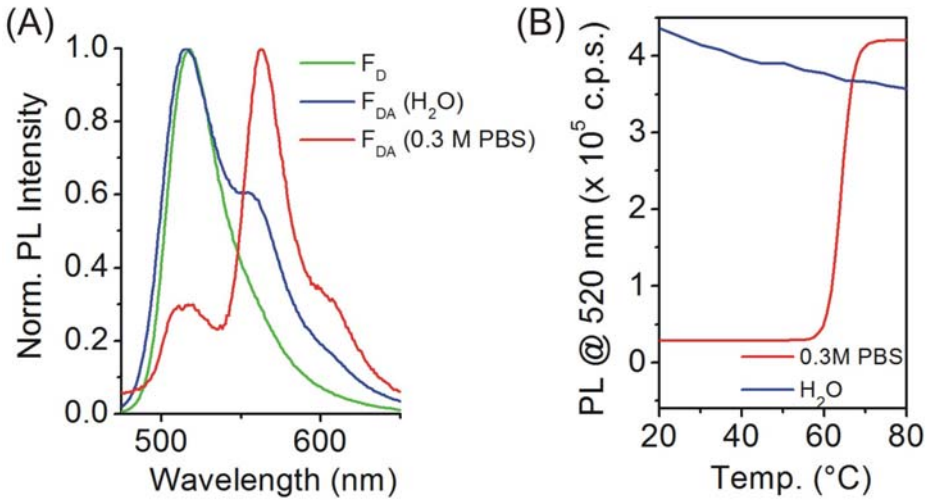

Figure 3-6. PL spectra of FAM-labeled DNA in the absence (F_D) and presence (F_{DA}) of complementary Cy3-DNA in (A) 0.3M PBS and water. (B) Corresponding melting curves by monitoring the FAM intensity at 520 nm.

Shown in **Figure 3-7** are melting transition profiles for plain DNA, simple micelles (PS@DNA) and meso-assemblies (PS@PS@DNA) with Cy3-DNA collected at the three different salt concentrations, 0M, 0.1M and 0.3M PBS at the same DNA concentration (in 1:4 ratio of donor DNA:acceptor DNA). Also shown in **Figure 3-7** are the corresponding PL spectra at three selective temperatures for all the melting transition profiles. Melting transition profiles of the three systems showed similar melting temperatures (T_m) at high salt concentrations such as 0.1 and 0.3M PBS. However, in solutions without the addition of any salt, plain DNA and PS@DNA did not hybridize with complementary Cy3-DNA, since the FAM intensity at 520 nm is not quenched in the presence of the acceptor. In the same conditions, in solutions without added salt, the meso-assemblies still showed a quenched FAM intensity at 520 nm which is regained with increasing temperature, indicating the DNA strands on the meso-assemblies hybridized with Cy3-DNA.

In **Figure 3-8**, the values of T_m and E_{FRET} for plain DNA, PS@DNA and PS@PS@DNA collected at the three different salt concentrations are shown in figure S3 are plotted for further comparison of the binding affinity of the three systems at different salt concentrations. It is interesting to point out that the E_{FRET} for plain DNA is higher than that of PS@DNA and PS@PS@DNA. This is most likely due to steric hindrance effect of the DNA being "packed" on a surface, where there will be considerable interactions from neighboring DNA versus in the case of plain DNA where the DNA are freely moving. The steric hindrance effect on the crowded surface of PS@DNA and PS@PS@DNA can also affect the orientation of the dye molecules, and thus the FRET process.

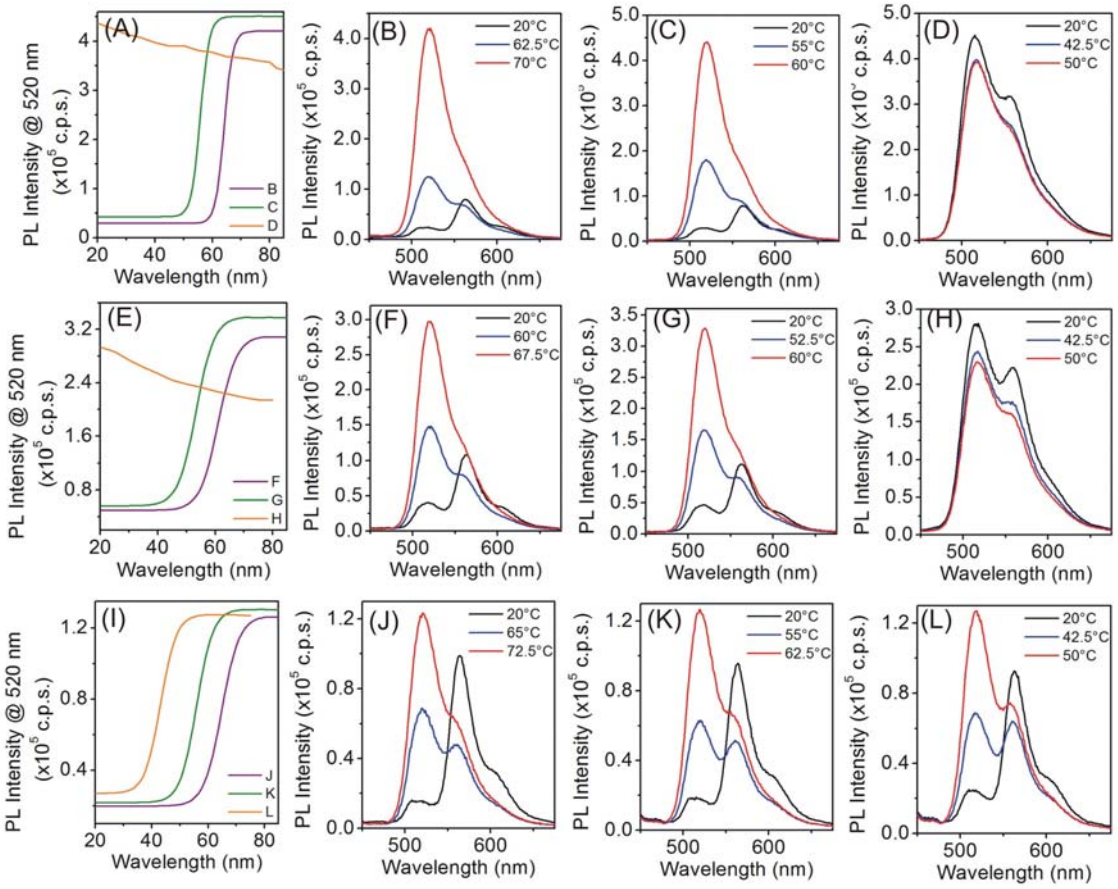

Figure 3-7. The melting transition profiles monitored by the change of FAM emission intensity at 520 nm for plain DNA (A), simple micelles (E), and meso-assemblies (I) with Cy3-DNA at three different salt concentrations, 0.3M PBS (purple), 0.1M PBS (green) and water (orange). Selected emission spectra at three different temperatures for each salt concentration are shown following the melting curves.

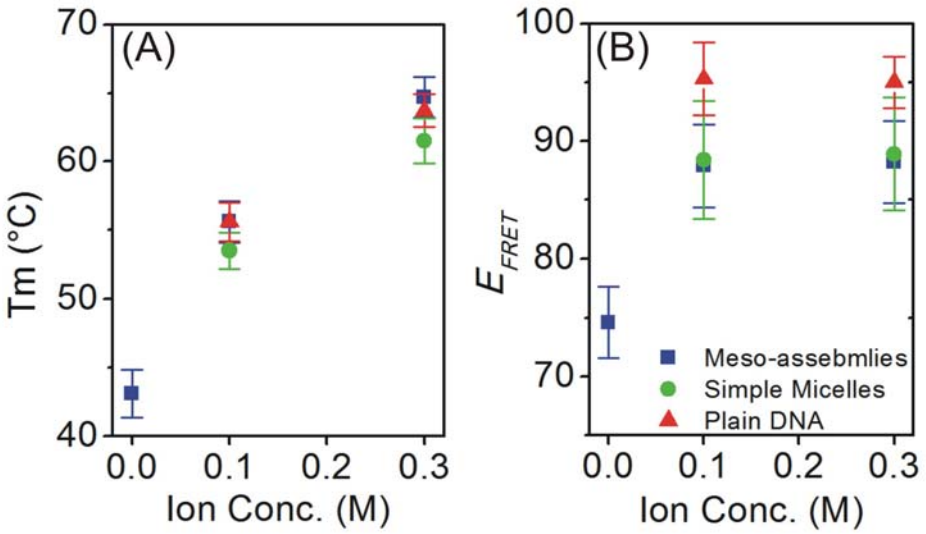

Figure 3-8. Plots of (A) T_m and (B) E_{FRET} for plain DNA, simple micelles and meso-assemblies in the presence of complementary Cy3-DNA for three different salt concentrations 0, 0.1 and 0.3M PBS.

3.4 Concentration Dependent Thermodynamic Analysis

3.4.1 Experimental Method

Concentration-dependent thermodynamic analyses were carried out for PS-filled meso-assemblies (PS@PS@DNA) and free DNA strands at varying DNA concentrations as well as varying salt concentrations of 0M, 100 mM and 300 mM NaCl. Melting curves were obtained at a series of different DNA concentrations. FAM-DNA and Cy3-DNA were mixed at 1:1 ratio for the measurements.

3.4.2 Thermodynamic Studies

Thermodynamic parameters of meso-assemblies and plain DNA were determined and compared to better understand the enhanced binding properties. These parameters were obtained by concentration dependent DNA melting analyses according to the van't Hoff's equation (**Equation 3-2**):

$$\frac{1}{T_m} = \frac{R}{\Delta H^o} \ln Ct + \frac{\Delta S^o - R \ln 4}{\Delta H^o} \qquad \textbf{(Eq. 3-2)}$$

where T_m is the melting temperature, R is the gas constant, C_t is the total DNA concentration, $\Delta H°$ is the enthalpy, and $\Delta S°$ is the entropy.

Parameters such as enthalpy $\Delta H°$ and entropy $\Delta S°$ were extracted from the fitted van't Hoff plots obtained from the concentration-dependent thermal denaturation measurements (**Figure 3-9B**) based on equation **Eq.3-3**. Other thermodynamic parameters such as free energy $\Delta G°$ and binding constants K_{eq} were subsequently determined using equations **Eq. 3-3** and **Eq.3-4**.

$$\Delta G° = \Delta H° - T\Delta S° \quad \textbf{(Eq. 3-3)}$$

$$\Delta G° = -RT\ln(K_{eq}) \quad \textbf{(Eq. 3-4)}$$

A list of melting temperature, T_m, and FRET efficiencies, E_{FRET}, collected are summarized in **Table 3-2 and 3-3** for plain DNA and PS@PS@DNA, respectively.

The concentration-dependent DNA melting analyses were carried out for meso-assemblies, simple micelles and plain DNA at three different salt concentrations. For these measurements, the molar ratio between the DNA block copolymer and complementary Cy3-DNA was set to 1. The free energy ($\Delta G°$) and equilibrium binding constants (*Keq*) of the systems were calculated from the $\Delta H°$ and $\Delta S°$ values extracted from the slope and the intercept of the equation 1. The calculated thermodynamic parameters are listed in **Table 3-4**, and the binding constants are plotted in **Figure 3-10**.

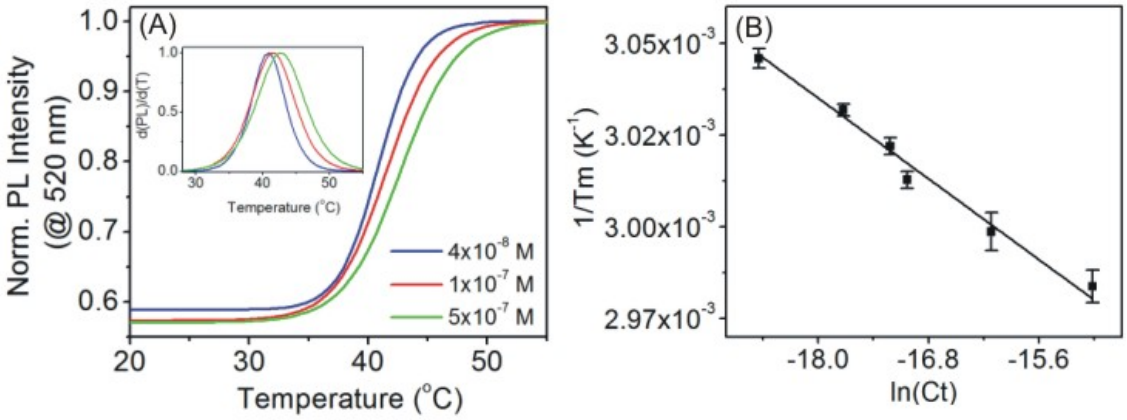

Figure 3-9. Concentration-dependent thermodynamic analysis of PS@PS@DNA in solution without added salt. (A) Melting curves at varying DNA concentrations plotted at the emission intensity of FAM (donor) at its emission maximum (520 nm) at increasing temperatures. (B) van't Hoff's plot of the concentration-dependent thermodynamic analysis where thermodynamic parameters of enthalpy and entropy were extracted.

Table 3-2. List of melting temperature (T_m) for plain DNA determined at a series of different DNA concentrations and two different salt concentrations.

0.1M PBS		**0.3M PBS**	
[DNA] (M)	**T_m (°C)**	**[DNA] (M)**	**T_m (°C)**
1.25E-07	48.3±0.4	1.73E-07	57.1±0.2
3.47E-07	49.7±0.3	3.30E-07	59.0±0.5
8.67E-07	51.8±0.3	7.29E-07	59.7±0.3
1.56E-06	53.0±0.1	1.63E-06	60.6±0.2
2.64E-06	53.7±0.3	2.26E-06	61.3±0.6
3.54E-06	53.9±0.4	4.06E-06	61.7±0.3

Table 3-3. List of T_m for PS@PS@DNA determined at a series of different DNA concentrations and three different salt concentrations.

0 M PBS		0.1M PBS		0.3M PBS	
[DNA] (M)	**T_m (°C)**	**[DNA] (M)**	**T_m (°C)**	**[DNA] (M)**	**T_m (°C)**
4.00E-08	39.0±1.8	3.33E-08	48.1±0.6	2.00E-08	55.2±0.3
7.50E-08	40.2±1.4	4.00E-08	48.4±0.8	3.33E-08	56.7±0.2
1.00E-07	41.0±0.5	5.00E-08	48.9±1.0	4.00E-08	57.8±0.3
2.00E-07	42.0±0.8	8.00E-08	50.3±0.6	1.00E-07	58.8±0.3
5.00E-07	43.2±0.8	1.00E-07	52.5±0.5	3.00E-07	60.3±0.6
6.00E-07	44.4±1.0	5.00E-07	55.6±0.1	5.00E-07	62.0±0.5

Table 3-4. Thermodynamic parameters of plain DNA and meso-assemblies obtained from melting analysis.

Ion Concentration	*Plain DNA*		*Meso-Assemblies*		
	100 mM	**300 m M**	**0 M**	**100 mM**	**300 m M**
ΔH° ***(kcal/mol)***	-92.4±7.5	-100.8±11.0	-73.9±3.7	-82.6±10.2	-112.3±12.8
ΔS° ***(cal/mol·K)***	-265.8±18.7	-280.5±22.8	-197.8±3.9	-219.9±31.9	-302.3±38.7
ΔG° ***(kcal/mol)***	-13.1±1.7	-17.1±0.4	-14.9±7.8	-17.0±0.7	-22.1±1.3
K_{eq} ***(M)***	(3.9±1.2)x 10^{9}	(3.6±1.3) x 10^{12}	(8.2±0.2) x 10^{10}	(3.0±1.1) x 10^{12}	(1.74±1.1) x 10^{16}

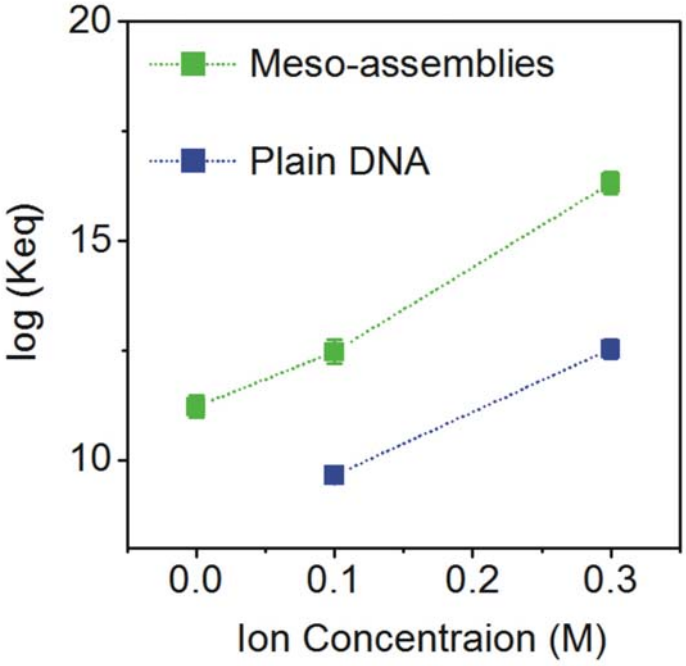

Figure 3-10. Binding constants, K_{eq}, of plain DNA, DNA block copolymer assemblies of homopolymer filled meso-assemblies at different salt conditions.

As presented in **Table 3-4** and **Figure 3-10**, the meso-assemblies have substantially higher binding constants than simple micelles and plain DNA strands at all three different salt concentrations. This is especially obvious at very low salt concentrations, where the simple micelles and plain DNA do not form duplex structure. The binding constant of meso-assemblies without added salt was comparable to that of plain DNA at 0.1 M PBS.

It is worth comparing the thermodynamic parameters of our meso-assemblies with those of DNA-modified gold nanoparticles which have been extensively studied for their enhanced binding properties.[4] The binding constant of meso-assemblies at 0.3 M PBS is two orders of magnitudes higher than that of DNA-conjugated gold nanoparticles.[4] In **Table 3-5**, the thermodynamic values of plain DNA and meso-assemblies determined from concentration dependent thermodynamic analysis in 0.3M PBS are compared with literature thermodynamic values of plain DNA and DNA-conjugated gold nanoparticles with the same DNA sequence in 0.3M PBS.

The thermodynamic parameters listed in **Table 3-4 and 3-5** indicated that both enthalpy and entropy terms contribute to the lower free energy of meso-assemblies compared to DNA-conjugated gold nanoparticles.

Table 3-5. Comparison of literature and experimental thermodynamic parameters for plain DNA, DNA-conjugated gold nanoparticles and meso-assemblies at 0.3M PBS.

	***Literature*[4]**		***Experimental***		
0.3M PBS	**Plain DNA**	**DNA-conjugated Au NP**	**Plain DNA**	**Simple Micelles**	**Meso-Assemblies**
ΔH° *(kcal/mol)*	-98±2.0	-117±3.9	-100.8±11.0	-74.8±9.4	-112.3±12.8
ΔS° *(cal/mol·K)*	-272±5.6	-326±11	-280.5±22.8	-191.4±46.2	-302.3±38.7
ΔG° *(kcal/mol)*	-16.7±2.0	-19.4±3.9	-17.1±0.4	-17.8±0.8	-22.1±1.3
K_{eq} *(M)*	1.8×10^{12}	1.8×10^{14}	$(3.6\pm1.3) \times 10^{12}$	$(1.05\pm0.3) \times 10^{13}$	$(1.74\pm1.1) \times 10^{16}$

The size-dependent DNA binding property suggests that the enhanced DNA binding of meso-assemblies is associated with the high DNA density. As depicted in **Figure 3-5A**, larger meso-assemblies have a smaller surface curvature compared to simple micelles. The smaller curvature is translated into a smaller space per DNA strand and a higher DNA density. This is in contrast to the size-dependence found in DNA-modified gold nanoparticles, where the average footprint of DNA becomes larger and the areal DNA density becomes smaller with increasing the nanoparticle size.[5] For DNA block-copolymers, a smaller curvature forces DNAs to pack more closely as every polymer is connected to a DNA. The close DNA packing creates an unusual environment for DNA on meso-assemblies, which leads to the extraordinary DNA binding properties of meso-assemblies. The hydrophobic nature of PS also contributes to the high DNA density on our meso-assemblies as DNA block-copolymers pack tightly to avoid the contact between water and PS. However, the size and the curvature effect is apparently important as simple micelles made of the same polymers behave similarly to plain DNA strands.

3.5 Estimate Number of DNA Strands per Assembly

As shown in equation **Eq.3-5**, the number of DNA strand per DNA block copolymer assembly in essence is the total number of DNA strands over the total number of assemblies in a given solution.

$$\text{\# DNA strands per assembly} = \frac{\text{Total \# of DNA strands}}{\text{Total \# of assemblies}} \quad \textbf{(Eq.3-5)}$$

To determine these two values, we prepared fluorescent-labeled PC DNA block copolymer assemblies with encapsulated gold nanoparticles (**Figure 3-11**).

3.5.1 Experimental Design

The number of DNA strands per meso-assembly was determined using photocleavable (PC) DNA strands (sequence: 5'-PC-FAM A_{10} ATC CTT ATC AAT ATT-3'). This method of releasing the DNA strands from the polymer cores allows for an accurate quantification of DNA without the interference of the scattering by meso-assemblies and the self-quenching of FAM PL that can occur on meso-assemblies due to the dense DNA packing. The photocleavable linker was inserted between PS and FAM dye to release FAM-modified DNA as free DNA strands for quantification. Gold nanoparticles (AuNP) were incorporated into the assemblies (AuNP@PS@PC-DNA) to determine the number of meso-assemblies.

3.5.2 Synthesis of PC DNA Block Copolymer Assembly

PC DNA block copolymer strands were synthesized by the same procedure{Chen, 2010 #125} as regular DNA block copolymers with the exception that a photocleavable phosphoramidite (4-(4,4'-dimethoxytrityloxy)butyramidomethyl)-1-(2-nitrophenyl)-ethyl]-2-cyanoethyl-(N,N-diisopropyl)-phosphoramidite, Glen Research) was added at

the 5’ end of the DNA sequence (5’-PC-FAM A_{10} ATC CTT ATC AAT ATT-3’). The synthesized PC DNA was then coupled to phosphoramidite-terminated PS at the 5’ end. The PC DNA block-copolymers were self-assembled with AuNP were prepared by the same procedure used for the non-photocleavable regular DNA block copolymers described above.

3.5.3 Characterization of PC DNA BCP Assembly

These assemblies were analyzed using TEM, DLS and also hybridization experiments in solutions without added salt to confirm that they are indeed structurally similar to other assemblies. As shown in Figure S6A and B, the PC assemblies contained 3 ± 2 gold nanoparticles per assembly, and the diameter of the assemblies by DLS is 153 ± 6 nm which is similar to the size of other meso-assemblies described above. These PC assemblies also possessed the enhanced DNA binding properties shown for other meso-assemblies (**Figure 3-11**), which indicated they are indeed very similar structurally to other non-photo cleavable assemblies that showed enhanced binding. These results indicate that the photo-cleavable moieties did not affect the binding properties of these meso-assemblies, and that they are characteristically similar to the other meso-assemblies studied. Thus making them reasonable models used to determine the number of DNA strands per meso-assembly of non-photocleavable meso-assemblies.

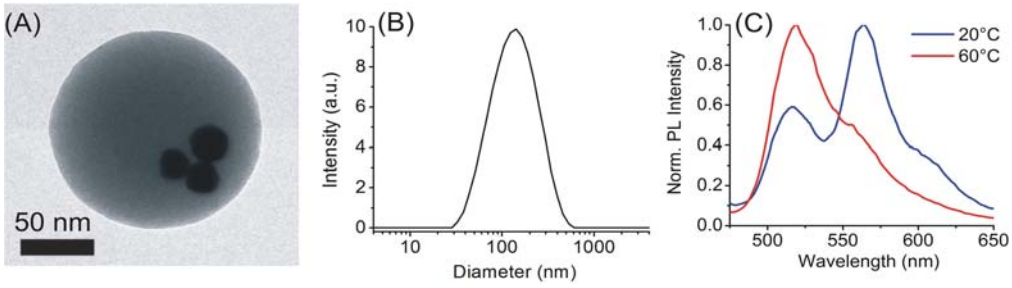

Figure 3-11. (A) TEM image and (B) DLS of AuNP@PS@PC-DNA. (C) Hybridization properties of AuNP@PS@PC-DNA assemblies with Cy3-labeled target in solutions with no added salt showing the assemblies enhanced binding properties.

3.5.4 Determining the DNA Density

The total number of assemblies in the solution was determined using the encapsulated gold nanoparticles as markers as shown in **Eq.3-6**, where the total number of encapsulated gold nanoparticles were determined using ICP-MS and the average number of gold nanoparticles per assembly was determined based on the statistical averaging of the number of gold nanoparticles per assembly using TEM images of AuNP@PS@DNA (**Figure 3-11**).

The FAM-modified PC-DNA was released from the meso-assemblies by the UV irradiation with a Spectroline Ultraviolet transilluminator (Spectronics Corporation TL-365R) (wavelength 365 nm) for 5 min.[6], **Figure 3-12A**. After the DNA cleavage, released DNA and PS beads were separated by centrifugation (14,000 rpm, 45 min). The precipitates of PS beads did not show any FAM emission, confirming that nearly all DNA strands were indeed released from the PS cores. The total number of DNA in the supernatant was determined by measuring the absorbance and the fluorescence of FAM attached to the released DNA. The value is in good agreement with the initial DNA concentration used to prepare the assemblies, suggesting almost all the DNA strands were cleaved off the assembly surface. Finally, the average number of DNA strands per assembly was determined by dividing the total number of cleaved DNA strands by the total number of assemblies.

From multiple measurements, the areal DNA density of AuNP@PS@PC-DNA was determined to be 62.5 ± 4.5 pmol/cm^2, which corresponds to the DNA foot-print of 2.6 ± 0.2 nm^2. Considering that the diameter of B-form DNA duplex is 2.0 nm[7], this foot print value is close to the smallest possible value. For comparison (**Figure 3-12B)**, the

areal DNA density of meso-assemblies is about four times higher than the highest value reported for DNA-modified gold nanoparticles of similar size (150 nm) with the same DNA sequence and spacer (15 pmol/cm^2).[5] The maximum areal DNA density reported for gold nanoparticles was 19 pmol/cm^2 using a PEG-spacer.[5] In the case of DNA functionalized gold nanoparticles, the calculated foot-print of each thiol-terminated DNA ranged from 4.9 nm^2 to 12.9 nm^2,[5] where the foot-print increases with increasing nanoparticle size as discussed above. To the best of our knowledge, the DNA density on our meso-assemblies is the highest reported value in the literature for DNA conjugated nanoparticles. We believe that the ultrahigh DNA density is responsible for the drastically enhanced DNA binding of our meso-assemblies.

3.6 Effect of High DNA Density on Enhanced Binding Property

In order to investigate the role of DNA density on the enhanced binding properties, a series of meso-assemblies of varying DNA density was prepared by the simultaneous self-assembly of block-copolymers with "diluent strand" DNA (DNA sequence: 5'FAM-CACAT3') and block copolymers with recognition DNA (DNA sequence: 5'-FAM A_{10} ATC CTT ATC AAT ATT-3') at varying compositions (**Figure 3-13**).

3.6.1 Experimental Method

Assemblies with varying percentages of diluent DNA block copolymer strands with DNA sequence of 5'FAM-CACAT3' were prepared by simultaneously self-assembling DNA block copolymers with recognition strands and DNA block-copolymers

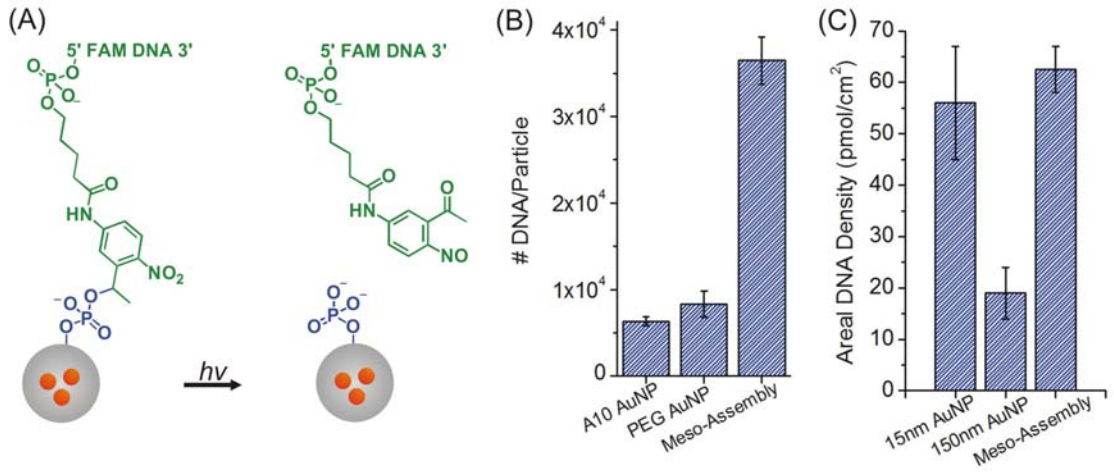

Figure 3-12. (A) Schematic description of the method used to determine the number of DNA strands using photocleavable DNA. (B) The number of DNA strands per meso-assemblies and the number of DNA strands per DNA functionalized gold nanoparticles (AuNP)[5] with A10 and PEG spacer and their (C) the corresponding areal DNA density.

with diluent strands at varying ratios. Diluent polymers (in DMF) were mixed with the recognition polymers in DMF at 5, 10, 33, 50, and 67% to total DNA block copolymer concentration of 3 μM in 1 mL solution. Appropriate amounts of core filling PS (10 μL, 2 mg/mL in DMF) were added to the solution. The three components were self-assembled by the slow water addition (10 μL at 30 sec intervals for a period of 15 min). After overnight stirring, 1 mL of purified water was added to the solution and it was subsequently dialyzed against water for one day. The assemblies were then purified by the above-described method used for typical meso-assemblies without diluent strands.

PS homopolymers were used as a filler to prepare sub-micrometer meso-assemblies (**Figure 3-13A**). The hydrodynamic diameter of the meso-assemblies with diluent strands was determined to be around 230 nm, which is slightly larger than that of meso-assemblies without diluent strands (160 nm), **Figure 3-13B, C**. This is expected as the diluent strand is shorter than the recognition strand, which should increase the aggregation number.[8] Nonetheless, all the assemblies with diluent strands were in the targeted sub-micrometer size range.

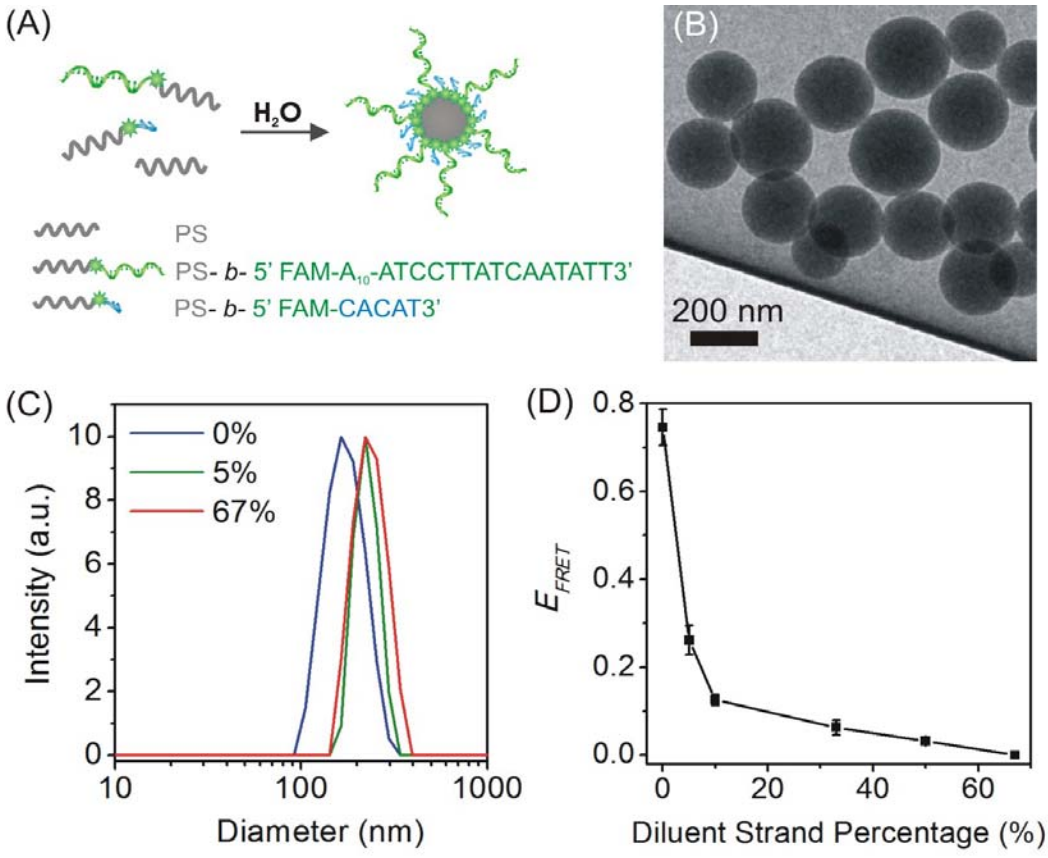

Figure 3-13. (A) Schematic description of the formation of meso-assemblies with diluent strands. (B) A TEM image of meso-assemblies with 10% diluent strand percentage. (C) DLS data of meso-assemblies with 0, 5, and 67% diluent strand percent-age. (D) A Plot of FRET efficiency as a function of diluent strand percentages.

3.6.2 FRET-monitored Hybridization of Diluent-Strand Assemblies

The FRET efficiency between the meso-assemblies and complementary Cy3-DNA was measured in water without added salt for a series of assemblies with varying percentages of diluent strands. As shown in **Figure 3-13D**, the FRET efficiency was sharply decreased as the number of diluent strand was increased to 10%. Eventually, the meso-assemblies with a diluent strand percentage exceeding 67% did not hybridize with complementary Cy3-DNA in water. This result indicates that an extremely high DNA density is necessary for the enhanced binding shown here for meso-assemblies in water without added salt. Note that the FRET efficiency is reduced even with very small amount of diluent strands (5%). This strong dependence of the FRET efficiency on the DNA density clearly indicates that the unusual enhanced binding of meso-assemblies is associated with the high DNA density and the unique local environment.

The high DNA density can affect the DNA hybridization in several different ways. It has been proposed for DNA-conjugated gold nanoparticles that the high DNA density on nanoparticles results in a high local salt concentration, leading to a higher binding constant.[4,9] We believe that the high local salt concentration should play an important role here in DNA block-copolymers as well.

3.7 Effect of Dye on Enhanced Binding Property

3.7.1 Experimental Method

Dye-diluent DNA block copolymer strands were synthesized by the same procedures in ref. [2] with the exception that they are not tagged with a fluorescent label to

the end of the DNA sequence (**Figure 3-14A**). Self-assembled structures of meso-assemblies containing up to 67% of dye-diluent DNA block copolymer strands (33% FAM-DNA block copolymer strands with a fluorescein dye) were prepared by the same procedures use for other homopolymer filled self-assemblies. The diameter of the resulting assemblies was determined to be 174 ± 3 nm based on DLS (**Figure 3-14B**), which is within the range of meso-assemblies with 100% FAM-DNA block copolymer.

3.7.2 FRET-monitored Hybridization of Dye Diluent-Strand Assemblies

FRET experiments with Cy3-labeled strands in solutions with no added salt showed that even at different ratios of dye diluent strands, the FRET efficiency stayed relatively unchanged, indicating that the dye density on the surface of the assemblies is not the important factor in the enhanced binding properties of the assemblies (**Figure 3-14C**).

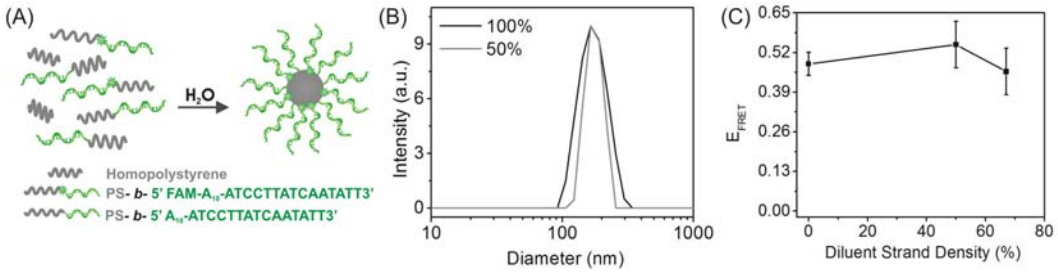

Figure 3-14. (A) Assembly scheme of meso-assemblies containing a mixture of DNA block copolymer strands with and without fluorescein (FAM). (B) DLS measurement of meso-assemblies with 100% and 50% FAM-DNA block copolymer strands. (C) FRET efficiencies of assemblies with 100%, 50% and 33% FAM-DNA block copolymer strands.

For meso-assemblies of DNA block-copolymers reported here, the hydrophobic core play a critical role in achieving the high DNA density needed for enhanced binding. The DNA stands tend to pack tightly to avoid the interaction between water and hydrophobic PS. In addition, the DNA strands can be forced to pack more tightly by introducing core fillers, which is responsible for the extraordinary DNA binding properties of meso-assemblies reported here. In our control experiment, meso-assemblies prepared from the mixture of FAM-labeled DNA block-copolymers and unlabeled DNA block-copolymers showed a similar FRET values as the typical meso-assemblies made of only FAM-labeled block-copolymers (**Figure 3-14C**), demonstrating that the inclusion of FAM is not responsible for the enhanced binding. While it is possible that the hydrophobicity and the aromatic structure of styrene monomers of PS might contribute to the DNA binding through the hydrophobic effect and the interaction between DNA bases and PS, it cannot solely explain the extraordinary DNA binding properties of meso-assemblies of PS-*b*-DNA, since simple micelles made of the same polymer did not show the level of enhanced binding. It is also important to note that the strong binding of meso-assemblies does not compromise the sequence-specific DNA binding.[2]

3.8 Summary and Conclusions

In summary, we have determined that DNA block copolymer assemblies with fillers (nanoparticles or homopolyers) in the core possessed an ultra-high surface DNA density, more than four times higher than the highest reported value in the literature. We have determined that this ultra-high DNA density is critical for enhanced DNA binding exhibited by these DNA block copolymer assemblies. As illustrated by diluent strands

experiments, where with the gradual diluent of the DNA strands on the surface while keeping the structure constant showed a drastic decrease in the DNA binding affinity of these assemblies with the target strands at extremely low salt conditions, and this enhanced binding decreased sharply when at as little at 10% of the DNA strands were "diluted", and almost completely disappeared for assemblies with 50% of diluent strands in the composition.

3.9 References

(1) Clegg, R. M.; David, M. J. L. a. J. E. D. In *Methods Enzymol.*; Academic Press, 1992; Vol. Volume 211; pp 353-388.

(2) Chen, X.-J.; Sanchez-Gaytan, B. L.; Hayik, S. E. N.; Fryd, M.; Wayland, B. B.; Park, S.-J.: Self-Assembled Hybrid Structures of DNA Block-Copolymers and Nanoparticles with Enhanced DNA Binding Properties. *Small*. 2010;**6**(20):2256-2260.

(3) Li, Z.; Zhang, Y.; Fullhart, P.; Mirkin, C. A.: Reversible and chemically programmable micelle assembly with DNA block-copolymer amphiphiles. *Nano Lett.* 2004;**4**(6):1055-1058.

(4) Lytton-Jean, A. K. R.; Mirkin, C. A.: A Thermodynamic Investigation into the Binding Properties of DNA Functionalized Gold Nanoparticle Probes and Molecular Fluorophore Probes. *J. Am. Chem. Soc.* 2005;**127**(37):12754-12755.

(5) Hurst, S. J.; Lytton-Jean, A. K. R.; Mirkin, C. A.: Maximizing DNA Loading on a Range of Gold Nanoparticle Sizes. *Anal. Chem.* 2006;**78**(24):8313-8318.

(6) Olejnik, J.; Krzymanska-Olejnik, E.; Rothschild, K. J.: Photocleavable Biotin Phosphoramidite for 5'-End-Labeling, Affinity Purification and Phosphorylation of Synthetic Oligonucleotides. *Nucleic Acids Res.* 1996;**24**(2):361-366.

(7) Voet, D.; Voet, J. G.; Pratt, C. W. *Fundamentals of Biochemistry: Life at the Molecular Level*; 4th ed., 2012.

(8) Zhang, L.; Eisenberg, A.: Multiple Morphologies and Characteristics of "Crew-Cut" Micelle-like Aggregates of Polystyrene-b-poly(acrylic acid) Diblock Copolymers in Aqueous Solutions. *J. Am. Chem. Soc.* 1996;**118**(13):3168-3181.

(9) Jin, R.; Wu, G.; Li, Z.; Mirkin, C. A.; Schatz, G. C.: What controls the melting properties of DNA-linked gold nanoparticle assemblies? *J. Am. Chem. Soc.* 2003;**125**(6):1643-1654.

Chapter 4. Cellular Uptake of DNA-*b*-Polystyrene (PS) Assemblies

4.1 Overview

This chapter presents results on the cellular uptake studies of the DNA-*b*-PS assemblies; mainly investigate 1) the efficiency of the uptake, 2) the stability of the

assemblies in cell medium and incubation conditions, 3) the stability of the DNA payload being delivered by the assemblies, and 4) the ability of these meso-assemblies in the down regulation of an exogenous gene.

4.2 Methodology

4.2.1 Aseptic Cell Culturing

HeLa cells were cultured with Dulbecco's modified Eagle's medium (DMEM, high glucose 4.5 mg/L, Invitrogen) supplemented with 10% fetal bovine serum (FBS, Hyclone) in 25 cm^2 cell culture flask (Thermoscientific, Nunc flask) at 37 °C, 5 % CO_2 and 95 % relative humidity in a Sanyo CO_2 cell culture incuabtor. The cells were trypsinized and passaged every two to three days.

4.2.2 Plasmid Amplification by Bacteria

4.2.2.1 Preparation of LB Broth and Agar Plates

The work area as well as anything used in the process was sterilized with 70% ethanol. Before opening and closing any of the autoclaved bottles, flame the neck of the containers using a Bunsen burner.

LB Miller broth was prepared by adding appropriate amount of LB Miller powder to de-ionized water to achieve a concentration of 25g of LB per 1 L of water. Add the mixture into an autoclavable container and keep a loose aluminum foil cap on the container, and authoclave the solution.

Agar plates were prepared by adding appropriate amount of LB Miller powder (25g of LB per 1 L of water) and add 1.5% of agarose by mass. That is, for 200 mL of

water, add 5g of LB Miller powder and 3 g of agarose. Add the mixture into an autoclavable container and keep a loose aluminum foil cap on the container, and authoclave the solution. While the medium is still warm, appropriate amount of antibiotic was added (**Table 4-1**). The solution was mixed by swirling gently to avoid bubbles, and poured into plates. The plates were then cooled in 4°C fridge until they set.

4.2.2.2 Transformation of Plasmid

In the typical transforming experiment, 1-10 ng of plasmid DNA to bacterial cells and mix with pipette. After incubation on ice for 30 min, heat shock the cells for 45 sec by incubation in a 42°C water bath, and then immediately place the tubes containing the cells on ice for 2 min. Then, 0.45 mL of S.O.C. medium was added to each tube and shake at 225 rpm for 1 hr at 37°C.

4.2.2.3 Plating/Culturing Transformed Bacteria

In a typical experiment, remove excess moisture in the agar plates by incubating at 37°C for a few mintutes with lids slightly ajar. Then about 200 uL of transformed bacteria cells was added to the agar plate and a flame-sterilize metal loop was used to spread the cells on the agar plates. The plates were then incubated at 37°C overnight.

4.2.2.4 Extraction and Purification of Plasmid

4.2.3 Transfecting Cells with Exogenous Plasmid

GFP plasmids were transfected into HeLa cells (**Scheme 4-1**) to be used to monitor the gene regulation capability of the DNA-b-PS meso-assemblies with antising GFP oligonucleotide sequence on the DNA block.

Incubate the HeLa cells in well plates overnight at 37°C or until the cells are 70 – 80% confluency. Determine the concentration of plasmid DNA by UV-vis. Calculate the volume of DNA needed for a total of 1.5 ug of DNA per well for 6-well plates. Prepare a solution of 10 uL to 12.5 uL lipofectamine transfection reagent with 1 mL Opti-MEM and 1.5 ug DNA, and incubate the solution at room temperature for 30 min. Aspirate off the spent medium and wash the cells in the wells with 1x PBS. Aspirate off the PBS. Add the transfecting agent/DNA medium solution to the wells. Add an additional 1 mL of Opti-MEM and incubate the solution at 37°C for 3 hrs (for short plasmid, ~ 3K bp) or 5-8 hrs (for long plasmid, > 3K bp). Aspirate off the transfecting solution and wash the cells in the wells with 1x PBS. Aspirate off the PBS and add new phenol red- free cell culture medium to the wells. Check the transfected cells using fluorescence microscopy. The transfected plasmid will be active for ~ 1 week. Usually the success rate of transfection is ~ 40 – 50%. If it is desired to select only transfected cells, flow-cytometry can be used to select fluorescent cells.

Table 4-1: Amount of antibiotic for agar plates for 200 mL volumes.

Antibiotic	Final Concentration (ug/mL)	Volume of Stock Solution
Ampicillin	100	0.8 mL of 25 mg/mL stock
Kanamycin	50	1 mL of 10mg/mL stock
Chloramphenicol	35	0.206 mL of 34 mg/mL stock

Scheme 4-1. Tranfection of exogenous GFP plasmid into cells.

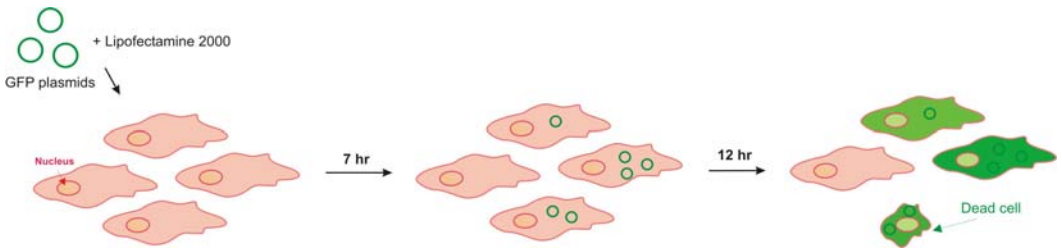

4.2.4 Antisensing Exogenous Genes with DNA BCP Meso-assemblies

Cells used for cellular uptake experiments were cultured with phenol red-free DMEM with 10% FBS. PS@PS@DNA (DNA sequence 5'- A_{10} ATC CTT ATC AAT ATT-FAM-3') or PS@PS@DNA hybridized with Cy3-modified complementary DNA strands at one equivalence (50 μL, 10 nmol total DNA concentration) were incubated with the cells grown in 200 μL phenol red-free DMEM with 10% FBS in Nunc Lab-Tek 4-well chambered cover glass at 37 °C with 5 % CO_2 and 95 % relative humidity for 24 hr. Cells were images by confocal microscopy using an Olympics FluoView FV1000 equipped with a 488nm, 559 nm and 633nm diode-gas laser combination and a SIM scanner.

4.3 Cellular Uptake of DNA Block Copolymer Assemblies

In general, negatively charged particles show very little cellular uptake efficiency due to the charge repulsion between the negative charged particles with the negatively charged cell membrane.[1] Cellular uptake studies of our meso-assemblies with HeLa cells showed that they can be efficiently taken up without any co-transfecting agents (**Figure 4-1)**. For cellular uptake studies, meso-assemblies of PS@PS@DNA were prepared by the self-assembly of DNA block-copolymers labeled with FAM at the 3' end. PS homopolymers were used as the core-filler. The cellular uptake of meso-assemblies was monitored by measuring FAM fluorescence. More than 99% of cells showed PL from the FAM-labeled meso-assemblies (**Figure 4-1A, top**). The z-section analysis of the cells incubated with the meso-assemblies showed even distribution of the assemblies throughout the cytoplasm (**Figure 4-1B**). Cells incubated with plain FAM-labeled DNA

did not show any uptake as expected (**Figure 4-2**). However, our meso-assemblies showed highly efficient cellular uptake presumably due to the extremely high DNA density as shown for DNA-modified gold particles.[2] It has been proposed that negatively charged nanoparticles can be taken up by cells by opsonization;[3, 4] where positively charged proteins in the cell medium bind to the surface of negatively charged nanoparticles, which can then be taken up by cells.

Moreover, these meso-assemblies can also be used to carry an additional load of therapeutic nucleic acid in addition to the DNA already present on the meso-assemblies. This was demonstrated using complementary DNA labeled with Cy3-DNA. In this way, both FAM and Cy3 fluorescence is visible without significant FRET between the two dyes. The meso-assemblies prehybridized with cCy3-DNA showed efficient cellular uptake. Moreover, the cCy3-DNA did not show signs of DNA degradation as indicated by the strong Cy3 fluorescence signal (**Figure 4-1A, bottom**). In comparison, cells incubated with the duplex of complementary Cy3-DNA and FAM-DNA did not such a significant uptake based on the FAM fluorescence signal (**Figure 4-2**). As shown for DNA-modified nanoparticles,[5] the ability of meso-assemblies to protect the hybridized complementary DNA can be used as a way to deliver siRNA. The meso-assemblies are advantageous over DNA-modified nanoparticles which attracted tremendous attention for gene detection and delivery.[2, 4, 5] First, additional therapeutic drugs can be readily loaded into the meso-assemblies by self-assembly. Secondly, the meso-assemblies can be fabricated with non-toxic low cost polymeric materials. Thirdly, the meso-assemblies show unprecedented high DNA binding constant, which should be useful in a number of and RNA DNA detection and regulation applications.

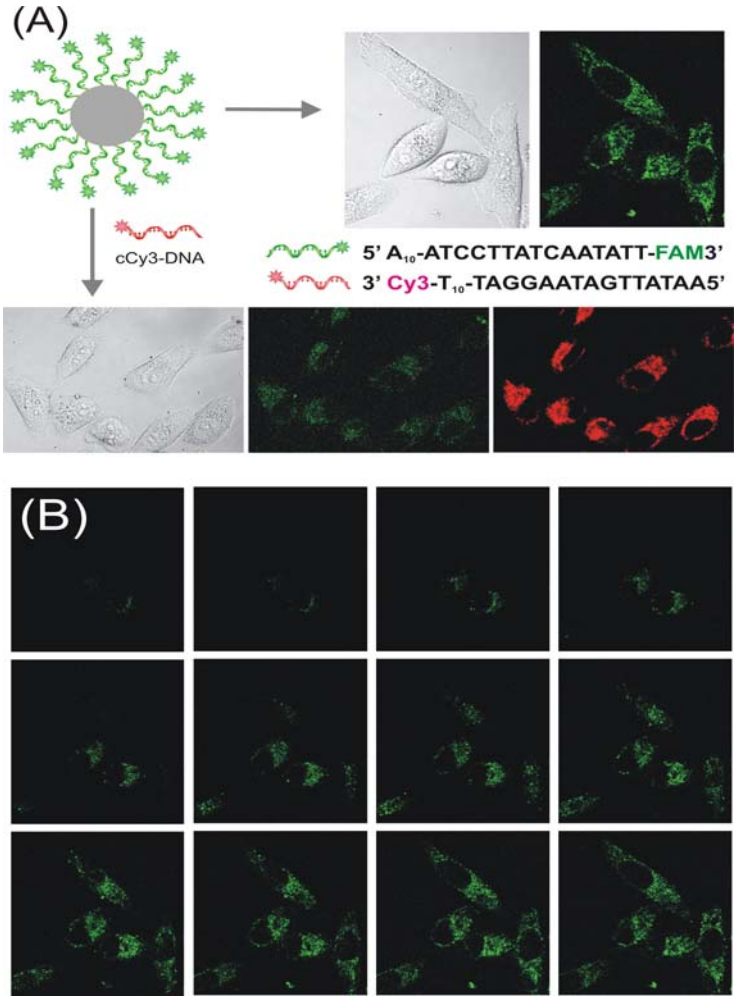

Figure 4-1. (A) Confocal images of HeLa cells after the incubation with PS@PS@FAM-DNA (top) and after the incuvation with PS@PS@FAM-DNA prehybridized with cCy3-DNA (bottom). (B) z-sectioning images of cells incubated with PS@PS@FAM-DNA using section size of 2 microns.

4.4 Cellular Uptake of Plain DNA

Confocal images of HeLa cells after incubation with single stranded DNA tagged with a fluorescein label (ssFAM-DNA) and double-stranded DNA with ssFAM-DNA and

ssCy3-DNA with a Cy3 label (dsFAM-DNA/Cy3-DNA) (**Figure 4-2**) showed that these plain DNA not efficiently uptake by cells. This is expected, since one of the major challenges in therapeutic DNA and RNA delivery has been the degradation of naked DNA by nuclease present in the cell medium[6]. This further demonstrated the importance of a dense layer of DNA on the surface. It should be noted that while the ssFAM-DNA and dsFAM-/Cy3-DNA did not show a significant FAM signal, a strong Cy3 signal was observed in the case of ssCy3-DNA (data not shown) and dsFAM-/Cy3-DNA in cells after incubation. We believe this signal is not that of intact Cy3-DNA strands, rather it is more likely to be Cy3-dye and or segmented Cy3-DNA, since as mentioned, it has been demonstrated that DNAse degrades naked DNA within minutes[7]. The uptake of the Cy3 dye is not surprising since it has a positive charge, and it has been shown that positively charged species are effectively uptake by cells due to the favorable interaction between the negative charged cell membrane and the cationic species.

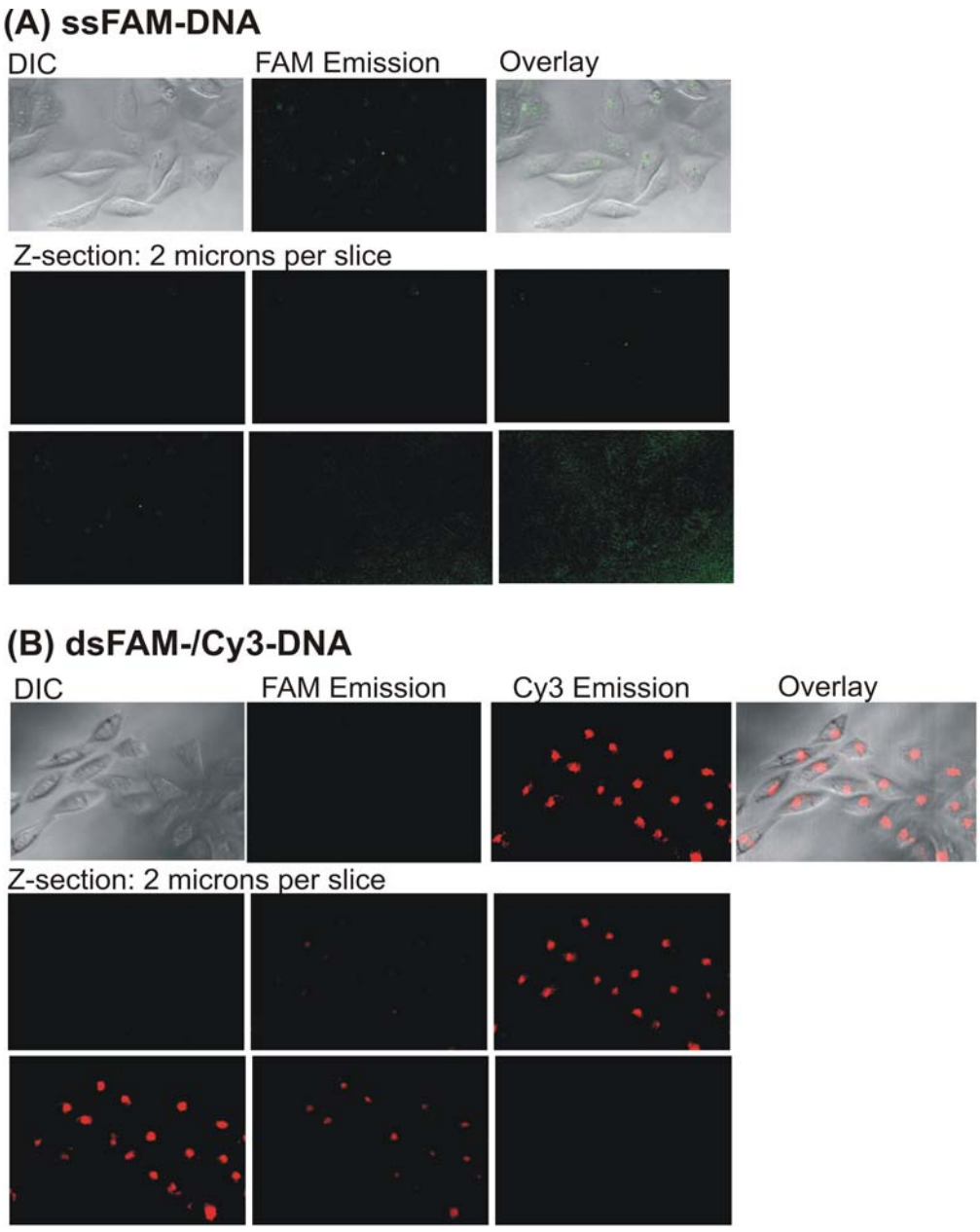

Figure 4-2. Confocal images of HeLa cells after incubation with ssFAM-DNA. The fluorescent image clearly showed that the ssFAM-DNA does not get uptake by the cells. The intense Cy3 signal without FAM signal indicates that the positively charged Cy3 dyes get taken up by cells after they are cleaved off from the DNA.

4.5 Stability of DNA BCP Assemblies

Stability studies of meso-assemblies in cellular uptake conditions showed that when the assemblies were mixed with cell medium (DMEM/10% FBS), the hydrodynamic diameter increased by about 10 nm (**Figure 4-3**), potentially due to opsonization of proteins onto the particle surface. More importantly, the assemblies did not show any sign of aggregation under stimulated physiological incubation conditions used for the cellular uptake studies, namely 37°C for 48hr at 95% humidity and 5%CO2 in cell medium DMEM/10%FBS. Importantly, the meso-assemblies were shown to be very stable in simulated physiological conditions, and did not show any aggregation after 48 hr of incubation in cell medium under the same conditions used to culture cells.

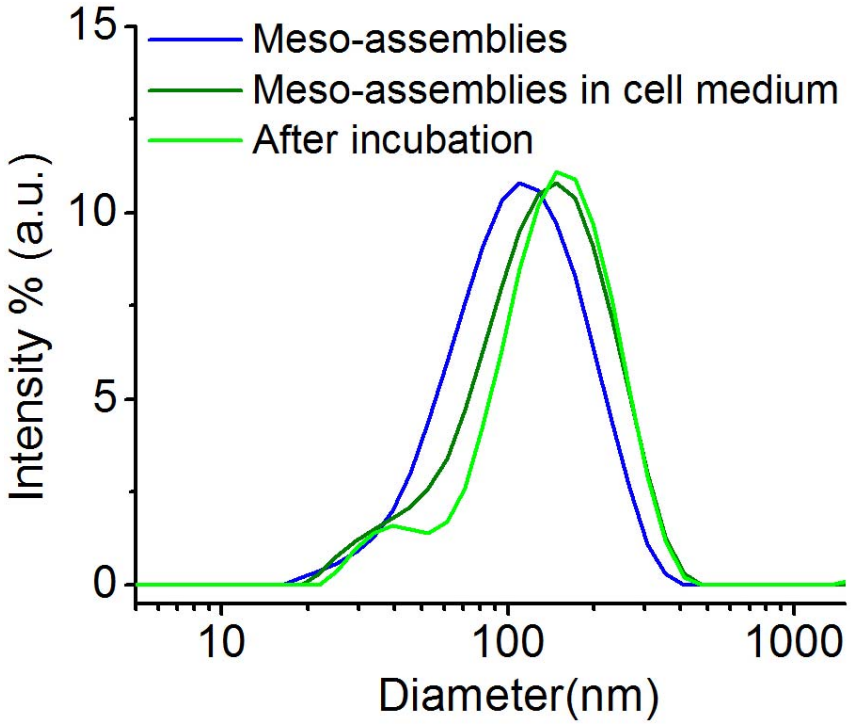

Figure 4-3. Dynamic light scattering measurements for the stability of meso-assemblies in cellular uptake study conditions; incubate condition: 37°C for 48 hr in cell medium, DMEM/10%FBS.

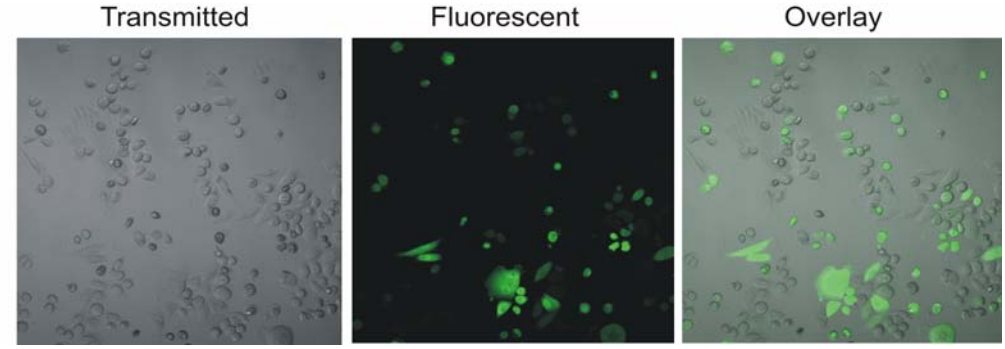

Figure 4-4. Confocal images of HeLa cells transfected with GFP plasmids.

4.6 Antisensing of GFP using DNA-*b*-PS Meso-assemblies

Antisensing experiments with DNA-*b*-PS assemblies where the DNA sequence on the assembly are the antisense sequence targeting green fluorescent protein (GFP) in GFP-transfected HeLa cells (**Figure 4-5**). GFP-HeLa cells treated with antisensing DNA block copolymer assemblies showed a significant decrease in the emission intensity of GFP after 48 hours of incubation, a 21.8 % decrease relative to cells not treated with the antisensing nanoparticles, **Figure 4-6**. Assemblies with scrambled DNA strands as well as the antisensing DNA alone do not show this down regulation. With longer incubation time (72 hr), **Figure 4-6B**, a bigger decrease in the GFP emission was observed 42.9 %; however, a 21.1% decrease in the GFP emission intensity was also observed with the DNA block copolymer assemblies with scrambled DNA strands. This decrease in the GFP emission from the controlled scrambled DNA block copolymer assemblies is speculated to be a result of cell death or perturbation to the normal cellular metabolism cycle which prevented the synthesis of GFP, thus making it difficult to determine whether or not longer incubation times in fact provide more efficient antisensing capabilities.

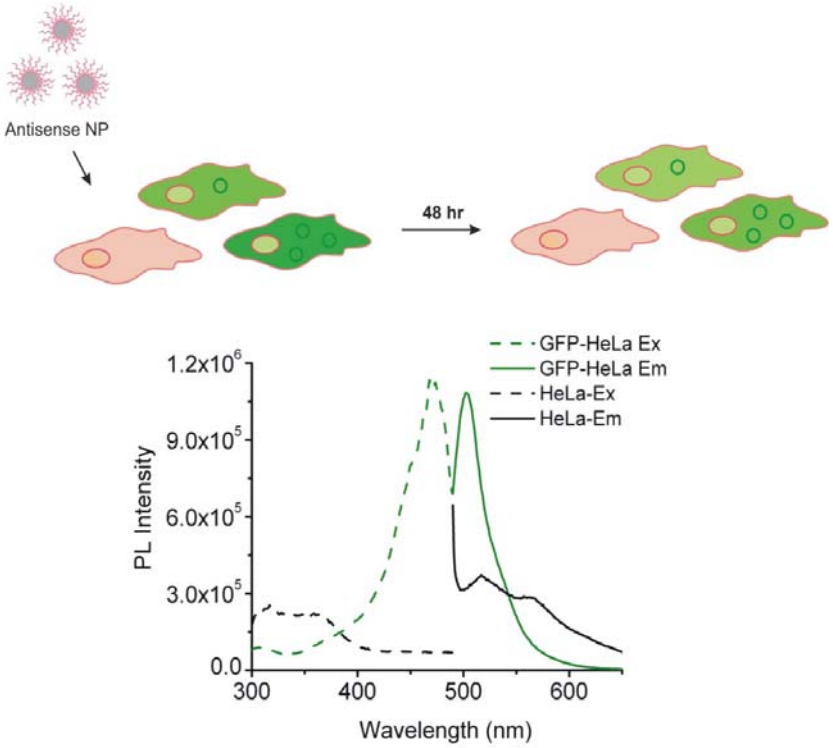

Figure 4-5. Confocal images of HeLa cells transfected with GFP plasmids.

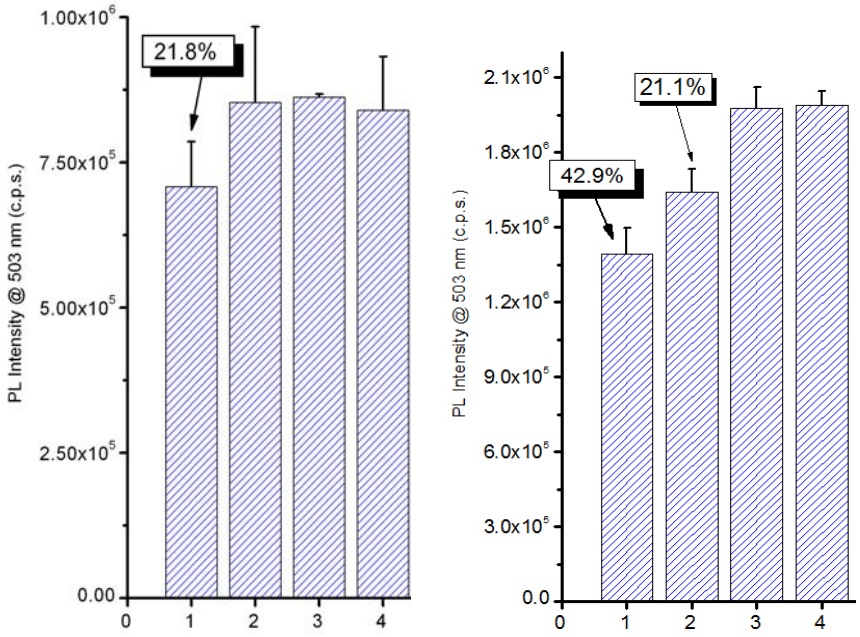

Figure 4-6. Plots of emission intensity of green fluorescent proteins (GFP) in GFP-transfected HeLa cells at 48 (A) and 72 (B) hours of incubation with (1) DNA block copolymer assemblies containing antisensing sequence. Also of (2) assemblies with non-antisensing sequence and (3) antisensing single-stranded DNA and (4) control with pristine GFP-transfected HeLa cells..

4.7 Summary and Conclusions

In summary, we have found that these self-assemblies of DNA block copolymers (specifically DNA-*block*-polystyrene, DNA-*b*-PS) with nanoparticles encapsulated in the core exhibited very efficient uptake by HeLa cells without the use of any co-transfecting agents. The DNA payload also appeared to be protected during the process. We have also demonstrated that the DNA-b-PS assemblies with antisense DNA strands for GFP can down regulate the expression of GFP in GFP expressing HeLa cells. While the work on DNA-*b*-PS is interesting and has great potential in DNA detection applications due to the enhanced binding properties, however, their application in delivery is limited due to the non-biocompatibility of polystyrene. To this end, we aimed toward the synthesis of biocompatible/biodegrable DNA block copolymer to be used for drug delivery and antisensing applications.

4.8 References

1. Verma, A. & Stellacci, F. Effect of Surface Properties on Nanoparticle–Cell Interactions. Small 6, 12-21 (2009).
2. Rosi, N. L. et al. Oligonucleotide-Modified Gold Nanoparticles for Intracellular Gene Regulation. Science 312, 1027-1030 (2006).
3. Alkilany, A. M. et al. Cellular Uptake and Cytotoxicity of Gold Nanorods: Molecular Origin of Cytotoxicity and Surface Effects. Small 5, 701-708 (2009).
4. Prigodich, A. E., Alhasan, A. H. & Mirkin, C. A. Selective Enhancement of Nucleases by Polyvalent DNA-Functionalized Gold Nanoparticles. Journal of the American Chemical Society 133, 2120-2123 (2011).

5. Giljohann, D. A., Seferos, D. S., Prigodich, A. E., Patel, P. C. & Mirkin, C. A. Gene Regulation with Polyvalent siRNA Nanoparticle Conjugates. Journal of the American Chemical Society 131, 2072-2073 (2009).
6. Luo, D. & Saltzman, W. M. Synthetic DNA delivery systems. Nat Biotech 18, 33-37 (2000).
7. Akita, H., Hatakeyama, H., Khalil, I. A., Yamada, Y. & Harashima, H. in Synthesis and Structural Design for Drug and Gene Delivery (Elsevier Ltd, 2011).
8. Chen, X.-J. et al. Self-Assembled Hybrid Structures of DNA Block-Copolymers and Nanoparticles with Enhanced DNA Binding Properties. Small 6, 2256-2260 (2010).

Chapter 5. Biocompitible DNA Block Copolymer for Antisensing Applications

5.1 Overview

This chapter presents the synthesis and cellular uptake studies on a second generation of DNA block copolymer, which uses biocompatible and biodegradable

hydrophobic polymer. Results on the size and shape effect on the cellular uptake of the DNA BCP of the same composition are also presented. Furthermore, preliminary results on biomedical applications of these DNA BCP assemblies in antisensing of Tau and Vimentin proteins are also presented.

5.2 Antisensing with Short Nucleic Acids

5.2.1 siRNA: RNA Interferance (RNAi)

Over the past couple of decades, there has been tremendous hype and excitement on using siRNA for gene therapy. Research in this area has helped develop a clearer understanding of the mechanism on how siRNA regulates the expression of targeted genes. The mechanism involves the binding of siRNA to the targeted mRNA. This duplex RNA then actives the RNA-induced silencing complex (RISC), where the RISC/siRNA complex will in turn cleave the mRNA. After the cleavage of the mRNA, the RISC/siRNA complex will release the cleaved mRNA and seek out new uncleaved mRNA and continue the cycle several times.[1] The RISC is composed of three components; one of the major components is a protein call argonaute which is responsible for cleaving the mRNA via a catalytic process which hydrolyzes the phosphate backbone.[2] (**Figure 5-1A**)

There is no typical size of double stranded (dsRNA) used in RNAi. However, the length of the dsRNA does matter in the efficiency of the silencing effect. It appears that longer dsRNA (300 to 600 nucleotides) have the best silencing effect in experiments using fruit flies compared to shorter dsRNA (150 nucleotides or less). However, increasing the concentration of the shorter dsRNA could increase the silencing effect to

the level of long dsRNA. Furthermore, dsRNA is not typically used in mammalian cell studies because they can invoke an antiviral immune response, so researchers usually use siRNA directly in RNAi studies in mammalian cells.[3]

5.2.2 DNA: RNAseH

Our system delivers synthetic oligo-DNA as the therapeutic nucleic acid instead of oligo-RNA given that the structure of DNA is more stable compared to that of RNA. In antisensing applications, antisensing oligo-DNA binds to a region of the targeted mRNA, then the mRNA is degraded by the RNAseH enzyme through the recognition of a DNA/RNA duplex.

RNAseH, the enzyme responsible for cleaving DNA/RNA duplex, cleaves the mRNA via hydrolysis of the phosphate backbone in the antisensing DNA/mRNA duplex.[5] (**Figure 5-1C**)

5.2.3 Steric Inhibition

In steric inhibition, an antisense oligomer can alternatively block the function of the ribosome or other proteins that are critical for elongation or splicing by binding to the targeted mRNA. (**Figure 5-1B**)

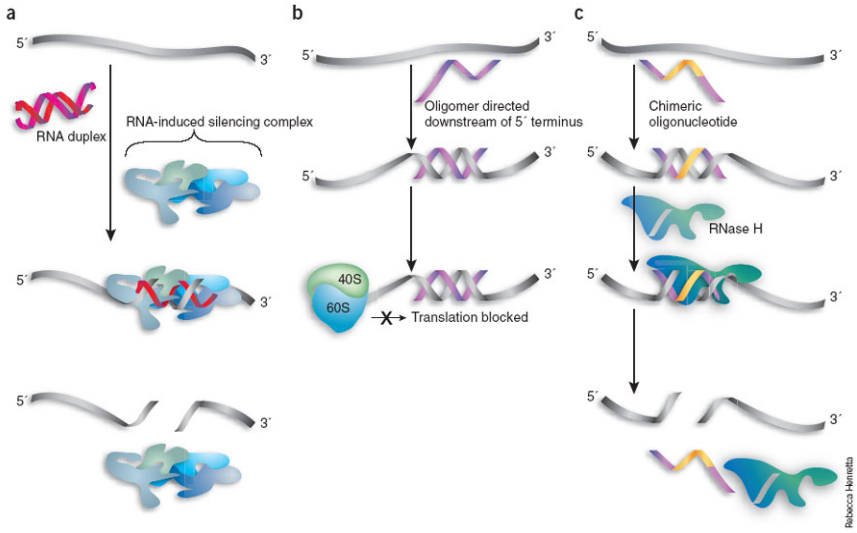

Figure 5-1. (A) RISC complex mechanism. (B) Steric inhibition mechanism. (C) RNAseH mechanism. Reprint with permission from ref [4].Copyright 2007 Nature Publishing Group.

5.3 Cellular Uptake Studies

5.3.1 Methodology

Cell studies were conducted with HeLa cells. Cells were cultured with phenol red-free DMEM with 10% FBS. Polymer assemblies (50 μL, 10 nmol) were incubated with the cells grown in 200 μL phenol red-free DMEM with 10% FBS in Nunc Lab-Tek 4-well chambered cover glass at 37 °C with 5 % CO_2 and 95 % relative humidity for 24 hr.

Cells were images by confocal microscopy using an Olympics FluoView FV1000 equipped with a 488nm, 559 nm and 633nm diode-gas laser combination and a SIM scanner. XTT assays were performed to evaluate the cytotoxicity of the assemblies following the recommended procedures by the manufacturer (Sigma Aldirch).

5.3.2 Azide-terminated PEG-*b*-PCL

Polymer assemblies of PEG-*b*-PCL loaded with Nile Red dye molecules in the hydrophobic PCL core prepared **Section 2-4.1** were first tested and were found to get uptake by cells rather rapidly. As can be seem in **Figure 5-2**, more than 99% of the cells incubated with the polymer structure show red fluorescence within less than 12 hr. Moreover, no inherent cytotoxicity was observed. It was also interesting to find that these assemblies appear to have the ability to by-pass the plasma membrane and be taken up even by cells that are known to be difficult to transfect, such as neuron and primary cell lines (**Section 5.5**).

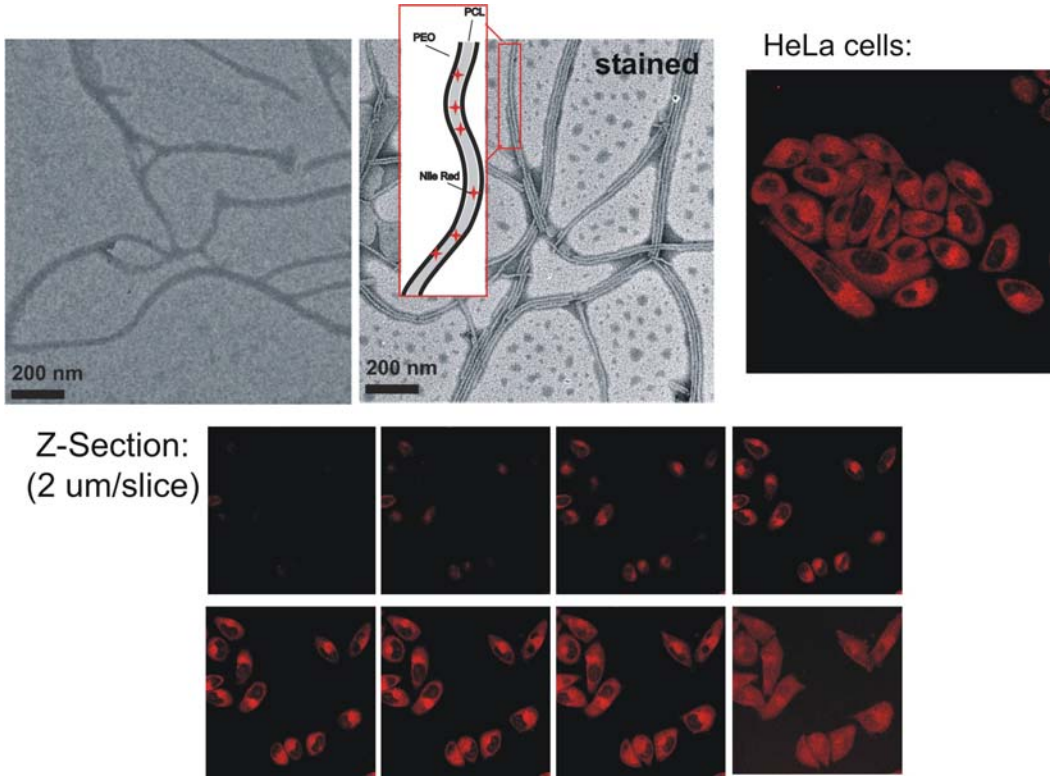

Figure 5-2. Cellur uptake of PEG-*b*-PCL with HeLa cells.

5.3.3 DNA-*b*-PEG-*b*-PCL

Nanostructures of DNA-*b*-PEG-*b*-PCL prepared in **Chapter 2** were first tested and found to get uptake by cells rather rapidly like of the PEG-*b*-PCL assemblies without DNA, (**Figure 5-3**, as shown by the green fluorescence from the FAM on the DNA. No inherent cytotoxicity was observed for the polymer assemblies conjugated with DNA as well as shown in the XTT assay. These assemblies were demonstrated to be efficient carriers for organic molecules as well. As demonstrated in **Figure 5-4**, the DNA-*b*-PEG-*b*-PCL assemblies loaded with Nile Red dye molecules in the hydrophobic core showed that cells incubated with this polymer carriers showed >99% transfection within 12 hr. The cells showed both green and red fluorescence and the both are co-localized indicating the polymer and DNA are both present and most likely intact. Furthermore, we demonstrate in Figure **5-5** that the polymer assemblies with varying DNA density on the surface are taken up by cells similarly.

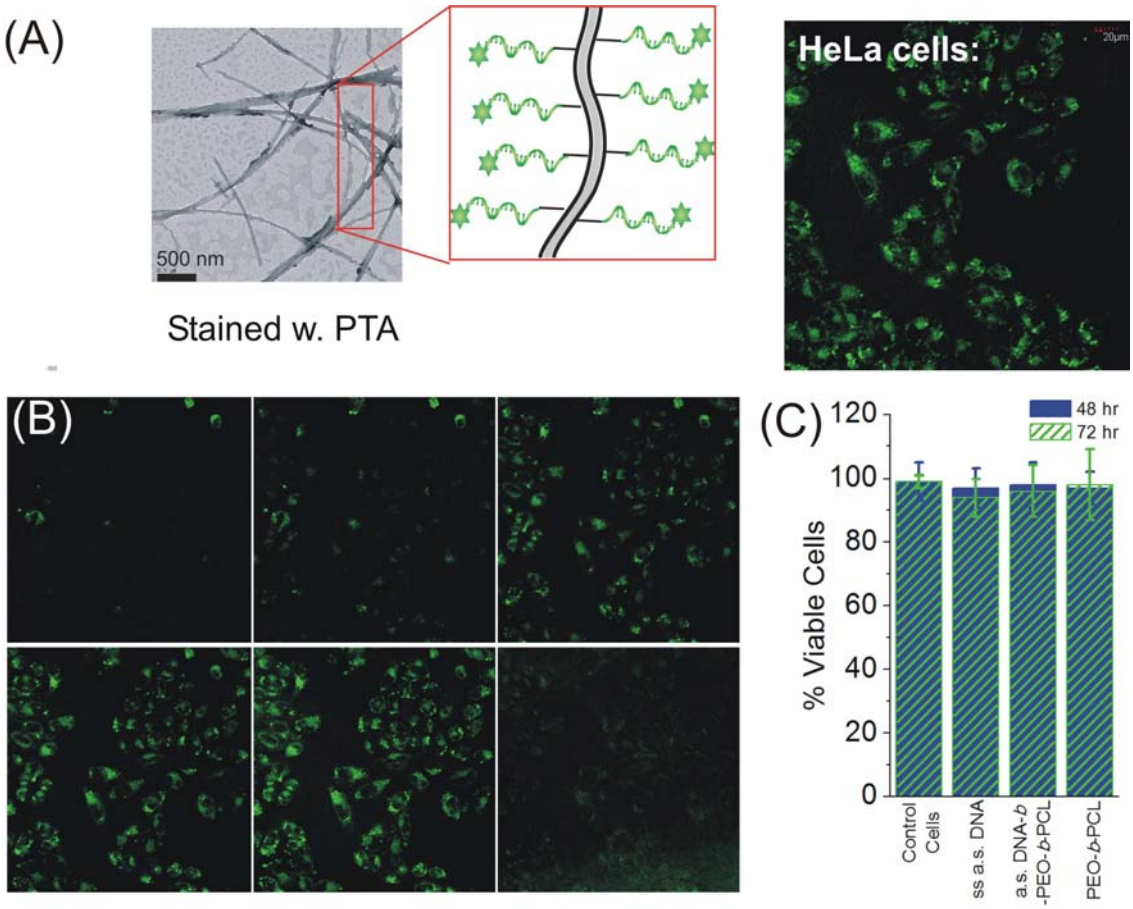

Figure 5-3. (A) Cellur uptake of DNA TCP with HeLa cells. (B) Z-section confocal images of the treated cells, 2 um per slice. (C) XTT assay analysis on the cytotoxicity of the biodegrable DNA block copolymer.

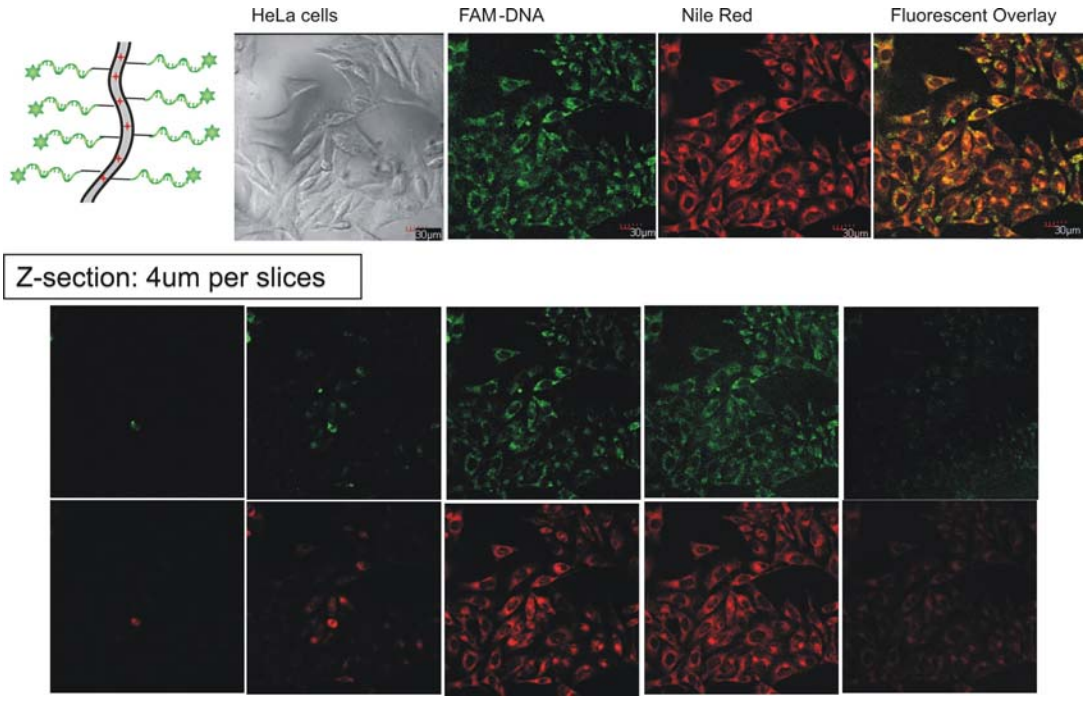

Figure 5-4. Cellur uptake of DNA TCP loaded with Nile Red.

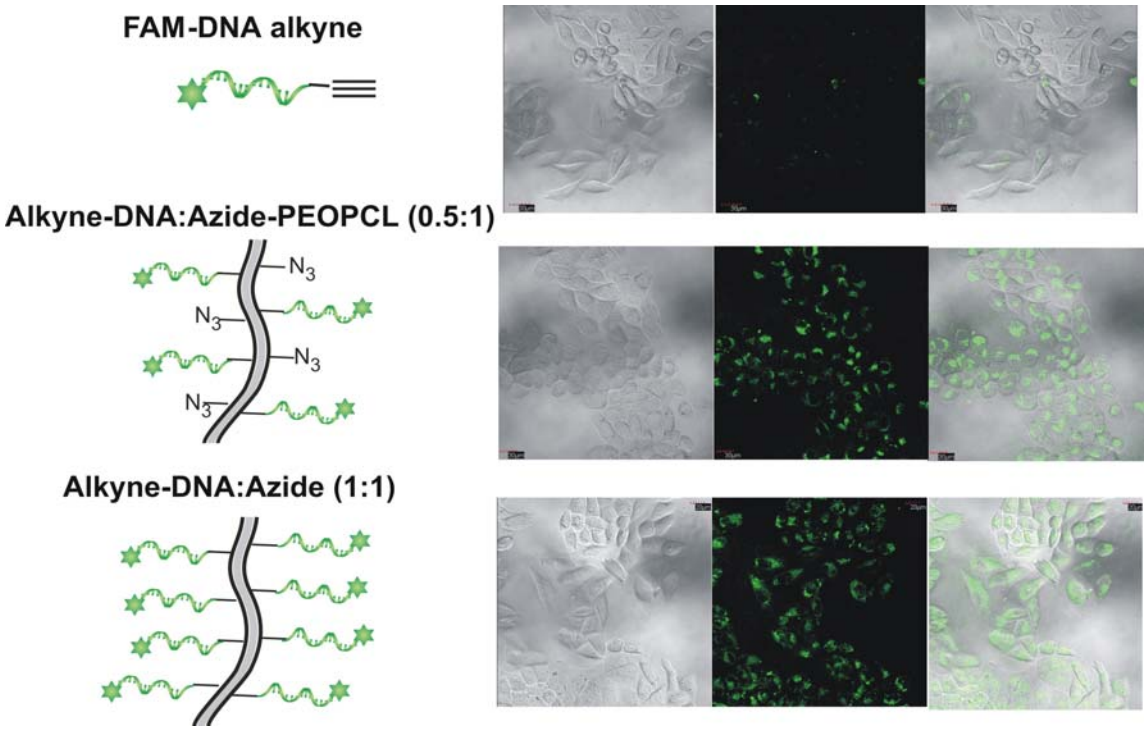

Figure 5-5. Cellular uptake of DNA TCP with HeLa cells with different DNA density.

5.3.4 Effect of Size and Shape on Cellular Uptake Efficiency

To investigate the effect size and shapes have on the cellular uptake on the DNA-b-PEG-b-PCL nanostructures, the uptake efficiency of spherical versus fibril-like structures were compared, and nanostructures with the sizes between 100 to 500 nm are also compared. (**Figure 5-6**). There appeared to be no significant difference observed in the effect of shape for this polymer system. However, the size appeared to play more of a role in the uptake. It was found that assemblies greater than 500 nm in size did not show significant uptake by cells.

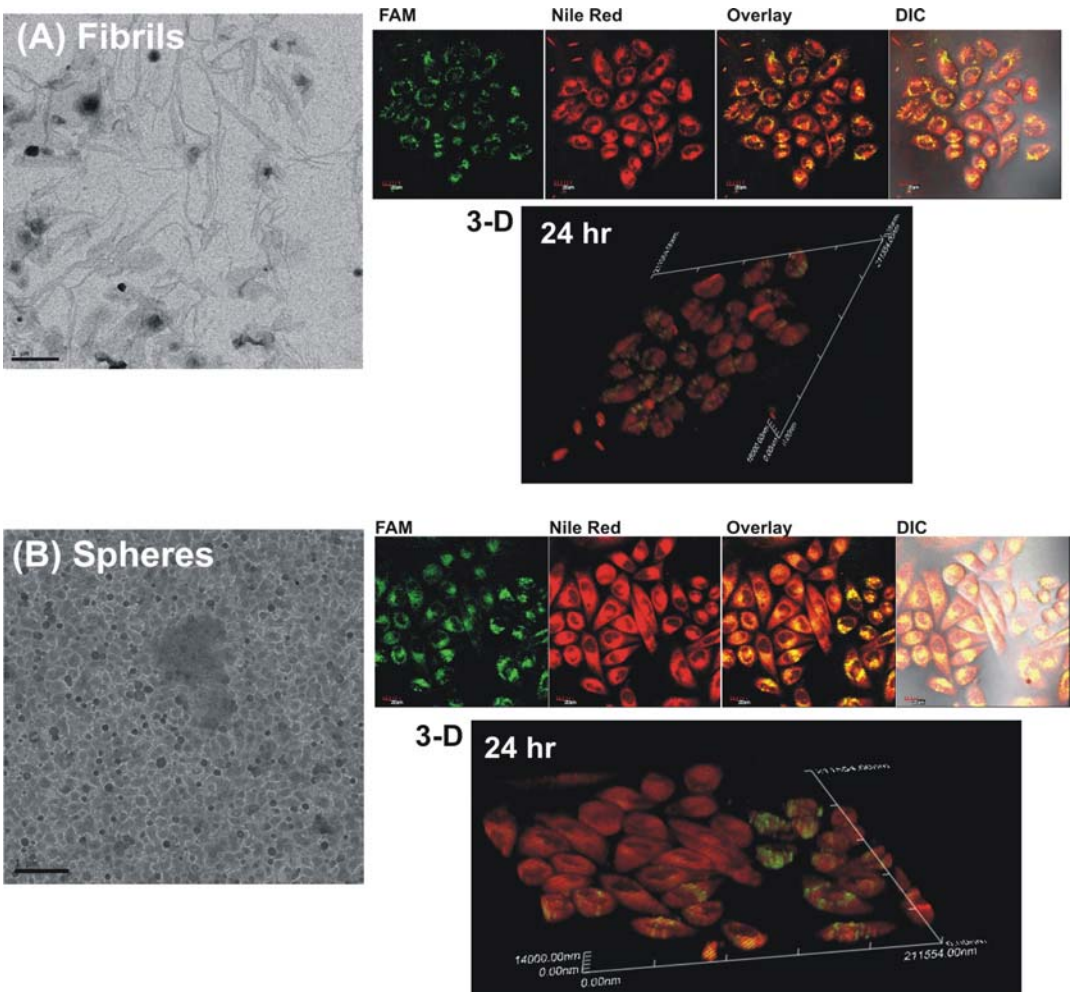

Figure 5-6. Cellular uptake of corresponding structures of different size and shape; (A) fibril and (B) spheres; DNA-b-PEG-b-PCL assemblies.

5.4 Gene Regulation via Antisensing

One of the major challenges in gene therapy is the efficient delivery of therapeutic nucleic acids in their active forms.[6, 7] Here, we propose to develop DNA block-copolymer (BCP) assemblies as an efficient and nontoxic delivery vehicle of short nucleic acids. A DNA BCP is consisted of a short single strand of DNA covalently attached to a strand of a hydrophobic polymer. In aqueous solutions, DNA BCPs self-assemble into nano- to meso-scale assemblies composed of a hydrophobic polymer core and a DNA corona. We have previously shown that the DNA binding constant of DNA-b-polystyrene mesoscale assembly is dramatically enhanced compared to regular DNA strands in solution owing to the very high DNA density on the surface of the assemblies.[8] They are also excellent candidates as gene delivery vehicles. Our initial studies with DNA BCP of DNA-b-polystyrene indicated that the cellular uptake of our assemblies is more efficient than DNA-modified gold nanoparticles (DNA-AuNP) which have been demonstrated to be an extraordinarily effective DNA delivery vehicle for many cell types.[9] It was hypothesized that the unusually efficient cellular uptake of DNA-AuNP is due to the opsonization of cell medium proteins onto nanoparticles with very high density DNA,[10] and we believe that the same mechanism is applied in our assemblies with a high density DNA.

5.4.1 Regulation of Vimentin

5.4.1.1 GFP/Vimentin 3T3 Cells

Constructs with antisensing Vimentin sequence in the DNA In addition to the Tau protein regulation, we will also evaluate our assemblies for the down regulation of Vimentin in 3T3 cells in collaboration of Dr. Paul Janmey (School of Engineering/Medicine, UPenn). It has been found that cells start to express Vimentin protein during the epithelial–mesenchymal transition (EMT), the process found in metastasis of cancer cells.[13] An effective method to regulate the expression of Vimentin will play a very important role in oncological studies of the metastasis of tumors. Our preliminary results using GFP/Vimentin showed reduced GFP fluorescence indicating that our assemblies can down regulate the expression of GFP-Vimentin (**Figure 5-7**).

5.4.1.2 Human Umbilical Vein Endothelial Cells (HUVEC)

We have examine the cellular uptake and the expression of Vimentin in human umbilical vein endothelial cells (HUVEC),these primary cells are of great interest but are notoriously difficult to transfect; conventional transfecting methods such as cationic liposomes failed to achieve high efficiency transfections. HUVEC (Lonza) used for experiments were cultured in EGM-2 medium supplemented with BulletKit (Lonza) as recommended by manufacturer. Prior to some experiments, HUVEC were subcultured onto glass coverslips or tissue-culture treated polystyrene at high density and incubated for a minimum of 4 days to allow a monolayer to form. HUVEC in 60mm dishes were transferred from their growth incubator to the live imaging chamber. A number of

locations within the dish were selected and imaging initiated for the experimental time courses, e.g., every 1min for 20min; every 5min for 60min, etc. After a few images were captured to establish the baseline condition, construct was added to the medium in the dish by gentle pipetting while imaging continued. To determine the loss of the fluorescent signal over time, replicates of dishes were seeded and incubated with construct; each dish was removed and imaged at a single 24hr interval following the addition of construct. Uptake experiments with HUVEC were imaged with a Leica DMIRE2 equipped with a camera (Hamamatsu model C4742-95), motorized stage (BioVision Technologies), and live imaging chamber capable of maintaining temperature, humidity and CO_2 (Tokai Hit), and controlled by iVision software (BioVision Technologies).

With our DNA polymeric assembled constructs, we were able to achieve an incredible transfection efficiency of >99% as shown in **Figure 5-8.** Cells showed both the green fluorescence from FAM and the red fluorescence from Nile Red within 15 mins of incubation (**Figure 5-9**). The uptake of this construct into 100% of the cells in a functional HUVEC monolayer is the first time that this degree of efficiency has been achieved. The timing of the addition of the construct after monolayer formation abrogates the possibility of the experimental perturbation affecting the formation of the monolayer, and reduces the potential dilution and degradation of constructs that accompany established transfection techniques.

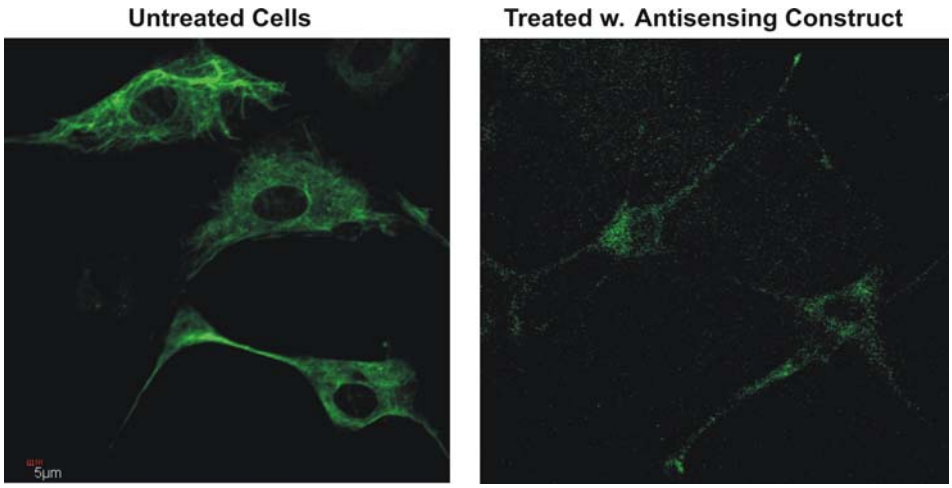

Figure 5-7. Vimentin down regulation in 3T3 cells using fibril DNA-*b*-PEG-*b*-PCL in 3T3 cells.

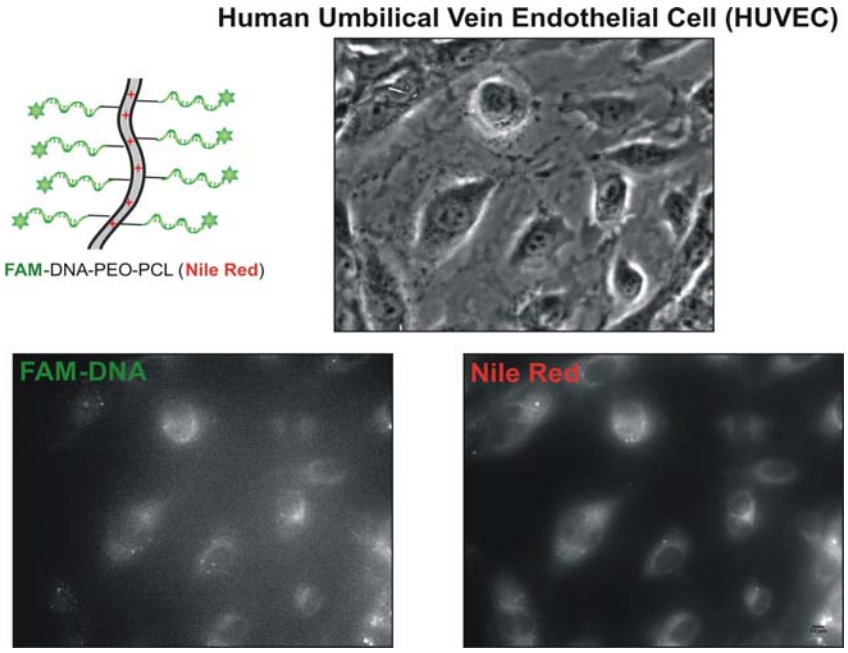

Figure 5-8. Cellular uptake of fibril DNA-*b*-PEG-*b*-PCL in HUVEC cells.

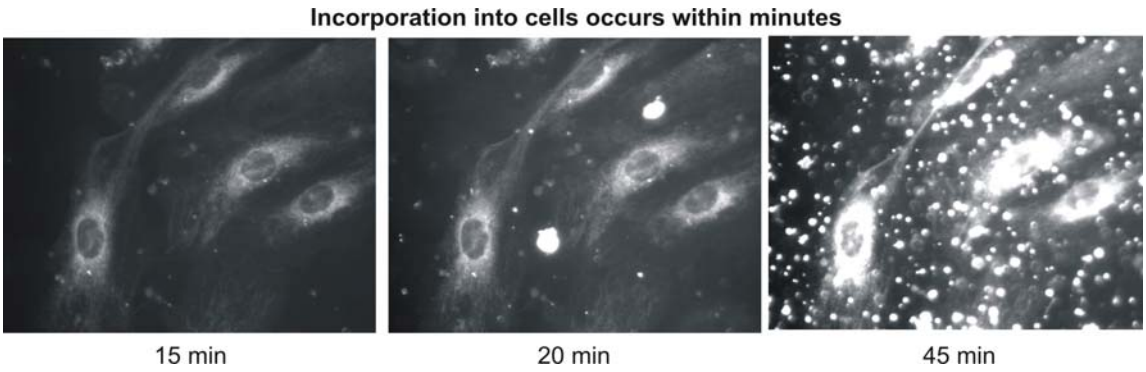

Figure 5-9. Kinetic studies on the uptake of DNA-*b*-PEG-*b*-PCL assemblies by HUVEC.

It was observed that over time, big spherical aggregates start to appear in the medium as seem in **Figure 5-9** over the course of 45 min. As mentioned in Chapter 2, these big aggregates were determined to be degraded products of PCL due to the basicity of the medium. To circumvent the fast degradation of PCL, a short segment of PBO was inserted in between PEG and PCL to provide an extra layer of hydrophobic shell to protect the PCL core from being degraded by hydrolysis of either base or enzymes. As shown in Chapter 2, the new DNA-*b*-PEO-*b*-PBO-*b*-PCL show great stability in the HUVEC medium over the course of many days. Uptake studies using this new construct were examined and it was found that these new constructs show similar uptakes as the DNA-*b*-PEO-*b*-PCL that is they were taken up by HUVEC very efficiently and effectively (**Figure 5-10A)**. Moreover, no big aggregates were observed in the medium (**Figure 5-10B**).

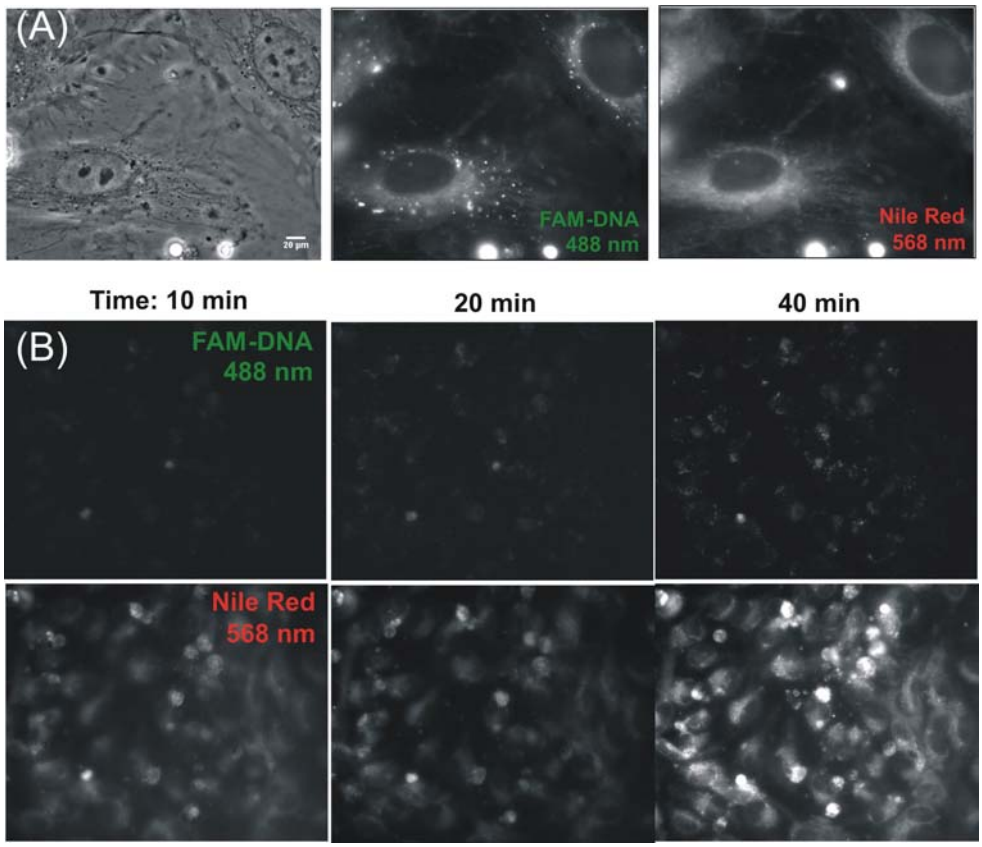

Figure 5-10. (A) Cellular uptake of DNA-*b*-PEG-*b*-PBO-*b*-PCL by HUVEC. (B) Kinetic studies on the uptake of DNA-*b*-PEG-*b*-PBO-*b*-PCL assemblies by HUVEC.

5.4.2 Regulation of Tau Protein

The over expression of Tau proteins has been suspected to be one of the causes of Alzheimer's disease.[11] Therefore, the ability to regulate its expression can potentially provide a new opportunity for a cure for Alzheimer's disease. We are currently collaborating with Dr. Gerard Schellenberg (School of Medicine, UPenn) to investigate the ability of our DNA BCP assemblies in the down regulation of the Tau protein in human IMR32 neuroblastoma cells.

Significantly, in our preliminary study, worm-like assemblies of DNA-*b*-PEO-*b*-PCL as well as the new polymer construct DNA-*b*-PEO-*b*-PBO-*b*-PCL were able to cross the plasma membrane of human IMR32 neuroblastoma cells (**Figure 5-11)**, which are notoriously difficult to transfect,[12] without the aid of any co-transfecting agent. For the down regulation of Tau protein, we will synthesize DNA-*b*-PEO-*b*-PCL with an effective antisense sequence found by the Schellenberg group using Morpholino DNA that binds to the region of the mRNA that is translated to Tau protein (5'TCA GCC ATC CTG GTT CAA AGT TCA C 3'). It is expected that the injection of the antisense sequence should reduce the Tau protein production.

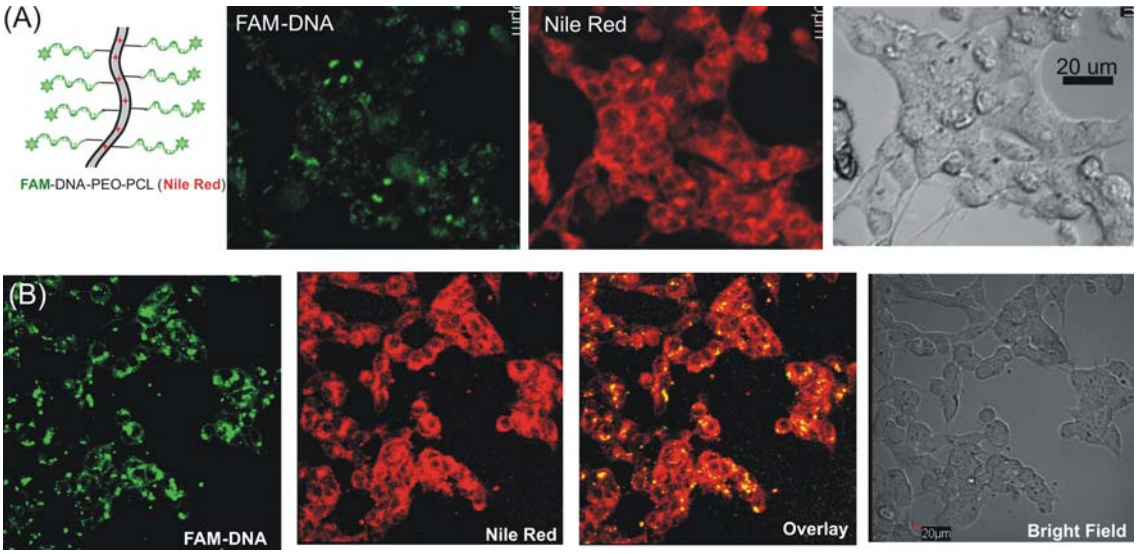

Figure 5-11. Cellular uptake of (A) DNA-*b*-PEG-*b*-PCL and (B) DNA-*b*-PEG-*b*-PBO-*b*-PCL in IMR32 cells.

5.5 Summary and Conclusions

Our DNA BCP assemblies offer important advantages over other existing non-viral gene delivery systems. Firstly, compared to conventional positively charged transfecting agents such as Lipofectamine, our negatively charged DNA BCP assemblies pose less toxicity concerns.[14] Secondly, despite the negatively charged surface of BCP assemblies, DNA BCP assemblies showed surprisingly high cellular uptake efficiency in our preliminary study without electroporation or co-transfecting agents. Futhermore, the densely packed DNA layer is expected to be resistant to the degradation by DNAase due to the high local salt concentration as mentioned above. Compared to the DNA-AuNP with the similar uptake efficiency and surface charge, our DNA BCP can be made from FDA approved biocompatible and/or biodegradable polymers such as polyesters to further reduce toxicity concerns. Moreover, pharmaceutical drugs can be loaded into the hydrophobic core of the assemblies during the self-assembling process for concomitant delivery of therapeutic DNA and other drugs. Similarly, we have previously demonstrated that nanoparticles can be readily incorporated into DNA BCP assemblies for imaging and controlled release of drugs.[8] This new delivery system is highly modular, and each component in the system (i.e., polymers, nanoparticles) can be tailored to meet the needs of specific applications. Finally, the mesoscale DNA BCP assemblies exhibit enhanced DNA binding properties compared to normal isolated oligonucleotides.[8] Thus, they are expected to bind efficiently to target RNA in cells for gene regulation.

5.6 References

1. Sioud, M. Therapeutic siRNAs (2004).
2. Pratt, A. J. & MacRae, I. J. The RNA-induced Silencing Complex: A Versatile Gene-silencing Machine. Journal of Biological Chemistry 284, 17897-17901 (2009).
3. Ngo, H., Tschudi, C., Gull, K. & Ullu, E. Double-stranded RNA induces mRNA degradation in Trypanosoma brucei. Proceedings of the National Academy of Sciences 95, 14687-14692 (1998).
4. Corey, D. R. RNA learns from antisense. Nat Chem Biol 3, 8-11 (2007).
5. Zalachoras, I., Evers, M. M., van Roon-Mom, W. M. C., Aartsma-Rus, A. M. & Meijer, O. C. Antisense-mediated RNA targeting: versatile and expedient genetic manipulation in the brain. Frontiers in Molecular Neuroscience 4 (2011).
6. Putnam, D. Polymers for gene delivery across length scales. Nat Mater 5, 439-451 (2006).
7. Sokolova, V. & Epple, M. Inorganic Nanoparticles as Carriers of Nucleic Acids into Cells. Angewandte Chemie International Edition 47, 1382-1395 (2008).
8. Chen, X.-J. et al. Self-Assembled Hybrid Structures of DNA Block-Copolymers and Nanoparticles with Enhanced DNA Binding Properties. Small 6, 2256-2260 (2010).
9. Rosi, N. L. et al. Oligonucleotide-Modified Gold Nanoparticles for Intracellular Gene Regulation. Science 312, 1027-1030 (2006).
10. Prigodich, A. E., Alhasan, A. H. & Mirkin, C. A. Selective Enhancement of Nucleases by Polyvalent DNA-Functionalized Gold Nanoparticles. Journal of the American Chemical Society 133, 2120-2123 (2011).
11. Buee, L., Bussiere, T., Buee-Scherrer, V., Delacourte, A. & Hof, P. R. Tau protein isoforms, phosphorylation and role in neurodegenerative disorders. Brain Research Reviews 33, 95-130 (2000).
12. Karra, D. & Dahm, R. Transfection Techniques for Neuronal Cells. The Journal of Neuroscience 30, 6171-6177 (2010).

13. Mendez, M. G., Kojima, S.-I. & Goldman, R. D. Vimentin induces changes in cell shape, motility, and adhesion during the epithelial to mesenchymal transition. The FASEB Journal 24, 1838-1851 (2010).
14. Massich, M. D. et al. Regulating Immune Response Using Polyvalent Nucleic Acid gold Nanoparticle Conjugates. Molecular Pharmaceutics 6, 1934-1940 (2009).

Chapter 6: Perspective and Future Directions

6.1 Perspective on DNA Block Copolymer as Non-Viral Carriers

Traditionally, the booming interest in bioinspired materials research has predominately focused on the understanding and the development of naturally occurring materials and the ability to create novel multifunctionality artificial materials by combination of different functional materials, *e.g.* the specific recognition properties of biological molecules (such as nucleic acid, peptides, proteins, *etc*) and the unique optical/physical properties of inorganic nanoparticles (such as quantum dots, noble metal nanoparticles, magnetic nanoparticles, *etc*). The expectation has always been that the resulting properties of the novel artificial material will simply be the combination of properties from the individual components. However, this is not always the case as demonstrated in our biohybrid DNA block copolymer nanomaterial.

The enhanced binding capability of the DNA strands on the DNA block copolymer self-assemblies i.e. DNA strands on the self-assembled nanostructure can form duplex with its complementary strand at solutions virtually without the addition of ions, a condition in which ordinary DNA strands do not form duplex, is a result of the high local salt concentration around the nanostructures caused by the ultra-high density of DNA packed on the surface of the nanostructures. Therefore, DNA strands on the nanostructure can still hybridize with complementary strands even if the global salt concentration does not promote hybridization for plain DNA strands. These hybrid self-assemblies of DNA block copolymers demonstrated the potential for the synthesis of novel artificial materials with novel properties that cannot be found in the individual components that they are composed of, by simply manipulating the microenvironment of the biohybrid nanostructures. This is an area in bioinspired materials that has been greatly overlooked and certainly deserves much greater consideration.

6.1.1 A Univerisal System

Engineer a universal delivery system for any type of antisensing applications. Design using a short "sacrificial" A20 strand to perform Thiol-ene Click reaction to avoid degradation commonly caused by UV-A radiation (wavelength 320 – 400 nm) commonly resulted in oxidation of guanine. This design will avoid any potential chance for degradation of the antisensing DNA strand during the conjugation step to the polymer assembly. A20-*block*-polymer assemblies can be used to hybridize with any antisensing DNA strands that have extra T20 at the terminal of the DNA sequence.

6.1.2 Concomitant Delivery

With the structure of the DNA block copolymer assemblies, this system can be used for concomitant delivery of therapeutic agents such as siRNA, functional nanoparticles and pharmaceutical drugs. This can increase the effectiveness of the therapy by targeting the problem using multiple solutions all packed into one type of nanoparticle carriers.

6.1.3 Topical Delivery

The meso-scale assemblies of DNA block copolymers using biodegradable polymer has been demonstrated to be able to be cross the plasma membrane efficiently, it is interested to see the uptake of these assemblies in topical delivery applications. DNA conjugated gold nanoparticles have been recently reported to be successful in the delivery of therapeutic siRNA for skin diseases.[1]

6.1.4 Kinetic Studies on Nulcease Degradation of Payload

Given the nature of the meso-structures, where they can achieved the areal DNA density of 13 nm gold nanoparticles, it is expected that these meso-structures should possess silimar properites such as the ability to slow the degradation of the DNA cargo by DNAse. [2] It will be interesting to study whether or not the DNA block copolymer assemblies also possess this interesting property due to the high density packing of DNA on the surface.

6.1.5 Endocytotic Mechanism

As have shown in **Chapters 4 and 5,** meso-assemblies are extremely efficient delivery carriers. It is a bit counterintuitive given that generally negatively charged species are considered poor choices in delivery since it is expected that electronic repulsion would play a major role since the cell membrane is negatively charged.

6.1.6 Long-term Toxicity Study of Carriers

Nanoparticles can undergo agglomeration or shape changes under certain conditions. In order to implement metal nanoparticles for *in vivo* and clinical applications, their biocompatibility and cytotoxicity issues must be resolved. Thus, it is important to evaluate the performance of nanoparticles at the cellular level and for *in vivo* applications. DNA-conjugated metallic nanoparticles have not been found to cause acute cytotoxicity.[4] In fact a recent detailed study on how nanoparticles change the genome expression profile of cells showed that DNA-conjugated nanoparticles do not induce significant changes in gene expression, while citrate-stabilized gold nanoparticles completely alters the entire genome expression of cells.[5] Moreover, Massich *et al.* reported that DNA functionalized gold nanoparticles induced 25 times less immune response compared to cationic liposome-DNA complex in macrophage and HeLa cells.[6] It is imperative to study the long-term cytotoxicity of the DNA block copolymer assemblies and how they compare to the DNA conjugated gold nanoparticles.

6.2 References

1. Zheng, D. et al. Topical delivery of siRNA-based spherical nucleic acid nanoparticle conjugates for gene regulation. Proceedings of the National Academy of Sciences of the United States of America 109, 11975-11980 (2012).
2. Prigodich, A. E., Alhasan, A. H. & Mirkin, C. A. Selective Enhancement of Nucleases by Polyvalent DNA-Functionalized Gold Nanoparticles. Journal of the American Chemical Society 133, 2120-2123 (2011).
3. Murphy, C. J. et al. Gold Nanoparticles in Biology: Beyond Toxicity to Cellular Imaging. Accounts of Chemical Research 41, 1721-1730 (2008).
4. Rosi, N. L. et al. Oligonucleotide-Modified Gold Nanoparticles for Intracellular Gene Regulation. Science 312, 1027-1030 (2006).
5. Massich, M. D., Giljohann, D. A., Schmucker, A. L., Patel, P. C. & Mirkin, C. A. Cellular Response of Polyvalent Oligonucleotide-Gold Nanoparticle Conjugates. ACS Nano 4, 5641-5646 (2010).
6. Massich, M. D. et al. Regulating Immune Response Using Polyvalent Nucleic Acid-Gold Nanoparticle Conjugates. Molecular Pharmaceutics 6, 1934-1940 (2009).